論文 / 著書情報
Article / Book Information

題目(和文)	窒素・酸素混合気体マイクロ波放電プラズマ中の一酸化窒素励起状態(A 2Σ+, B 2Π, C 2Π)に関する実験・数値分光学的研究
Title(English)	Experimental and numerical spectroscopy examinations of NO (A 2Σ+, B 2Π, C 2Π) excited states in N2-O2 mixture microwave discharge
著者(和文)	譚 浩
Author(English)	TAN HAO
出典(和文)	学位:博士（学術）, 学位授与機関:東京工業大学, 報告番号:甲第10252号, 授与年月日:2016年3月26日, 学位の種別:課程博士, 審査員:赤塚 洋,奥野 喜裕,沖野 晃俊,肖 鋒,脇 慶子
Citation(English)	Degree:, Conferring organization: Tokyo Institute of Technology, Report number:甲第10252号, Conferred date:2016/3/26, Degree Type:Course doctor, Examiner:,,,,
学位種別(和文)	博士論文
Type(English)	Doctoral Thesis

Tokyo Institute of Technology

Experimental and Numerical Spectroscopy Examinations of NO ($A\ ^2\Sigma^+$, $B\ ^2\Pi$, $C\ ^2\Pi$) Excited States in N_2-O_2 Mixture Microwave Discharge

A Dissertation

By

Hao Tan (譚　浩)

Supervisor: Prof. Hiroshi Akatsuka (赤塚　洋)

Department of Energy Sciences

Submitted in partial fulfillment of the requirements

for the degree of

Doctor of Philosophy

Date 2016/1

東京工業大学
Tokyo Institute of Technology

ABSTRACT

This research focuses on low-pressure and low-temperature gaseous plasma. We theoretically calculate the γ-band radiation spectrum of the NO molecule. By matching the calculated spectra with the experimental spectra, the molecular parameters in the plasma can be obtained. From the results, we found that the vibrational and rotational temperatures of NO molecules range from 0.42-0.76 and 0.13-0.21 eV, respectively, while the vibrational and rotational temperatures of N_2 range from 0.45-0.75 and 0.12-0.17 eV, respectively. From these results, besides a normal cooling process as the plasma flows to the downstream along the tube, we also find an unusual increase of the NO vibrational temperature when O_2 partial pressure ratio approaches to 100%.

We also improve our kinetic model to calculate the reaction rates and number densities of different species in N_2-O_2 mixture plasma. We find good agreements between the simulated and experimental results of the NO A $^2\Sigma^+$ state number densities. The radiation bands of β and δ are observed only when the oxygen partial pressure is less than 3. We discuss the de-excitation processes for the NO B $^2\Pi$ and C $^2\Pi$ states in this low-pressure plasma and propose an assumption that the de-excitation processes involve collision with O_2 X $^3\Sigma^-_g$ for these two levels are much faster than their generating processes, which can explain the observed spectral disappearance. Further results show that, as the ratio of the number density of NO C $^2\Pi$ and A $^2\Sigma^+$ increases, the vibrational temperature of the NO A $^2\Sigma^+$ state increases synchronously. This indicates the NO C $^2\Pi$ state experiences a de-excitation collision and turns into A $^2\Sigma^+$ state, which finally leads to the vibrational temperature increase of NO A $^2\Sigma^+$state.

TABLE OF CONTENTS

LIST OF TABLES

LIST OF FIGURES

CHAPTER I: Introduction

1.1 Applications of Mixture Plasma

The interest in discharges of N_2-O_2 mixtures is furthered by researches on air breakdown, optical characteristics of the atmosphere under perturbed non-equilibrium conditions, chemical processes for surface treatments, synthesis of nitrogen oxides, nitrogen isotope separation, cleaning of polluted atmospheric gases, and so on. [1] Figure 1.1 shows the main chemical products during the nighttime activities of the human beings. From the figure, we can find that NO_x widely exist in the chemical reactions, which can be accelerate under the plasma conditions (combustion and high energy light exposure). NO molecule is very important because it is harmful to the organisms. There have always been investigations on this kind of processes. Figure 1.2 shows the rate coefficient dependence against to the various altitudes of the stratospheric eddy coefficient values.

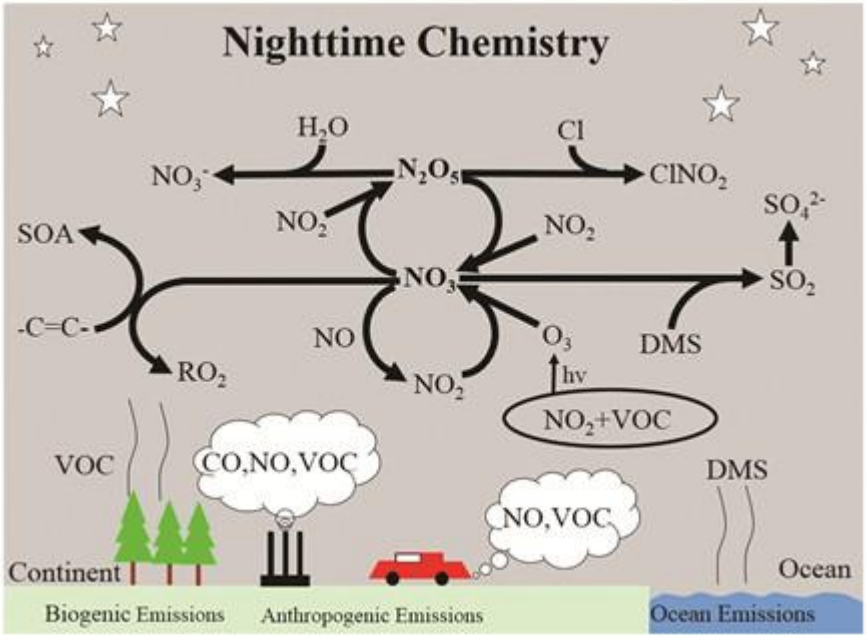

Figure 1.1. Chemical processes in atmosphere.

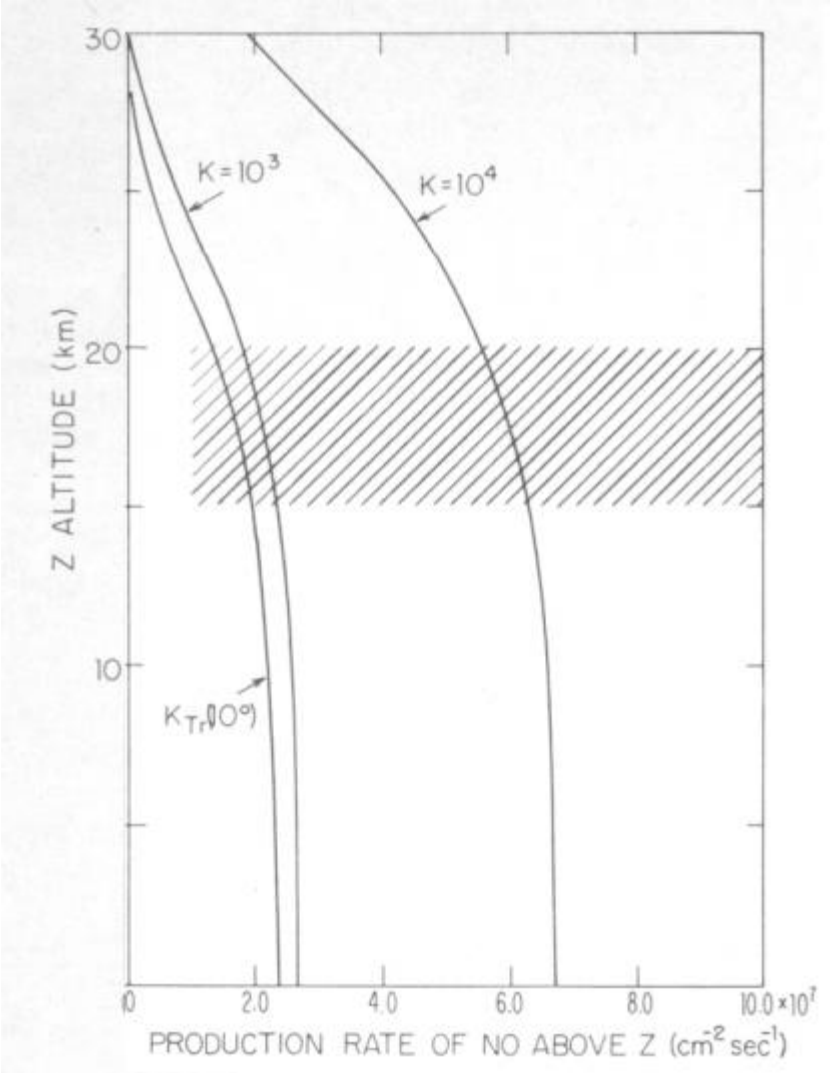

Figure 1.2. The production rate of NO above the altitude *z* from $O+N_2O \rightarrow 2NO$ for various values of the stratospheric eddy coefficient. (Mcelroy and Mcconnell, 1971)

Because the main compositions of the atmosphere and ionosphere are N_2-O_2 gases, this kind of plasma usually relates to the earth (normal or high pressure) as well as the space (low pressure) investigations, including the engine development of fighters especially for the 5th generation, the coating materials of the space shuttle surfaces at the moment of re-entry or in order to study the surface glow produced by the spacecrafts in low Earth orbits. [2–3] When studying these discharges, we know that a number of

unstable species are produced, such as excited states of O and N atoms, O_2 and N_2 metastables, and many kinds of the nitric oxides. All these species usually have very active properties both physically and chemically. On the other hand, under these kinds of plasma conditions, some of them also have strong emission bands locate at the UV or IR radiation range, which can leads to further molecular performance. [4–8]

The active species in N_2-O_2 discharges can be applied in the plasma biology and plasma medicine treatment. For example, at first, the low-pressure plasma sterilization is implied using gas mixtures containing components with germicidal properties such as H_2O_2 and aldehydes. After that, it is extended to use other mixture gases for some further plasma processes including the He-air, He-O_2 and N_2-O_2. [9,10] These studies and application, have been performed using radiofrequency (RF) or microwave low-pressure discharge in oxygen and N_2-O_2 mixtures. In some cases, under the strong radiation of plasmas, the efficiency of sterilization can be more than 50% improvement than other methods even at a short time.

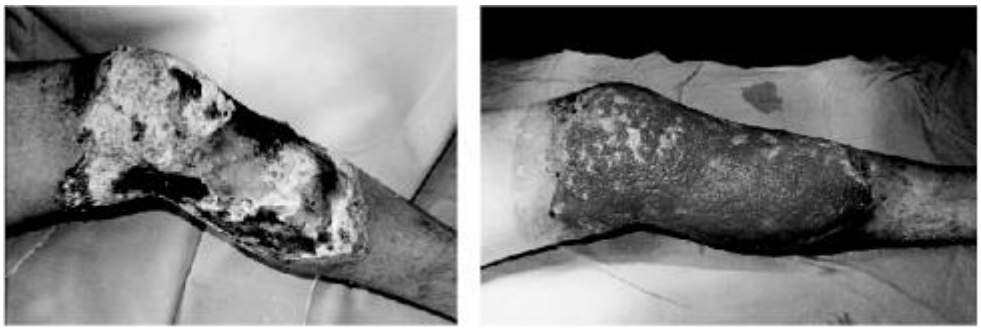

Figure 1.3. Healing dynamics of the festered burn wound in process of the plasma NO therapy: (a) prior to the beginning of treatment; (b) after five sessions of the therapy. [9]

As one of the important resultants in N_2-O_2 mixture discharge, the NO molecule is also applied in medical treatment. Figure 1.3 shows an effective treatment of plasma NO therapy, which is used for healing a festered burn wound. From the photographs, it is obviously seen that this effect is observed independently of the location of the wound on the body and also of the plastic material used. The effectiveness of NO therapy in treatment of early and late radiation reactions allows for the surgeon to carry out a full course in radiation therapy in around 88% of the patients. Meanwhile, this treatment is also used in some other cures, such as apparent with the erysipelatous inflammation.

Another application of the gas discharges is the envelope (lamps). There are three types of the continuous-discharge lamps.[11] Gas-discharge lamps emit light as result of optical transitions in atoms and molecules. The discharges are usually generated by glows of direct current (DC) discharges, microwave discharge in tubes, and dielectric barrier discharges (DBD), and so on. Because there are many emission bands when using different mixture gases, or even in a single gas, some optional radiation peaks can be obtained. Moreover, under different plasma conditions, the emission bands are able to change their densities or locations even using the same mixture. Therefore, the gas discharges can apply in many areas, including the laser technology, lighting systems, and photodetectors.[12]

1.2 Spectroscopic Investigations on N_2-O_2 Plasmas

The spectroscopic method is also very useful when coordinating with a kinetic model calculation for the concentrations of neutral and charged particles. As a classical measurement of detecting concentrations of particles, the mass spectrometer cannot be

used for detecting the metastables of the neutral particles. It is also very difficult to detect the concentrations within or along the plasma flow. This makes the spatial investigation on plasma impossible. The spectroscopic method can solve this problem perfectly by contactless diagnosing. Nowadays, this technology has been widely used for checking the correctness of the plasma kinetic models. [13–23] This method requires strong radiation peaks so that it has been often applied in diagnosing the atmosphere-like gases which has strong emission even at a low pressure.

Many kinds of N_2-O_2 plasmas have been characterized through different kinds of experimental and theoretical efforts. Generally, we can divide this mixture plasma into high-pressure (close-to) and low-pressure (far-from) conditions because they are similar status to the atmospheric and ionospheric plasmas. About the atmospheric plasma, Park and Lee [24] developed a multi-temperature nozzle flow code. It was used to determine rotational, vibrational, and electron-electronic temperatures by Park and Lee and Babikian *et al* [25] of NASA Ames Research Center. In their research, the heavy-particle translational temperature is assumed to equal to rotational temperature, and vibrational temperatures of NO, N_2 and O_2 are different from each other. Abe *et al* [26] characterized eight temperatures to describe arc-heated nozzle flows, that is, translational, N_2-, O_2-, and NO-rotational, N_2-, O_2-, and NO-vibrational, and electron temperatures. Especially, the NO rotational and vibrational temperatures are unusual to N_2 and O_2, which leads that people present many assumptions about these molecular processes to explain this temperature difference. Figure 1.4 shows the spectra obtained by S-. Hyun *et al* [27] and Park *et al* [25]. In their spectra, we can find the calculated spectra include some peaks

which are not seen in the experimental result. This indicates that even the spectra can be calculated, it is still insufficient.

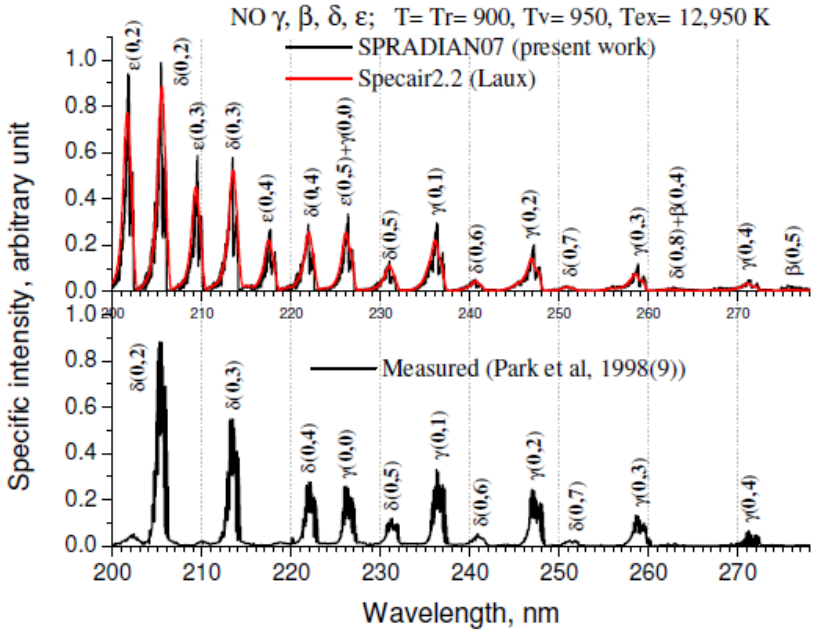

Figure 1.4. Comparison of NO spectra calculated by S. Hyun *et al* (present work [27]) and by Babikian *et al* [25].

Since this research about the atmospheric pressure N_2-O_2 plasma often involves the environment issues, the calculation are mature and able to present precise estimations on the concentration of chemically active particles and chemical reaction products in a pulsed microwave discharge as showed in Fig. 1.5. [16] From the presented result, we can find the oxynitrides are even far more less than the O and O_3 which are also products during this plasma process. However, this process is complicated because the concentrations are keeping changing in time and spatial domain.

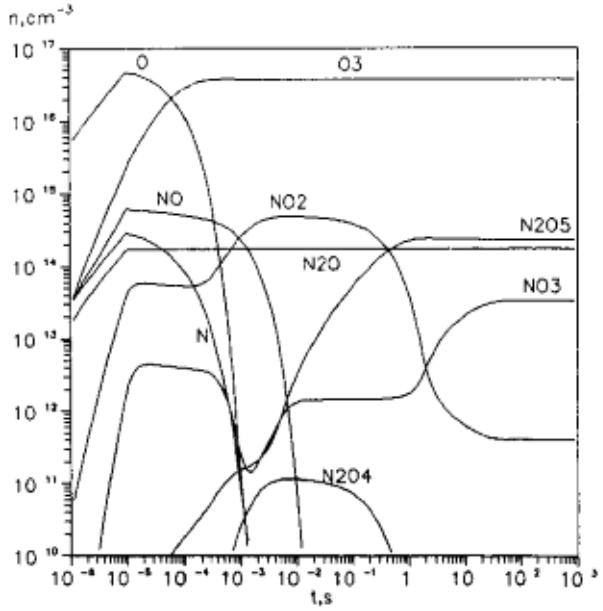

Figure 1.5. The concentration of some chemically active particles and chemical reaction products in a pulsed microwave discharge.[16]

Meanwhile, about the low-pressure N_2-O_2 plasma, the calculation investigations are even more mature. Figure 1.6 shows the NO concentration change against the O_2 percentage in the N_2-O_2 plasma. This implies many conditions will vary the plasma properties besides temperature effects. This is very useful in the application of the waste gas treatment.

Not only some relatively few particles but also the vibrational excitations for some ground state particles can be calculate precisely shown in Fig. 1.7. T. Sakamoto *et al* [16] examined N_2 vibrational excitations for different vibrational levels both numerically and experimentally. This makes a big improvement on the knowledge about the N_2 excitation process.

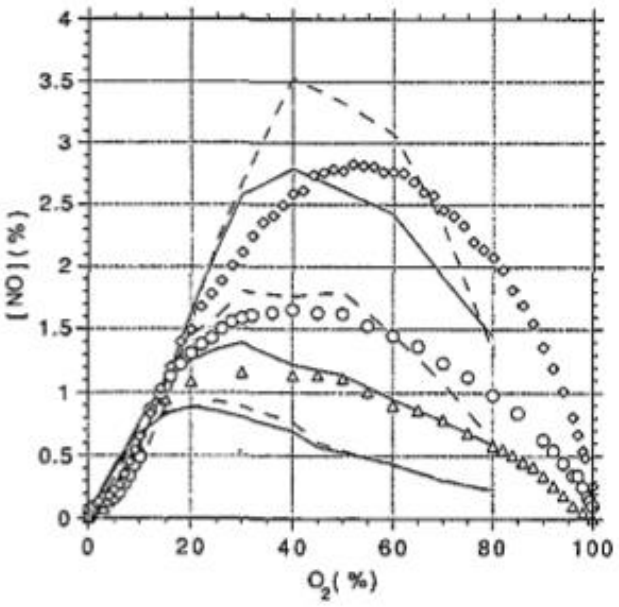

Figure 1.6. Variation of NO concentration against O_2 percentage for 12, 30 and 80 mA.

[15]

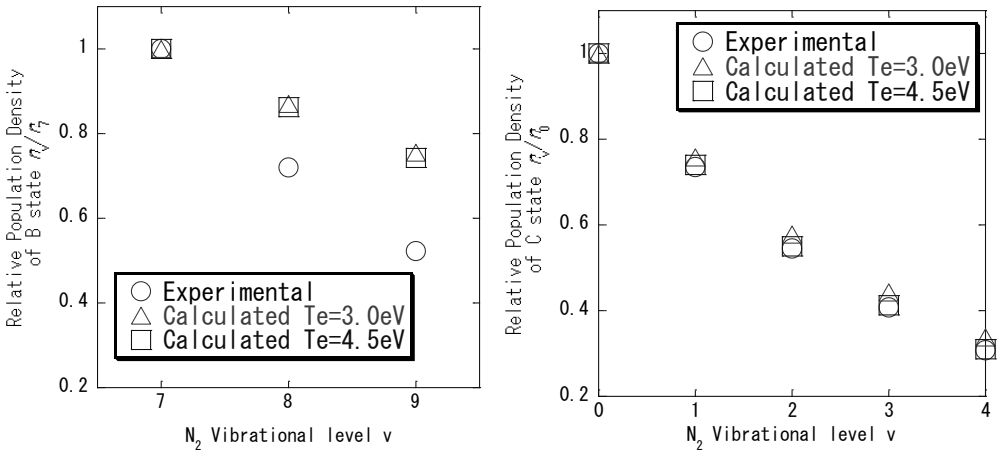

Figure 1.7. Measured and calculated number densities of vibrational levels of N_2. (left) B $^3\Pi$ (v=7, 8 and 9) and (right) C$^3\Pi$ (v=0 and 1) [41].

1.3 Low Pressure N_2-O_2 Plasmas in Geophysics

The NASA website locates many under-going investigations on the most forward N_2-O_2 plasma applications. Especially in the "Spacecraft and Orbital Environments" part, we can see their achievement about the low pressure air plasmas.

In their research issues, there is a team working on the analysis of international space station plasma interaction named "Plasma Interaction Model". This team created a model to predict the voltage difference between the ISS (International Space Station) of the US and the plasma background. The ionospheric plasma (low pressure N_2-O_2 plasma) interacts with the ISS solar arrays and conducing surfaces. In order to diagnose and protect the surfaces, many models are developed and used for the plasma processes. For example, if the free charges are accumulated in excess, this potential voltage will make a dielectric breakdown and finally speed the destroy process. This requires not only the surface property simulation, but also the background plasma simulation for the physical and chemical kinetics characters as many as possible. On the other hand, the diagnosing measurement is usually done by the remote observation, which is the spectroscopic method. For example, the Maui analysis of upper atmospheric injections (MAUI) group, usually watches the exhaust of the spacecraft by Maui Space Surveillance Surveillance Site in Hawaii. The technicians can analysis the images and data taken by a telescope and all-sky imagers in order to better understand interaction between the exhaust plume and the Earth's upper atmosphere. From all the introductions above, we can see the significance of the investigations on low pressure N_2-O_2 plasmas roughly.

The research of the spectroscopic measurement started hundreds years ago since Newton divided the sun light into seven different colors. Till 1960s, Kirchhoff founded the practical spectroscopy, after that, this technology is used for diagnosing the Universe. This technology promotes the development of our knowledge to the world, because at that time, the place is able to obtain the natural light is the sky. Throughout this curiosity, scientists keep investigating the basic physics processes and make it into the application. Nowadays, researches can deduce the material construction of another planet, only by the radiation we obtained. This is very helpful for us to take advantage of the extraterrestrial energy and resource in the future.

This thesis is a kind of continue of many predecessors, who devoted their lives to the research on N_2-O_2 plasma. In the discussion section of this thesis, I mention the B. Gordiets group frequently because this group achieves many important findings on low-temperature and low-pressure N_2-O_2 plasma. B. Gordiets also extended his ideas to geophysics by considering the mechanism of energy transfer fron geomagnetic disturbances to the lower atmosphere via the upper-atmospheric IR flux. One important study of his is also devoted to the role of the IR emission of CO_2 in the cooling process of the lower atmospheres of Venus, Earth and Mars, his analysis being again investigated and extended many years after. [28]

The reason of his huge achievement on this kind of plasmas should relate to his collaboration with some different French, Italian, Portuguese and Spanish groups. Since his collaboration stated in 1986 with a chapter in a book, more than 20 years have passed, his knowledge about the N_2-O_2 plasma, is partly a combination of different theories.

After a longtime work at Portugal, he came back to his motherland (Moscow) to continue his research. However, still he return to Lisbon for 1 or 2 months almost every year. As a result, his reports about N_2-O_2 plasma reflect the most cutting-edge all over the world.

1.4 Objectives

This research focuses on low-pressure and low-temperature gaseous plasma, which often involves atmospheric and ionospheric physics. Among these applications, the basic process and theoretical knowledge about the plasma status should be investigate deeply enough for available estimations. For this purpose, I set up a self-consistent research on our microwave plasma, to verify the accuracy of some general classical conclusion about this kind of discharges, it is very necessary to carry out both calculation and experimental examination.

Chapter 1 is devoted to the explanation of the background of this study. That is, the interest in discharges of N_2-O_2 mixtures is furthered by researches on air breakdown, optical characteristics of the atmosphere under perturbed non-equilibrium conditions, chemical processes for surface treatments, synthesis of nitrogen oxides, nitrogen isotope separation, cleaning of polluted atmospheric gases, and so on.

In Chapter 2, I review the backgrounds of the microwave discharges as well as the microwave itself, concerning analysis of these non-equilibrium plasmas. I also describe the summary of his experimental apparatus, not only for the discharge apparatus but also for the spectroscopic measurement system, together with general review of molecular spectroscopic principle to analyze properties of vibrational and rotational excited states kinetics in the plasmas.

In Chapter 3, I concentrate on the NO molecule in N_2-O_2 mixture microwave discharge because it is generated in oxidation processes in chemical and biological systems, which not only causes environmental problems but is also toxic to organisms. I observe this kind of plasma by optical emission spectroscopy measurements to obtain the spectra ranges at 200-850 nm. The plasma is generated and forced to flow in a quartz tube. In the experiment, I diagnose the spectra at different positions along the tube and different plasma conditions (electron density and temperature, total pressure, and partial pressure ratio).

I also theoretically calculates the γ-band radiation spectrum of the electronic transition from NO A $^2\Sigma^+$ to X $^2\Pi$ state. By matching the calculated spectra with the experimental spectra, the molecular parameters in the plasma can be obtained. From results, the plasma process is discussed.

In Chapter 4, in order to quantify the analysis in Chapter 3, I improve his kinetic model to calculate the reaction rates and number densities of different species in N_2-O_2 mixture plasma. According to my results, I make an assumption to explain the disappearance of β- and δ-bands. In order to prove my assumption, I carried out some experimental and calculation results. As expected, my assumption is right, but still this analysis is indirect.

In Chapter 5, I summarized my study and describe further perspective of the present contribution. This is not limited to the low-pressure N_2-O_2 plasma. I state that my finding can also explain the appearance of the NO β-band and δ-band at atmosphere.

CHAPTER II: Background Theory

2.1 Microwaves in Plasma

Waves widely exist in the world, meanwhile are ones of the basic motions of the matter. Since Langmuir found the plasma wave, many investigations on the generation, propagation and damping of waves in plasma are performed. [29] In the early researches about the astrophysics, the magneto-fluid mechanics are used to explain the reason of the formation of the macula and all kinds of the signals of different celestial bodies. In radio physics, people need the theory to study the propagating principle of radio waves in the ionosphere. In the controlled thermonuclear fusion, the plasma stability, microwave heated plasma, and plasma parameter diagnosing relate to the plasma wave theory. Therefore, both experimental and theoretical investigations on plasma waves are very important.

Properties of plasma waves depend on the plasma properties and the plasma conditions. Plasma is a kind of gas which consists of charged particles, as a result, there are three kinds of forces in the plasma: thermal gradient, electrostatic force and magnetic force. This indicates that the electrostatic and magnetic waves can generate and propagate in plasmas. Meanwhile, since the electron mass is far smaller than that of ions, they have different effects on the plasma waves. Generally speaking, waves in plasma are very complicated.

2.1.1 Dielectric Tensors and General Dispersion of Plasma Waves [30-33]

Before discussing the microwaves in plasmas, two important parameters should be specified. The plasma system consists of a large number of charges. In order to diagnose its physical properties, a disturbance is usually suggested. And as a response between ions and electrons, the dielectric tensor is one of the parameters which describe the plasma macroscopic response.

Suppose set a electric field $E(\boldsymbol{r}',t')$ at the place r' and time t', there will generate the induced current in plasma. If the induced current density is $j(\boldsymbol{r},t)$ at the place r and time t, this can be treated as the response to the disturbance of electric field from the plasma. Generally speaking, the relationship between $\boldsymbol{j}$ and $\boldsymbol{E}$ can be expressed as:

$$j(\vec{r},t) = \sigma(\vec{r},\vec{r}',t,t') \cdot E(\vec{r}',t'), \tag{2.1.1.1}$$

here the σ is the dielectric tensor of plasma. The tensor property originates from the plasma anisotropy. Meanwhile, considering the law of causation, we have

$$\sigma(\vec{r},\vec{r}';t,t') = 0, \ (t < t'). \tag{2.1.1.2}$$

If the disturbance is small, we can assume that the relationship between $\boldsymbol{j}$ and $\boldsymbol{E}$ is linear. A linear response satisfies the superposition principle. Therefore, as a function of $\boldsymbol{r}$ and t, the current density can be expressed as:

$$j(\vec{r},t) = \int d\vec{r}' \int_{-\infty}^{t} dt' \sigma(\vec{r},\vec{r}';t,t') \cdot E(\vec{r}',t'), \tag{2.1.1.3}$$

where the integration crosses throughout the whole space of the plasma.

Beside the linear response, if the medium is homogeneous and still, then the σ is only the function of the relative position $\boldsymbol{r}-\boldsymbol{r}'$ and time $t-t'$, which can be expressed as the follow:

$$j(\vec{r},t)=\int d\vec{r}'\int_{-\infty}^{t}dt'\sigma(\vec{r}-\vec{r}';t-t')\cdot E(\vec{r}',t'), \tag{2.1.1.4}$$

It is not convenient to substitute Eq. (2.1.1.4) in to Maxwell Equations. However, using the spatial Fourier Transform, Eq. (2.1.1.4) can be converted into a simple form as:

$$j(\vec{k},\omega)=\sigma(\vec{k};t-t')\cdot E(\vec{k},\omega), \tag{2.1.1.5}$$

including the follows:

$$j(\vec{k},\omega)=\int d\vec{r}\int_{-\infty}^{\infty}dt\,j(\vec{r};t)\cdot e^{i(\omega t-\vec{k},\vec{r})},$$

$$E(\vec{k},\omega)=\int d\vec{r}\int_{-\infty}^{\infty}dtE(\vec{r};t)\cdot e^{i(\omega t-\vec{k},\vec{r})}, \tag{2.1.1.6}$$

$$\sigma(\vec{k},\omega)=\int d\vec{r}\int_{0}^{\infty}dt\sigma(\vec{r}';t)\cdot e^{i(\omega t-\vec{k},\vec{r})},$$

As shown Eq. (2.1.1.6), it is obvious that the current density $\boldsymbol{j}$ is a linear function by the dielectric tensor, where the plasma properties are included.

On the other hand, when studying the linear waves in plasma, it is more convenient to include the current density in the electric displacement vector $\boldsymbol{D}$:

$$\mu_0\vec{j}+\varepsilon_0\mu_0\frac{\partial\vec{E}}{\partial t}\equiv\mu_0\frac{\partial\vec{D}}{\partial t}, \tag{2.1.1.7}$$

and the same as in a usual dielectric medium, the plasma dielectric tensor should be included as:

$$\vec{D} \equiv \varepsilon_0 \varepsilon \vec{E} . \tag{2.1.1.8}$$

Thus, after doing the Fourier Transfer to Eq. (2.1.1.7) and (2.1.1.8), the current density can be expressed as:

$$j(\vec{k},\omega) = -i\omega\varepsilon_0(\varepsilon(\vec{k};t-t') - \vec{I}) \cdot E(\vec{k},\omega), \tag{2.1.1.9}$$

where ***I*** is the unit tensor. It follows that, the dielectric tensor completely determines the plasma linear response property. As a result, the dielectric tensor completely determines the plasma wave property.

After obtaining the dielectric tensor of plasma, the induced current in Maxwell equation can be expressed by the dielectric tensor of plasma. Thus, without an external charge, the Maxwell equations that electric field ***E*** and magnetic field ***B*** satisfy are shown as:

$$\begin{aligned}
&\nabla \times \vec{E} = -\frac{\partial \vec{B}}{\partial t}, \\
&\nabla \times \vec{B} = \mu_0 \vec{j} + \frac{1}{c^2}\frac{\partial \vec{E}}{\partial t} = \mu_0 \vec{j} + \frac{\partial \vec{D}}{\partial t} = \frac{1}{c^2}\vec{\varepsilon} \cdot \frac{\partial \vec{E}}{\partial t}, \\
&\nabla \cdot \vec{D} = 0, \\
&\nabla \cdot \vec{B} = 0.
\end{aligned} \tag{2.1.1.10}$$

After doing a Fourier Transform to Eq. (2.1.1.10), we have:

$$\vec{k} \times \vec{E} = \omega \vec{B}, \tag{2.1.1.11}$$

$$\vec{k} \times \vec{B} = -\omega \mu_0 \vec{D} = -\frac{\omega}{c^2} \vec{\varepsilon} \cdot \vec{E}, \tag{2.1.1.12}$$

$$\vec{k} \cdot \vec{D} = 0, \tag{2.1.1.13}$$

$$\vec{k} \cdot \vec{B} = 0. \tag{2.1.1.14}$$

Eliminating ***B*** by Eqs. (2.1.1.11) and (2.1.1.12), the wave field ***E*** formula can be obtained as:

$$\vec{k} \times (\vec{k} \times \vec{E}) + (\frac{\omega^2}{c}) \vec{\varepsilon} \cdot \vec{E} = 0, \tag{2.1.1.15}$$

or if we extend the first term on the left side, we can get

$$[kk - k^2 \vec{I} + (\frac{\omega^2}{c}) \varepsilon(\vec{k}, \omega)] \cdot \vec{E} = 0. \tag{2.1.1.16}$$

The condition of the existence of a non-trivial solution for Eq. (2.1.1.16) is its coefficient determinant equals to zero:

$$\mathrm{Det} \left| kk - k^2 \vec{I} + (\frac{\omega^2}{c}) \varepsilon(\vec{k}, \omega) \right| = 0. \tag{2.1.1.17}$$

This formula determines the wave frequency ω and number ***k*** in plasma, and this is the plasma dispersion relationship.

In an isotropic plasma (without magnetic field), the most important direction is the direction that the wave propagates. The dielectric tensor can be written as:

$$\varepsilon(\vec{k},\omega)=\varepsilon_{\perp}(\vec{k},\omega)(\vec{I}-\frac{\vec{k}\vec{k}}{k^2})+\varepsilon_{\parallel}(\vec{k},\omega)\frac{\vec{k}\vec{k}}{k^2}, \tag{2.1.1.18}$$

where the $\varepsilon_{\perp}$ and $\varepsilon_{//}$ are the perpendicular and axial components, respectively, and they are both scalar functions of $\boldsymbol{k}$ and ω. Substituting Eq. (2.1.1.18) into Eq. (2.1.1.17), we can obtain the dispersion relationship of an isotropic plasma as:

$$\mathrm{Det}\left|\frac{\vec{k}\vec{k}}{k^2}\varepsilon_{\parallel}(\vec{k},\omega)+[\varepsilon_{\perp}(\vec{k},\omega)-N^2](\vec{I}-\frac{\vec{k}\vec{k}}{k^2})\right|=0. \tag{2.1.1.19}$$

After extending the determinant in Eq. (2.1.1.19), the following equations can be obtained:

$$\begin{aligned}&\varepsilon_{\parallel}(\varepsilon_{\perp}-N^2)^2=0,\\&\varepsilon_{\parallel}(\vec{k},\omega)=0,\\&\varepsilon_{\perp}(\vec{k},\omega)=N^2=(\frac{kc}{\omega})^2.\end{aligned} \tag{2.1.1.20}$$

Up to now, we have obtained the dispersion relationships for both transverse and longitudinal waves. With the corresponding, the wave fields can be shown as:

$$\begin{aligned}&\varepsilon_{\parallel}\vec{E}=0,\\&(N^2-\varepsilon_{\perp})\vec{E}=0.\end{aligned} \tag{2.1.1.21}$$

It implies that, the transverse and longitudinal waves in isotropic plasma are mutually independent.

2.1.2 Microwave in Plasma [34, 35]

In many cases, it is convenient to analyze plasma wave using the hydrodynamics theory. However, some important properties of plasma are unable to simulate, especially some effect from the thermal motion of particles, such as the damping effect. For a cold or with high density (the thermal motion can be ignored) plasma, the hydrodynamics is sufficient for a normal approximation. It should be specified that, when the phase velocities of all kinds of waves are small enough to compare with the oscillation of charges in plasma or are damping, this approximation is not appropriate.

For simplicity, we ignore the friction between different particles, and suppose it is an adiabatic system. The hydrodynamics equation for the plasma is shown as:

$$\begin{aligned} &mn\frac{d\vec{u}}{dt} = -\nabla p + en\vec{E}, \\ &\frac{dn}{dt} + n\nabla \cdot u = 0, \\ &\frac{d}{dt}(pn^{-r}) = 0, p = nT. \end{aligned} \tag{2.1.2.1}$$

Supposing $\mathbf{E}_0 = \mathbf{u}_0 = 0$, $p = p_0 + p_1$, $n = n_0 + n_1$ and the disturbing values p_1, n_1, and $\mathbf{E}_0$ and $\mathbf{u}_0$ are plane waves in ~exp [$i(\mathbf{k} \bullet \mathbf{r} - \omega t)$] changing. After linearizing the Eq. (2.1.2.1), we have the following for the pressure p_1:

$$-i\omega p_1 = -\gamma p_0 \nabla \cdot \vec{u} = -i\gamma(\vec{k} \cdot \vec{u}) p_0 . \tag{2.1.2.2}$$

It follows that, the pressure gradient is nonzero only at the direction of the propagation of waves. Supposing the direction of the propagation of waves is z axis, in the z direction we have:

$$
\begin{aligned}
-i\omega u_{\perp} &= \frac{e}{m} E_{\perp}, \\
-i\omega u_{z} &= -i\gamma \frac{k^2 T}{m\omega} u_{z} + \frac{e}{m} E_{z}.
\end{aligned}
\tag{2.1.2.3}
$$

Then, the current density $j=\Sigma e n_0 \mathbf{u}$ is:

$$
\begin{aligned}
j_{\perp} &= i\sum \frac{n_1 e^2}{m\omega} E_{\perp}, \\
j_{z} &= -i\sum \frac{n_0 e^2 \omega}{m\omega^2 - \gamma k^2 T} E_{z}.
\end{aligned}
\tag{2.1.2.4}
$$

It is easily seen that the $E_{\perp}$and E_z relates to the $\sigma_{\perp}$ and $\sigma_{/\!/}$. Therefore, the dielectric tensors of the unmagnetized plasma are:

$$
\begin{aligned}
\varepsilon_{\perp} &= 1 - \sum \frac{n_0 e^2}{\varepsilon_0 m\omega^2}, \\
\varepsilon_{\parallel} &= 1 - \sum \frac{n_0 e^2}{(m\omega^2 - \gamma k^2 T)\varepsilon_0}.
\end{aligned}
\tag{2.1.2.5}
$$

and the dispersion relationships can be obtained as:

$$
\begin{aligned}
N^2 = \varepsilon_{\perp} &= 1 - \sum \frac{n_0 e^2}{\varepsilon_0 m\omega^2}, \\
\varepsilon_{\parallel} &= 1 - \sum \frac{n_0 e^2}{(m\omega^2 - \gamma k^2 T)\varepsilon_0} = 0.
\end{aligned}
\tag{2.1.2.6}
$$

They represent the transverse and longitudinal waves in unmagnetized plasma.

Firstly we discuss the transverse waves. For simplicity, we limit the discussion to the plasma containing only one kind of the ion and electron. When we ignoring the

movement of ions because the ion mass is far larger than the electron, the dispersion relationship is:

$$N^2 = 1 - \frac{\omega^2_{pe}}{\omega^2} - \frac{\omega^2_{pi}}{\omega^2} \approx 1 - \frac{\omega^2_{pe}}{\omega^2},$$
$$\omega_{pe} = \sqrt{\frac{n_e e^2}{\varepsilon_0 m_e}}. \tag{2.1.2.7}$$

where the ω_{pe} is called plasma frequency or Langmuir frequency. From Eq. (2.1.2.7), we know that, if $\omega < \omega_{pe}$, N is a pure imaginary number, which means that the parameter k becomes an imaginary as the follow equation shown:

$$k = \frac{\omega}{c} N = i \frac{\omega_{pe}}{c} (1 - \frac{\omega^2}{\omega^2_{pe}})^{1/2} \equiv ia. \tag{2.1.2.8}$$

Moreover, the wave variation is an exponentially damping wave:

$$E(z,t) = E_0 e^{i(kz - \omega t)} = E_0 e^{-az} e^{-i\omega t}. \tag{2.1.2.9}$$

This indicates that the wave cannot propagate in unmagnetized plasma, if the wave frequency is smaller than the plasma frequency. We define the wave propagation distance in the plasma when its amplitude decreases to 1/e of the initial value as reflection skin depth δ. Then the formula will be:

$$\delta = \frac{1}{\alpha} = \frac{c}{\omega_{pe}} (1 - \frac{\omega^2}{\omega^2_{pe}})^{-1/2}. \tag{2.1.2.10}$$

The wave with smaller frequency than plasma frequency cannot propagate in the plasma, this is because the electromagnetic waves are shielded by the polarization

currents. However, in this case, there is no energy transformation, which means that the absorption and energy flux are both zero, hence the induced electromagnetic waves are all reflected. The critical frequency is called cut-off frequency as $\omega = \omega_{pe}$. We can summarize the cut-off frequency and density as:

$$\omega_c = \omega_{pe} = \sqrt{\frac{n_e e^2}{\varepsilon_0 m_e}} \approx 5.64 \times 10 \sqrt{n_e} \text{ [rad/s]}, \tag{2.1.2.11}$$

$$n_c = \frac{\varepsilon_0 m_e \omega_c^{\,2}}{e^2} \approx 1.2 \times 10^{-2} \, f_c^{\,2} \text{ [m}^{-3}\text{]; } f \text{ [s}^{-1}\text{]}, \tag{2.1.2.12}$$

If $\omega > \omega_{pe}$, the electromagnetic waves can propagate in the plasma, and the relationship between wave frequency and wave number is:

$$\omega^2 = \omega_{pe}^{\,2} + k^2 c^2. \tag{2.1.2.13}$$

2.1.3 Absorption and Resonance [36, 37]

When we talk about the wave absorption, this is very similar to a normal vibration energy transformation between two oscillators. In this case, the two oscillators are the microwave and the charges in plasma. The energy transformation efficiency have a maximum at the resonant point, which means $N^2 = \infty$ ($k^2=\infty$, $v_p=0$). For unmagnetized plasma, we can easily obtain that the farther the plasma and microwave frequencies differ from each other, the larger the N is. Therefore, in our experiments, the microwave absorption efficiency of gaseous plasma only depends on the relative position of the standing wave and the gas area. As shown in Fig. 2.1, TE (transverse electric) and TM

(transverse magnetic) waves will have standing waves of different shapes, which means the energy in the waveguide is not uniform distribution.

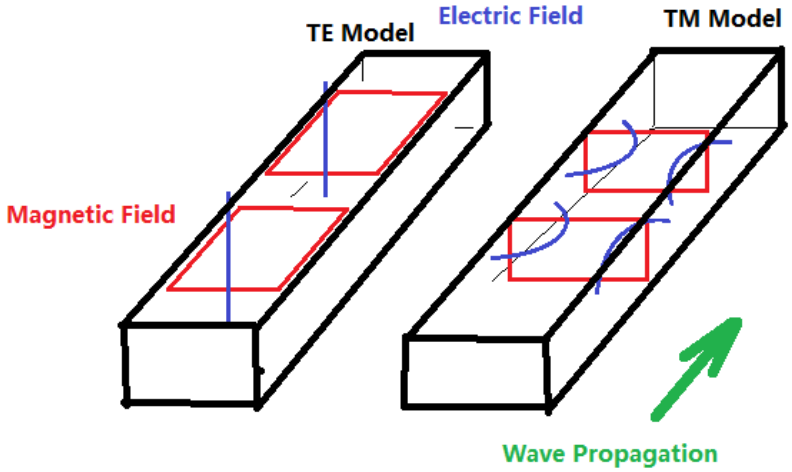

Figure 2.1. Schematic diagram of the TE and TM wave propagations in a rectangular waveguide.

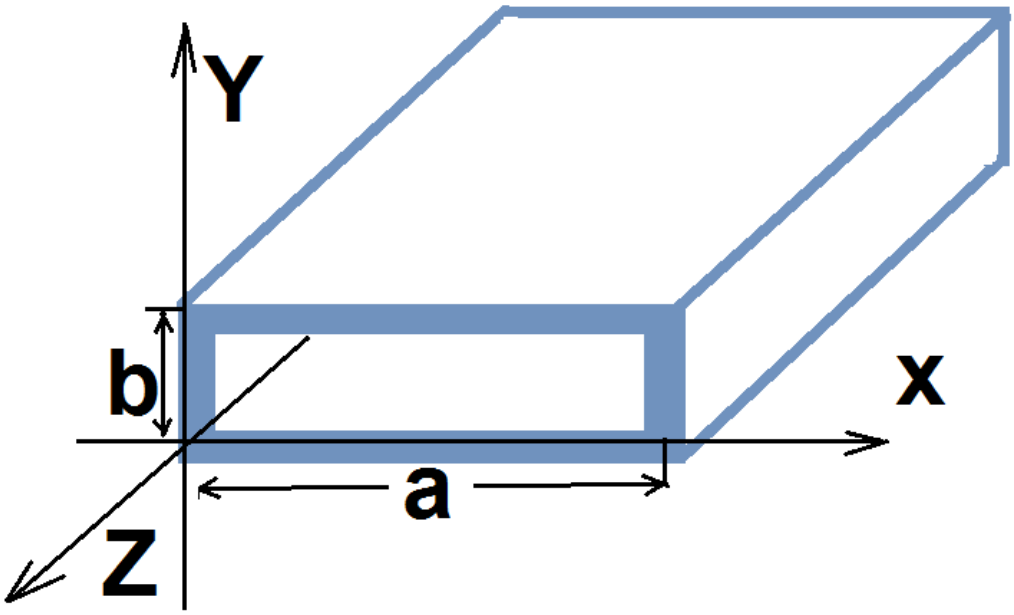

Figure 2.2. Schematic diagram of a rectangular waveguide.

Figure 2.2 shows a normal rectangular waveguide, which is usually made of metal materials. Inside the cavity, there is the air without any conductors. Hence the power loss and capacity are large. Meanwhile, since it is an enclosed construction, it has a very good anti-interference ability and no radiative loss. Considering a TM wave in the waveguide, we have the follow formula:

$$k_c^2 = k_x^2 + k_y^2 = (\frac{m\pi}{a})^2 + (\frac{n\pi}{b})^2, \quad (2.1.3.1)$$

where *x* and *y* footnotes remark the directions and *c* remark the coefficient for the light. The *m* and *n* indicate the half-wave numbers in *x* and *y* directions and we use TM_{mn} to indicate the field mode with and the *m* and *n* parameters. However, *m* and *n* cannot be zero or else the fields are all zero. Therefore, TM_{11} is the wave at lowest mode that exists in this waveguide. Considering that the different gases have different impedance, during the experiments, we should do the impedance matching by some stubs and a short plunger in order to keep the high power area at the gas position and provide a highest output power for the plasma generation.

2.1.4 Experimental Equipments

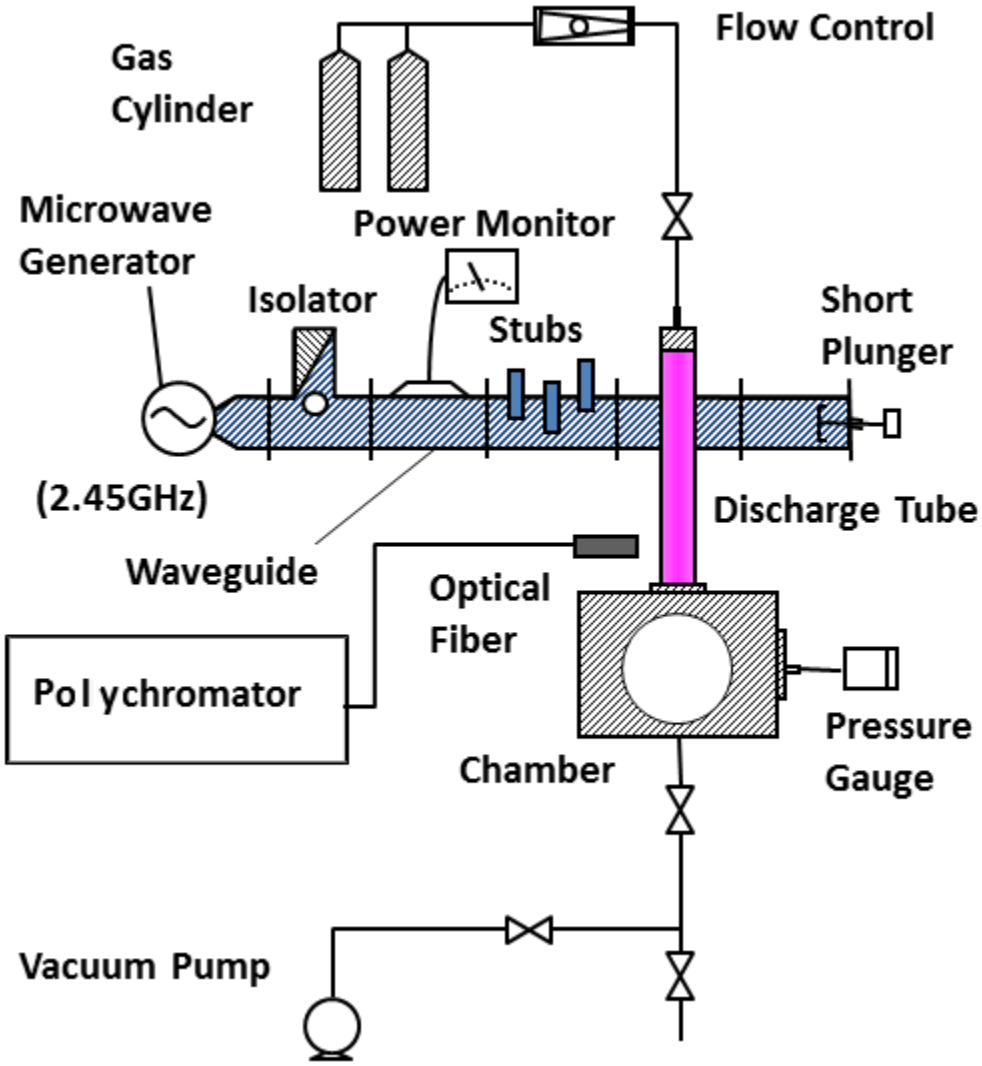

Figure 2.3. Schematic diagram of experimental setup.

Figure 2.3 shows a schematic diagram of our present experimental setup. A N_2-O_2 gas mixture microwave discharge is generated using a vertically placed rectangular waveguide. A quartz tube with a 26 mm inner diameter is aligned in the vertical direction of the waveguide. One end of the quartz tube is connected to the gas entrance, where N_2

and O_2 are mixed beforehand. The other end of the quartz tube serves as the outlet to a vacuum chamber, which is evacuated by a rotary pump. The pressure of the chamber is monitored using a membrane manometer, which also shows that the minimum pressure of the chamber is 0.01 Torr. A microwave generator (2.45 GHz) is used to drive the gaseous discharge, with flow controllers for both nitrogen and oxygen (purity 99.5%). The discharge apparatus is similar to that described elsewhere. [38–45] Figure 2.4 shows the longitudinal position of the present line-of-sight side-on measurement in detail. That is, for the spectroscopic examination, the distance along the discharge tube from the intersection with the waveguide *z* is chosen to be 0, 60, 100, and 140 mm.

In the vibrational and rotational temperature experiments, we applied a CCD spectrometer as a polychromator (BWTEK BRC112E-U) for the measurement of the emission spectrum, whose wavelength range of 200 – 850 nm, with its spectral resolution of 1.5 nm.

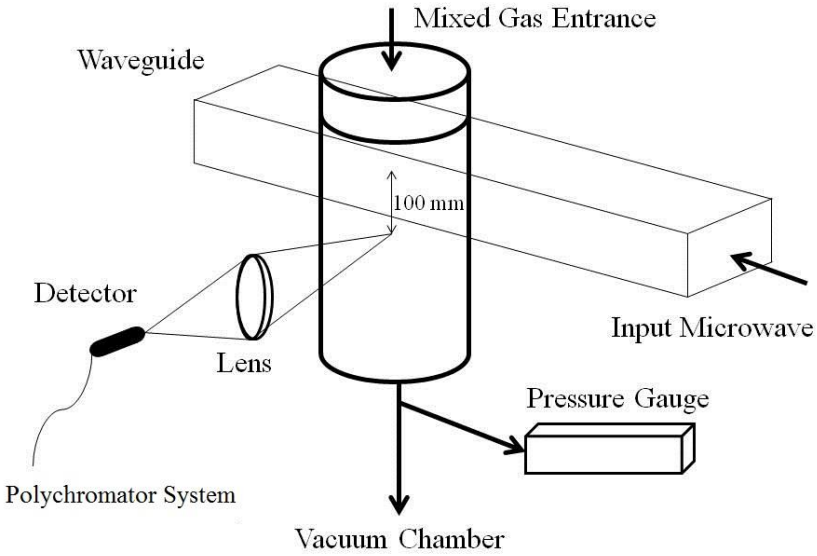

Figure 2.4. Schematic diagram of quartz tube and lens system.

In the kinetics model experiments, we also placed a lens between the quartz tube and the detector to collect the plasma radiation at the detector to enhance the collected spectrum as shown in Fig 2.4. We applied a polychromator system (imaging polychromator spectrograph SOL Instruments MS 3504i and cooled CCD detector Andor Technology DU420A-OE), which has a 0.08-nm-wavelength resolution with a 1200/250 grating [groove spacing (mm^{-1})/blaze wavelength (nm)], achieving a detection sensitivity outside the 190 – 500 nm range (> 40% efficiency). The wavelength dependence of detection sensitivity is calibrated automatically using software by default.

Model structure parameters of some other important equipment are shown in the following table.

Table I. Instrument Model.

Microwave Generator	Model: Toshiba TNG-491C Microwave Frequency: 2.45±0.03 GHz Rated Output Power: 0.5 ~ 4.9 kW Power Supply: AC 200 V, 9.7 kVA Efficiency: 52%
Isolator	Model: Toshiba TMU-261B

	Position: Inside the Microwave Generator
Power Monitor	Model: Toshiba TMU-613A Detect Incident and Reflected Power
Stub	Model: Toshiba TMU-224A (Triple Type)
Rotary Pump	Model: Alcatel-2025SD Exhaust Speed: 250 l/min Ultimate Pressure: 2 Pa
Pressure Monitor	Model: Japan MKS-622A Indicated Value: 0.01 ~ 100 Torr

2.2 Emission of Diatomic Molecular Transition [46]

For a diatomic molecule, there are two modes of motion, which do not occur for atoms, and these two molecular motions are able to have the infrared emission: Firstly, the molecule can rotate like a crabstick around the center of gravity and perpendicular to the nuclei line (internuclear axis), and second, the atoms can vibrate facing to each other along the internuclear axis. In order to investigate the emission spectrum, the structure of diatomic molecules and the detailed motion mechanism should be understood.

2.2.1 Vibration and Rotation of Diatomic Molecules

If we treat the diatomic molecules as a harmonic oscillator, which is the simplest form of the vibration motions, we can consider that each atom moves toward or away from the other one. In this case, the displacement from the center of gravity is approximately a sine function at the time domain. We can use mechanics for a classical harmonic oscillator to define this vibration motion by defining the mass point *m* as the following:

$$F = -kx = m\frac{d^2x}{dt^2}. \tag{2.2.1.1}$$

Hence, the vibratinoal frequency v_{osc} is given by:

$$v_{osc} = \frac{1}{2\pi}\sqrt{\frac{k}{m}}. \tag{2.2.1.2}$$

The potential energy *V* can be obtained as:

$$V = \frac{1}{2}kx^2 = 2\pi^2 m v_{osc}^2 x^2. \tag{2.2.1.3}$$

Thus we can define a harmonic oscillator as a system whose potential energy is proportional to the square of the distance from its equilibrium position; as a result, the potential energy curve should be a parabola.

When we consider the wave mechanics, the vibrations of these two nuclei can be regarded as a motion of a single particle of mass μ as a whole. In this case, the displacement *x* from its equilibrium position equals the change from the internuclear distance. The wave equation that describes the motion of the particle can be expressed as:

$$\frac{d^2\psi}{dx^2} + \frac{8\pi^2\mu}{h^2}(E - \frac{1}{2}kx^2)\psi = 0. \qquad (2.2.1.4)$$

From a study of this equation [47], we know the solutions of this kind of functions have finite single values, and are continuous, but asymptotically become zero at an infinite distance. We can discuss the *E* value as follows, which has a certain physics meaning:

$$E(v) = \frac{h}{2\pi}\sqrt{\frac{k}{\mu}}(v + \frac{1}{2}) = h\nu_{osc}(v + \frac{1}{2}), \qquad (2.2.1.5)$$

where the vibrational quantum number *v* can take only integer values, 0, 1, 2, ⋯. If we transform the energy values as this term (by dividing by *hc*), we obtain the function for the vibrational terms:

$$G(v) = \frac{E(v)}{hc} = \frac{\nu_{osc}}{c}(v + \frac{1}{2}) = \omega(v + \frac{1}{2}), \qquad (2.2.1.5)$$

where ω is the vibrational frequency in cm^{-1}.

Similar to the vibrational analysis, a rigid rotator is also able to assume the rotational motion. Therefore, the classical mechanics of the energy of rotation *E* is given by:

$$E = \frac{1}{2}I\omega^2, \qquad (2.2.1.6)$$

where ω is the angular velocity of the rotation and *I* is the moment of inertia of the whole system. Just like the vibrational case, the wave equation analysis leads to the following for the different energy levels *J* (rotational quantum number):

$$E = \frac{h^2 J(J+1)}{8\pi^2 \mu r^2} = \frac{h^2 J(J+1)}{8\pi^2 I}, \tag{2.2.1.7}$$

Just as well, the transform energy values to term values are given by:

$$F(J) = \frac{E}{hc} = \frac{hJ(J+1)}{8\pi^2 cI} = BJ(J+1), \tag{2.2.1.8}$$

where the constant:

$$B = \frac{h}{8\pi^2 cI}, \tag{2.2.1.9}$$

is called the rotational constant.

2.2.2 Radiation Position (Frequency) from Electronic Transition

The band spectra observed in the visible and ultra-violet regions cannot be simply considered as the vibration-rotation spectra, because the structure is generally too complicated to explain by vibration-rotation spectral theory, including the frequencies in the visible and ultra-violet regions are much too large than the vibrational and rotational calculated values. The diatomic system contains two atoms, which means the system has two positive charge centers, and the gravitation and repulsion forces occur more complicated than a single atom. However, just like an atom, we can expect different electronic states of the molecule, depending on the orbits where the electrons locate. The electronic states are defined as different terms marked as Σ, Π, Δ, ⋯. The total energy of the molecule (neglecting spin and magnetic interactions) consists of the potential and kinetic energies of the electrons and the nuclei. It is obvious that the electronic energy

(potential + kinetic energy) depends on the internulear distance *r*. Meanwhile, this dependence varies for different electronic states because the relative center positions of positive and negative charges change, for example, considering a H_2 molecule exciting process. One electron jumps to a higher orbit and effect on both the positive and negative centers.

Because the mass of the electrons is much smaller than that of the nuclei, electrons move much faster than the nuclei. And when the nuclei are no longer fixed, figuratively speaking the two nuclei vibrate, and the momentary positions of the nuclei vary. Thus in order to change the position of the nuclei, it is clear that the Coulomb repulsion of the nuclei changes. However, it should be remarked that the sum of the electronic energy and the Coulomb potential of the nuclei that acts as the potential energy obeys the law of conservation energy. But there are still two cases, if the potential energy, in its dependence on the internuclear distance, has a minimum, this is a stable electronic state of the molecule. Otherwise if there is no minimum, the electronic state is unstable, that is, the two atoms repel each other from any moment they combine into a molecule. Each electronic state is characterized by a definite potential curve which may have a more or less deep minimum (stable molecular state) or may have no minimum (unstable molecular state).

The Schrödinger equation of a diatomic molecule may be written as:

$$\frac{1}{m}\sum_i\left(\frac{\partial^2\psi}{\partial x_i^2}+\frac{\partial^2\psi}{\partial y_i^2}+\frac{\partial^2\psi}{\partial z_i^2}\right)+\sum_k\frac{1}{M_k}\left(\frac{\partial^2\psi}{\partial x_k^2}+\frac{\partial^2\psi}{\partial y_k^2}+\frac{\partial^2\psi}{\partial z_k^2}\right)+\frac{8\pi^2}{h^2}(E-V)\psi=0\,, \qquad (2.2.2.1)$$

where x_i, y_i, z_i are the coordinates of the electrons (mass m) and x_k, y_k, z_k are those of the nuclei (mass M_k). An approximate solution is given by:

$$\psi = \psi_e(\cdots, x_i, y_i, z_i, \cdots)\psi_{vr}(\cdots, x_k, y_k, z_k, \cdots), \tag{2.2.2.2}$$

where ψ_e and ψ_{vr} are the solutions of the equations:

$$\sum_i \left(\frac{\partial^2\psi_e}{\partial x_i^2} + \frac{\partial^2\psi_e}{\partial y_i^2} + \frac{\partial^2\psi_e}{\partial z_i^2}\right) + \frac{8\pi^2 m}{h^2}(E^{el} - V_e)\psi_e = 0, \tag{2.2.2.3}$$

and

$$\sum_k \frac{1}{M_k}\left(\frac{\partial^2\psi_{vr}}{\partial x_k^2} + \frac{\partial^2\psi_{vr}}{\partial y_k^2} + \frac{\partial^2\psi_{vr}}{\partial z_k^2}\right) + \frac{8\pi^2}{h^2}(E - E^{el} - V_n)\psi_{vr} = 0, \tag{2.2.2.4}$$

respectively. The first equation is the Schrödinger equation describing the electrons moving in the field of the fixed nuclei system, where includes a potential energy V_e (which is a function of the electronic coordinates x_i, y_i, z_i). From the analysis above, it is obvious that the eigenfunctions ψ_e and eigenvalues E^{el} depend on the internuclear distance as parameter. Equation (2.2.2.4) is the Schrödinger equation of the nuclei moving under the action of the potential $E^{el} + V_n$ where V_n is the Coulomb potential of the nuclei. For a diatomic molecule system including two charges Z_1e and Z_2e and the distance r from each other we have:

$$V_n = \frac{Z_1 Z_2 e^2}{r}. \tag{2.2.2.5}$$

If we substitute Eq. (2.2.2.2) into the previous wave equation (2.2.2.1), and consider the Eqs. (2.2.2.3) and (2.2.2.4), we will see it at once that Eq. (2.2.2.1) is satisfied only if:

$$\sum_k \frac{2}{M_k}[\frac{\partial\psi_e\partial\psi_{vr}}{\partial x_k^2}+\frac{\partial\psi_e\partial\psi_{vr}}{\partial y_k^2}+\frac{\partial\psi_e\partial\psi_{vr}}{\partial z_k^2}+(\frac{\partial^2\psi_e}{\partial x_k^2}+\frac{\partial^2\psi_e}{\partial y_k^2}+\frac{\partial^2\psi_e}{\partial z_k^2})], \tag{2.2.2.6}$$

can be neglected. It implies that when ψ_e varies as internuclear distance, it is sufficiently slow so that its first and second derivatives $\partial\psi_e/\partial x_k$, $\cdots\partial^2\psi_e/\partial x_k^2$, $\cdots$ can be neglected. The detailed discussion for this solution condition has been shown by Born and Oppenheimer. [48] Therefore, we can use $E^{el} + V_n$ as the potential energy for the motion of the nuclei and at the same time in resolving ψ into a product ψ_e and ψ_{vr} according to Eq. (2.2.2.2).

After some mathematical derivation, the eigenfunction ψ_{vr} of the vibrating rotator, can be expressed as the result $(1/r)\psi_v\psi_r$, where ψ_v is the vibrational eigenfunction of a linear oscillator, depending on the internuclear distance $(r\text{-}r_e)$, and ψ_r is the rotational eigenfunction, depending on the spatial orientation of the molecule. Thus we have a simple approximation for the total eigenfunction:

$$\psi = \psi_{\mathrm{e}} \cdot \frac{1}{r}\psi_{\mathrm{v}} \cdot \psi_{\mathrm{r}}. \tag{2.2.2.7}$$

As mentioned above the electronic eigenfunction depends on the internuclear distance as a parameter. While the variation is slow, we ignore this electronic position change.

From the discussion above, we know that the base energy of the non-rotating molecule E_{e} must be considered as vibrational energy E_{v} since the similar order of

magnitudes. Moreover, the molecule has rotational energy E_r which can also affect the shape of the energy curve. Thus the total energy E of the molecule consists of, to a very good approximation, three component parts,

$$E = E_e + E_v + E_r, \tag{2.2.2.8}$$

hence we can re-write the equation in wave-number units for a convenience for both calculation and understanding,

$$T = T_e + G + F, \tag{2.2.2.9}$$

Concerning the vibrations and rotations of the molecule in a general electronic state, we use the model of the vibrating rotator and detail these two energy part

$$G = \omega_e(v+\frac{1}{2}) - \omega_e x_e(v+\frac{1}{2})^2 + \omega_e y_e(v+\frac{1}{2})^3 + \cdots, \tag{2.2.2.10}$$

and

$$F = B_v J(J+1) - D_v J^2(J+1)^2 + \cdots. \tag{2.2.2.11}$$

Generally speaking, F is smaller than G and nearly the same order of magnitude with the second term in Eq. (2.2.2.10). Also, for F the second term is very small compared to the first and can be neglected entirely in many cases. The vibrational and rotational constants presenting to G and F depend on the molecule properties.

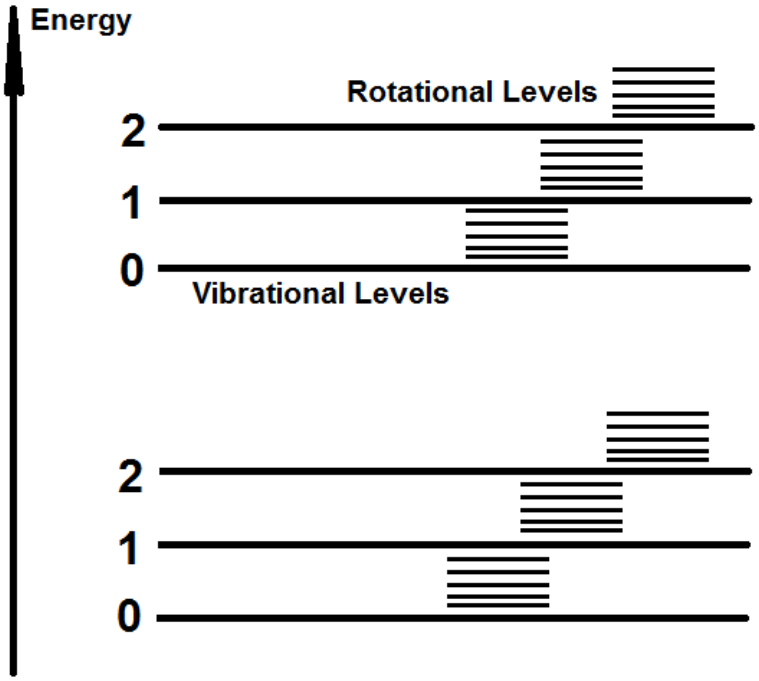

Figure 2.5. Vibrational and rotational levels of the two electronic states of a normal molecule.

In this introduction, we are neglecting the interaction between electronic motion and rotation of the molecule. From the Fig. 2.5, two different electronic states with their vibrational and rotational levels are schematically represented. This diagram shows the orders for vibrational and rotational levels and at the same time, we can easily recognize the way that the energy changes with the vibrational and rotational levels.

2.2.3 Strength Distribution (Intensity) of Vibration and Rotation

After discussing all the energy levels considered during analysis a molecule motion, we know that when the electronic transition occurs, every radiation line has a special molecular state, including both vibrational and rotational states. Hence, all the

line positions from the electronic transitions can be determined. Now, we can begin to consider that the line intensities of radiation from electric transition can be calculated as

$$I(n',v',J' \rightarrow n'',v'',J'') \propto h\nu A(n',v',J' \rightarrow n'',v'',J'')N_{n',v',J'}, \quad (2.2.3.1)$$

where single quote denotes the upper state and double denotes the lower state, $I(n',v',J' \rightarrow n'',v'',J'')$ is the intensity of the spectrum, and n is the electronic state, v is the vibrational quantum number, and J is the rotational quantum number, h is the Planck's constant, $A(n',v',J' \rightarrow n'',v'',J'')$ is the transition probability, and $N_{n',v',J'}$ is the number density of the molecules in the upper states. The transition probability $A(n',v',J' \rightarrow n'',v'',J'')$ can be expressed as

$$A = \frac{64\pi^4 \nu^3}{3hc^3 g_{n'}} 2(J'+1)^{-1} \sum_{J'J''} |\bar{R}_{J',J''}|^2 \, q_{v',v''} S_{J',J''}, \quad (2.2.3.2)$$

where c is the light velocity, $\Sigma_{j'j''}|R_{j'j''}|^2$ is the transition moment, $g_{n'}$ is the statistical weight of the electronic state n', $q_{v'v''}$ is the Franck-Condon factor, and $S_{j'j''}$ is the Hönl-London factor, which indicate the probabilities of vibrational and rotational transitions, respectively. [49]

As we have talked above, the $N_{n',v',J'}$ (the number density of the molecules) determine the intensity of the radiation line belongs to the n',v',J' energy level, thus a theoretical prediction of the numbers of molecules in the various initial states is necessary.

According to the Maxwell-Boltzmann distribution law, the number of molecules dN_g that have a classical vibrational energy between E and $E+dE$ is proportional to $e^{-E/kT}dE$, where k is the Boltzmann constant and T is the absolute temperature. In quantum

theory, only the discrete values are possible for the vibrational energy. The number of molecules at every vibrational state is proportional to the Boltzmann factor as

$$e^{-E/kT} = e^{-G0(r)hc/kT}, \qquad (2.2.3.3)$$

where the zero-point energy can be ignored, since to add this to the exponent means only adding a constant factor for all the vibratinoal levels.

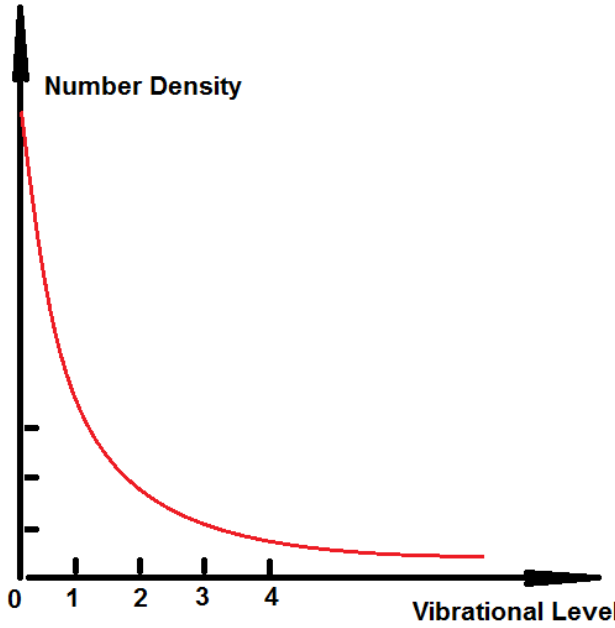

Figure 2.6. Maxwell-Boltzmann distributions of number densities of different energy levels.

Concerning the rotational levels, which are different from the vibrational levels, are not simply given by the Boltzmann factor $e^{-E/kT}$. It cannot be ignored that, according to quantum theory, each state of an atomic system with total angular momentum J consists of $(2J+1)$ levels which coincide in the absence of an external field, which we call multiplicity. Therefore, the final distributions should be in direct proportion to $e^{-E/kT}$ and

at the same time $2J+1$. Thus, the number density dependence should have its maximum when $J > 0$ as shown in Fig. 2.7.

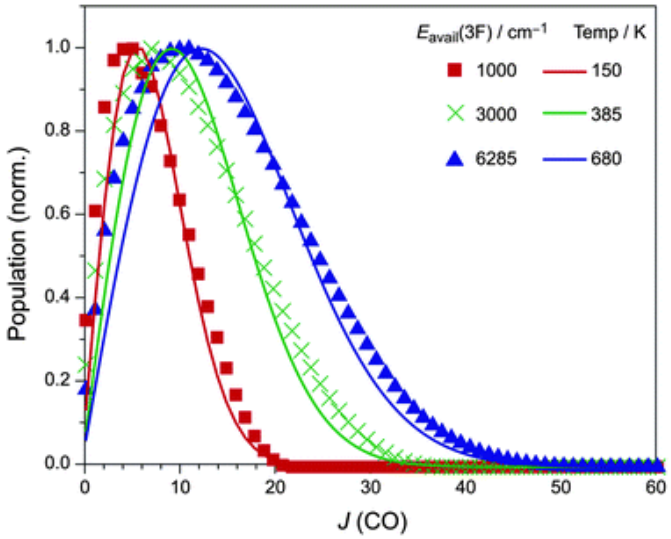

Figure 2.7. Example of CO distributions of number densities of different energy levels at different temperatures.[50]

2.2.4 Hund's Cases

Beside the main energy parts introduced, there are some small energy correction terms should be considered because there are some different coupling forms for the fine structures of the spectrum. Different angular momentums have different coupling styles. J denotes the sum of the electronic spin (S), electron orbit momentum (Λ) and nuclei rotational momentum. When the molecular axis component of the electronic orbit angular momentum is non-zero, and the spin of the molecule S is non-zero, the coupling of rotation and electronic motion has different cases. There are five cases named Hund's coupling case (a), (b), (c), (d), and (e).

Hund's case (a) and (b).

For Hund's case (a), it is assumed that the interaction of the nuclear rotation with the electronic motion (spin as well as orbital) is very weak, while the electron motion interaction with nuclei axis is strong. Thus this case is a very good approach to a two-center system. Here, even for the rotating molecule, the electronic angular momentum is well defined. The component of the angular momentum, which perpendicular to the molecular axis, is rotating so fast, so that it can be treated as zero. This implies that we can use a sum value to show the *S*, Λ (component along the molecular axis of the angular momentum *L*) and Σ (component along the molecular axis of the electronic spin) as showed below

$$\begin{aligned} J &= \Omega + N \\ \Omega &= \Lambda + \Sigma \end{aligned}, \qquad (2.2.4.1)$$

But when $\Lambda = 0$ and $S \neq 0$, the spin *S* is not coupled to the internuclear axis at all, which implies the Ω is not defined. Therefore, the Hund's case (a) cannot apply and

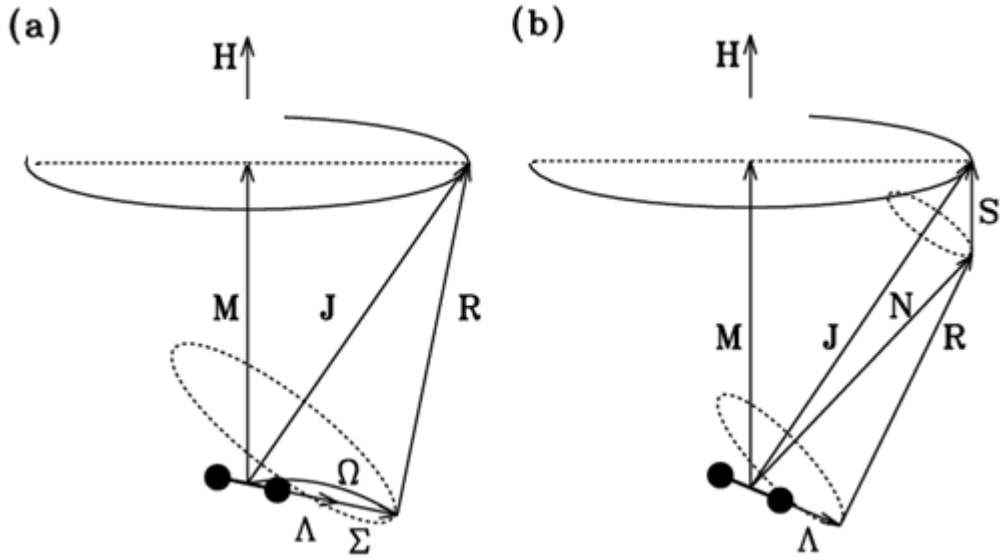

Figure 2.8. Vector diagram for Hund's case (a) and (b).

particularly to light molecules, even when $\Lambda \neq 0$, the S does couple with the nuclei axis weakly. This weak coupling is the characteristics of Hund's case (b). Thus, we have some (b) case formula below

$$\begin{aligned} K &= \Lambda + N \\ J &= K + S \\ |K - S| &\leq J \leq |K + S| \end{aligned} \quad , \tag{2.2.4.2}$$

where K is the whole angular momentum beside the electronic spin.

The coupling way can be referred in Fig. 2.8. As to the singlet, Hund's case (a) and (b) cannot be applied, because $\Lambda = \Omega$, and $N = J$. Therefore, some more complicated couplings are necessary. However, Hund's case (a) and (b) are the most important.

Other Hund's cases (c), (d), and (e).

In some cases, for example some heavy molecules, the interaction between L and S is stronger than those with the nuclei axis. Thus, Λ and Σ are not defined. We can consider that L and S combine to a sum vector J, and then, the nuclei axis component Ω of this J can couple with the nuclei axis. This is the Hund's case (c).

If the interaction between L and the nuclei axis is weak, while the interaction between L and the rotation axis is strong, we achieve the Hund's case (d). N and S are similar to the Hund's case (b), but in the Hund's case (d), their interaction is weak, which leads to an ignorance for both of them.

The Hund's case (e) is not examined experimentally yet, while theoretically the interaction between *L* and *S* is strong but the interaction between them and the nuclei axis is weak, which is the same form as the case (c). All these three cases are shown in Fig. 2.9.

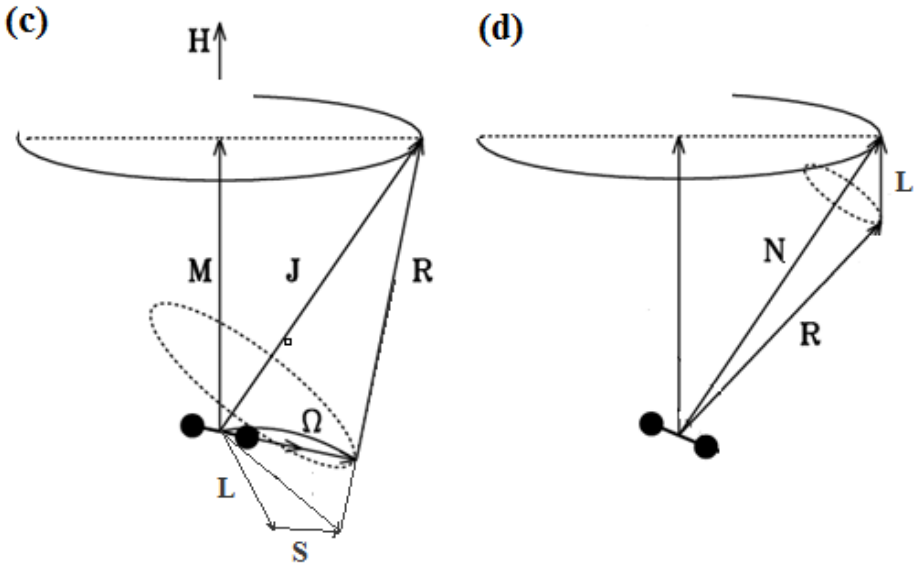

Figure 2.9. Vector diagram for Hund's case (c) and (d).

2.3 Kinetic Model for the Number Densities of Species in N_2-O_2 Plasma [59]

In order to enable a numerical discussion, a simulation for the number densities of various excited states and atomic species in the plasma should be applied. Mr. Ichikawa originally designed the numerical code to calculate the number densities of important particles in the N_2-O_2 gas mixture microwave discharge plasma as functions of the following parameters: the gas temperature T_g, electron density N_e, total discharge pressure P, reduced electric field E/N, and the N_2 to O_2 partial pressure ratio in the

mixture. The plasma parameters including plasma gas temperature and electron density were modified during the calculation, in order to maintain this quasi-neutrality. Throughout the analysis, gas temperature is approximated by the rotational temperature obtained from the N_2 second positive system (2PS).

2.3.1 EEPF Obtained from the Boltzmann Equation and VDF

In order to calculate the various rate coefficients to solve the total changing rate for different species, the electron energy probabilistic function (EEPF) is necessary. Therefore, the Boltzmann equation is solved and the equation term formulated as follows:

$$-\frac{d}{d\varepsilon}\left[\frac{1}{3}\left(\frac{E}{N}\right)^2\frac{\varepsilon}{\sigma_c(\varepsilon)}\frac{df_0(\varepsilon)}{d\varepsilon}\right]+\frac{2m_e}{M}\varepsilon^2\sigma_c(\varepsilon)\left[f_o(\varepsilon)+\frac{kT_g}{e}\frac{d}{d\varepsilon}f_o(\varepsilon)\right], \\ +\sum_l \varepsilon\frac{N_l}{N}\sigma_l^{si}(\varepsilon)f_0(\varepsilon)-\sum_l(\varepsilon+\varepsilon_l^{si})\frac{N_l}{N}\sigma_l^{si}(\varepsilon+\varepsilon_l^{si})f_0(\varepsilon+\varepsilon_l^{si})=0 \qquad (2.3.1.1)$$

where e is the elementary charge, k is Boltzmann constant, ε is the electron energy, σ_c is the momentum transfer cross section, σ_l^{si} is the lth inelastic collision cross section with the energy change of ε_l^{si}, m_e is the electron mass, M denotes the molecular mass of the elastic collision partner of the electron, and N_l is the number density of the lth inelastic collision partner. In Eq. (2.3.1.1), the EEPF $f_0(\varepsilon)$ is specified in Sec. 4.2.1.

Considering the number densities of the ground-state oxygen atoms, the model solves the Boltzmann equation simultaneously and self-consistently with the rate equations to obtain the density of oxygen atoms in the plasma, which will be specified in Section 2.3.3. For nitrogen molecules, we consider inelastic collisions that make $N_2(a\ ^1\Pi_g)$, $N_2(w\ ^1\Delta_u)$, $N(2p\ ^4S^0)$, and $N_2^+(X\ ^2\Sigma_g^+)$. Considering the superelastic collision terms of Eq. (2.3.1.1), the model treat electron collisions with the vibrationally excited states of

$N_2(X\ ^1\Sigma_g^+,\ v=1-8)$, whose number densities are also calculated self-consistently as specified in Sec. 4.2.1. Table I summarizes the inelastic collisions included in the collision terms of the Eq. (2.3.1.1).

Table II. List of inelastic collisions in the collision terms in the Boltzmann equation.

Inelastic collisions with N_2	
$N_2(X^1\Sigma_g)+e \rightarrow 2N(^4S)+e$	$N_2(X^1\Sigma_g)+e \rightarrow N_2(A^3\Sigma_u)+e$
$N_2(X^1\Sigma_g)+e \rightarrow N_2(B^3\Pi_g)+e$	$N_2(X^1\Sigma_g)+e \rightarrow N_2(C^3\Pi_u)+e$
$N_2(X^1\Sigma_g)+e \rightarrow N_2(a'^1\Sigma_u)+e$	$N_2(X^1\Sigma_g)+e \rightarrow N_2(a^1\Pi_g)+e$
$N_2(X^1\Sigma_g)+e \rightarrow N_2^+ + 2e$	$N_2^+ + e \rightarrow N(^4S)+2e$
$N_4^+ + e \rightarrow 2N_2(X^1\Sigma_g)$	
Inelastic collisions with O_2	
$O_2\left(X^3\Sigma_g\right)+e \rightarrow O_2\left(a^1\Delta_g\right)+e$	$O_2\left(X^3\Sigma_g\right)+e \rightarrow O_2\left(b^1\Sigma_g\right)+e$
$O_2\left(a^1\Delta_g\right)+e \rightarrow O_2\left(b^1\Sigma_g\right)+e$	$O_2\left(X^3\Sigma_g\right)+e \rightarrow O_2^+ + 2e$
$O_2\left(X^3\Sigma_g\right)+e \rightarrow O^- + O\left(^3P\right)$	$O_2\left(a^1\Delta_g\right)+e \rightarrow O^- + O\left(^3P\right)$
$O_2\left(X^3\Sigma_g\right)+e \rightarrow 2O\left(^3P\right)+e$	$O_2\left(a^1\Delta_g\right)+e \rightarrow 2O\left(^3P\right)+e$
$O_2^+ + e \rightarrow 2O\left(^3P\right)+e$	$O_3 + e \rightarrow O\left(^3P\right)+O_2\left(X^3\Sigma_g\right)$

To evaluate the effect of inelastic and superelastic collisions with the vibrationally excited levels of the N_2 molecule on the EEPF, the master equations that describe the vibrational distribution function (VDF) of the ground state of the nitrogen molecule. This model considers the following elementary processes to describe the population kinetics of vibrational excitation and de-excitation, vibration-vibration (V-V) energy transfer collisions between N_2 vibrational levels, vibration-translation (V-T) energy relaxation due to collisions with N_2 molecules, and dissociation by the V-V and V-T processes. In this kind of low-temperature and low-pressure plasma, the N_2 dissociation degree is about 10^{-3}, and consequently, we neglect the V-T relaxation process by nitrogen atoms. However, the relaxation process of vibrationally excited states due to collision with the discharge

tube wall is neglected, because the discharge pressure is low, at which the V-V and V-T processes dominate the wall relaxation. In the V-V and V-T processes, only single-quantum transition is considered. In the VDF model, for simple analysis, it is assumed that the total density of nitrogen molecules is constant owing to their small dissociation degree. As a result, the dissociated nitrogen atoms are assumed to associate into the vth vibrational levels with probability R_v immediately after dissociation, which is assumed to be constant over v. Hence, the master equation of the VDF could be taken as:

$$\begin{aligned}\frac{dN_v}{dt} &= N_e \sum_{w=0,\neq v}^{M} N_w C_{wv} - N_e N_v \sum_{w=0,\neq v}^{M} C_{wv} + N_{v-1} \sum_{w=0,\neq v}^{M-1} N_{w+1} Q_{v-1,v}^{w+1,w} + \\ & N_{v+1} \sum_{w=0,\neq v}^{M-1} N_w Q_{v+1,v}^{w,w+!} - N_v \left(\sum_{w=0,\neq v}^{M-1} N_{w+1} Q_{v,v+1}^{w+1,w} + \sum_{w=0,\neq v}^{M-1} N_w Q_{v,v-1}^{w,w+1} \right) + \\ & [\mathrm{N_2}](N_{v-1} P_{v-1,v} + N_{v+1} P_{v+1,v}) - N_v [\mathrm{N_2}](N_{v-1} P_{v-1,v} + N_{v+1} P_{v+1,v}) + R_v \end{aligned} \quad , \qquad (2.3.1.2)$$

where N_v is the number density of the N_2 X state at the vth vibrationally excited level, C_{wv} is the rate coefficient of the electron impact vibrational excitation ($w < v$) or de-excitation ($w > v$) from level w to v, Q and P are the rate coefficients of V-V transfer and V-T relaxation, respectively, between the levels given by the following suffixes for N_2-N_2 collisions, and R_v is the rate of atomic nitrogen re-combination into the vth level. The upper limit of the summation M is set at $v = 45$, which is considered to be the dissociation level of the nitrogen molecule, considered to be followed by instantaneous association into level v, which corresponds to the term R_v in Eq. (2.3.1.2). Strictly speaking, we should include the effect of vibrational relaxtion with O_2 molecules in the plasma. However, in this model, this has been neglected since the effect of an O_2 admixture on the N_2-VDF is less significant than the effect of nitrogen atoms. These reactions included are summarized in the following table.

Table III. List of inelastic collisions in the master equation used to determine the VDF of N_2 X state.

$N_2(X^1\Sigma_g, v=0-8)+e \leftrightarrow N_2(X^1\Sigma_g, v=0-8\neq v)+e$
$N_2(X^1\Sigma_g, v)+N_2(X^1\Sigma_g, w) \leftrightarrow N_2(X^1\Sigma_g, v+1)+N_2(X^1\Sigma_g, w-1)$
$N_2(X^1\Sigma_g, M)+N_2(X^1\Sigma_g, w) \leftrightarrow 2N(2p\ ^4S^0)+N_2(X^1\Sigma_g, w-1)$
$N_2(X^1\Sigma_g, v)+N_2(X^1\Sigma_g, w) \leftrightarrow N_2(X^1\Sigma_g, v-1)+N_2(X^1\Sigma_g, w+1)$

2.3.2 Atomic and Molecular Reactions in the Model

Likewise, in this model, the atomic and molecular collision processes are included as the follow table. Meanwhile, there include the reactions such as atomic and molecular reactions, radiative transitions and wall loss processes.

Table IV. List of collision processes relate to molecules and atoms.

Atomic and molecular processes
$N_2(a'^1\Sigma_u)+N_2(X^1\Sigma_g) \rightarrow N_2(B^3\Pi_g)+N_2(X^1\Sigma_g)$
$N_2(C^3\Pi_u)+N_2(X^1\Sigma_g) \rightarrow N_2(a'^1\Sigma_u)+N_2(X^1\Sigma_g)$
$N_2(a^1\Pi_g)+N_2(X^1\Sigma_g) \rightarrow N_2(a'^1\Sigma_u)+N_2(X^1\Sigma_g)$
$N_2(a'^1\Sigma_u)+N_2(X^1\Sigma_g) \rightarrow N_2(a^1\Pi_g)+N_2(X^1\Sigma_g)$
$N_2(B^3\Pi_g)+N_2(X^1\Sigma_g) \rightarrow N_2(X^1\Sigma_g)+N_2(X^1\Sigma_g)$
$N_2(A^3\Sigma_u)+N_2(X^1\Sigma_g) \rightarrow N_2(X^1\Sigma_g)+N_2(X^1\Sigma_g)$
$N_2(A^3\Sigma_u)+N(^4S) \rightarrow N_2(X^1\Sigma_g)+N(^4S)$
$N_2(A^3\Sigma_u)+N_2(A^3\Sigma_u) \rightarrow N_2(B^3\Pi_g)+N_2(X^1\Sigma_g)$
$N_2(A^3\Sigma_u)+N_2(A^3\Sigma_u) \rightarrow N_2(C^3\Pi_u)+N_2(X^1\Sigma_g)$
$N_2(a'^1\Sigma_u)+N_2(X^1\Sigma_g) \rightarrow N_2^+ + N_2(X^1\Sigma_g)$
$N_2(a'^1\Sigma_u)+N_2(a'^1\Sigma_u) \rightarrow 2N_2^+ + 2e$
$N_2(A^3\Sigma_u)_{(v>6)}+N_2(A^3\Sigma_u) \rightarrow N_2(B^3\Pi_g)+N_2(X^1\Sigma_g)$
$N_2(B^3\Pi_g)+NN_2(X^1\Sigma_g) \rightarrow N_2(A^3\Sigma_u)+N_2(X^1\Sigma_g)$
$2N+N \rightarrow N_2(B^3\Pi_g)+N$
$N_2(a'^1\Sigma_u)+N_2(A^3\Sigma_u) \rightarrow N_4^+ + 2e$
$N_2(a'^1\Sigma_u)+N_2(a'^1\Sigma_u) \rightarrow N_4^+ + 2e$
$O_2\left(a^1\Delta_g\right)+O^- \rightarrow O_3+e$

$$O_2\left(b^1\Sigma_g\right)+O^- \rightarrow O\left(^3P\right)+O_2\left(X^3\Sigma_g\right)$$
$$O^- + O_2^+ \rightarrow O\left(^3P\right)+O_2\left(X^3\Sigma_g\right)$$
$$O_3 + O_2\left(X^3\Sigma_g\right)\rightarrow O\left(^3P\right)+2O_2\left(X^3\Sigma_g\right)$$
$$O\left(^3P\right)+2O_2\left(X^3\Sigma_g\right)\rightarrow O_3 + O_2\left(X^3\Sigma_g\right)$$
$$O\left(^3P\right)+O_3 \rightarrow 2O\left(^3P\right)+O_2\left(X^3\Sigma_g\right)$$
$$2O\left(^3P\right)+O_2\left(X^3\Sigma_g\right)\rightarrow O\left(^3P\right)+O_3$$
$$O\left(^3P\right)+O_3 \rightarrow O_2\left(a^1\Delta_g\right)+O_2\left(X^3\Sigma_g\right)$$
$$O_2\left(b^1\Sigma_g\right)+O_3 \rightarrow O\left(^3P\right)+2O_2\left(X^3\Sigma_g\right)$$
$$O_2\left(a^1\Delta_g\right)+O_2\left(X^3\Sigma_g\right)\rightarrow 2O_2\left(X^3\Sigma_g\right)$$
$$O_2\left(a^1\Delta_g\right)+O_3 \rightarrow O\left(^3P\right)+2O_2\left(X^3\Sigma_g\right)$$
$$O\left(^3P\right)+O_3 \rightarrow 2O_2\left(X^3\Sigma_g\right)$$
$$N(^4S)+O_2\left(X^3\Sigma_g\right)\rightarrow NO+O\left(^3P\right)$$
$$N(^4S)+O\left(^3P\right)+N_2\left(X^1\Sigma_g\right)\rightarrow NO+N_2\left(X^1\Sigma_g\right)$$
$$N_2\left(B^3\Pi_g\right)+NO\rightarrow N_2\left(A^3\Sigma_u\right)+NO$$
$$N_2\left(a'^1\Sigma_u\right)+NO\rightarrow N_2\left(X^1\Sigma_g\right)+NO$$
$$N_2\left(A^3\Sigma_u\right)+O_2\left(X^3\Sigma_g\right)\rightarrow N_2\left(X^1\Sigma_u\right)+O_2\left(X^3\Sigma_g\right)$$
$$N_2\left(A^3\Sigma_u\right)+O_2\left(X^3\Sigma_g\right)\rightarrow N_2\left(X^1\Sigma_u\right)+2O\left(^3P\right)$$
$$N_2\left(B^3\Pi_g\right)+O_2\left(X^3\Sigma_g\right)\rightarrow N_2\left(X^1\Sigma_u\right)+2O\left(^3P\right)$$
$$N_2\left(C^3\Pi_u\right)+O_2\left(X^3\Sigma_g\right)\rightarrow N_2\left(X^1\Sigma_u\right)+2O\left(^3P\right)$$
$$N_2\left(a'^1\Sigma_u\right)+O_2\left(X^3\Sigma_g\right)\rightarrow N_2\left(X^1\Sigma_u\right)+2O\left(^3P\right)$$
$$N_2^+ + O_2\left(X^3\Sigma_g\right)\rightarrow N_2\left(X^1\Sigma_u\right)+O_2^+$$
$$N_2^+ + O\left(^3P\right)\rightarrow NO^+ + N(^4S)$$
$$N_2^+ + NO \rightarrow N_2\left(X^1\Sigma_u\right)+NO^+$$
$$N_4^+ + O_2\left(X^3\Sigma_g\right)\rightarrow 2N_2\left(X^1\Sigma_u\right)+O_2^+$$
$$N_4^+ + O\left(^3P\right)\rightarrow 2N_2\left(X^1\Sigma_u\right)+O^+$$
$$N_4^+ + NO \rightarrow N_2\left(X^1\Sigma_u\right)+NO^+$$
$$O_2^+ + N(^4S)\rightarrow NO^+ + O(^3P)$$
$$O_2^+ + NO \rightarrow NO^+ + O_2\left(X^3\Sigma_g\right)$$
$$O^+ + N_2\left(X^1\Sigma_u\right)+O_2\left(X^3\Sigma_g\right)\rightarrow NO^+ + N(^4S)+O_2\left(X^3\Sigma_g\right)$$
$$N_2\left(A^3\Sigma_u\right)+O_2\left(X^3\Sigma_g\right)\rightarrow N_2\left(X^1\Sigma_u\right)+O_2\left(a^1\Delta_g\right)$$
$$N_2\left(A^3\Sigma_u\right)+O_2\left(X^3\Sigma_g\right)\rightarrow N_2\left(X^1\Sigma_u\right)+N_2\left(B^3\Pi_g\right)$$
$$N_2\left(a'^1\Sigma_u\right)+NO\rightarrow N_2\left(X^1\Sigma_u\right)+O(^3P)+N(^4S)$$

$N_2(a'^1\Sigma_u) + NO \rightarrow N_2(X^1\Sigma_u) + O(^3P) + N(^4S)$

$N(^4S) + N(^4S) + O_2(X^3\Sigma_g) \rightarrow N_2(A^3\Sigma_u) + O_2(X^3\Sigma_g)$

$N(^4S) + N(^4S) + NO \rightarrow N_2(A^3\Sigma_u) + NO$

$N(^4S) + N(^4S) + O(^3P) \rightarrow N_2(A^3\Sigma_u) + O(^3P)$

$N(^4S) + N(^4S) + O_2(X^3\Sigma_g) \rightarrow N_2(B^3\Pi_g) + O_2(X^3\Sigma_g)$

$N(^4S) + N(^4S) + NO \rightarrow N_2(B^3\Pi_g) + NO$

$N(^4S) + N(^4S) + O(^3P) \rightarrow N_2(B^3\Pi_g) + O(^3P)$

$O_2(a^1\Delta_g) + NO \rightarrow O_2(X^3\Sigma_g) + NO$

$O_2(b^1\Delta_g) + N_2(X^1\Sigma_u) \rightarrow O_2(a^1\Delta_g) + N_2(X^1\Sigma_u)$

$O(^3P) + O(^3P) + N_2(X^1\Sigma_u) \rightarrow O_2(X^3\Sigma_g) + N_2(X^1\Sigma_u)$

$O(^3P) + O_2(X^3\Sigma_g) + N(^4S) \rightarrow O_3 + N(^4S)$

Radiative transitions	
$N_2(B^3\Pi_g) \rightarrow N_2(A^3\Sigma_u) + h\nu$	$N_2(C^3\Pi_u) \rightarrow N_2(B^3\Pi_g) + h\nu$
$N_2(a^1\Pi_g) \rightarrow N_2(a'^1\Sigma_u) + h\nu$	$N_2(a^1\Pi_g) \rightarrow N_2(X^1\Sigma_g) + h\nu$
$N_2(a'^1\Sigma_u) \rightarrow N_2(X^1\Sigma_g) + h\nu$	

Wall loss processes	
$N_2(A^3\Sigma_u) + wall \rightarrow N_2(X^1\Sigma_g)$	$N + wall \rightarrow \frac{1}{2} N_2(X^1\Sigma_g)$
$N_2^+ + wall \rightarrow N_2(X^1\Sigma_g)$	$N_2(a'^1\Sigma_u) + wall \rightarrow N_2(X^1\Sigma_g)$
$N_2(a^1\Sigma_u) + wall \rightarrow N_2(X^1\Sigma_g)$	$O_2(a^1\Delta_g) + wall \rightarrow O_2(X^3\Sigma_g)$
$O_2(b^1\Sigma_g) + wall \rightarrow O_2(X^3\Sigma_g)$	$O(^3P) + wall \rightarrow \frac{1}{2} O_2(X^3\Sigma_g)$
$O_2^+ \rightarrow O_2(X^3\Sigma_g)$	

2.3.3 Numerical Procedure

Taking the elementary processes described above into account, the model calculates the number densities of the excited species involved in the model by the procedure depicted in Fig. 2.10.

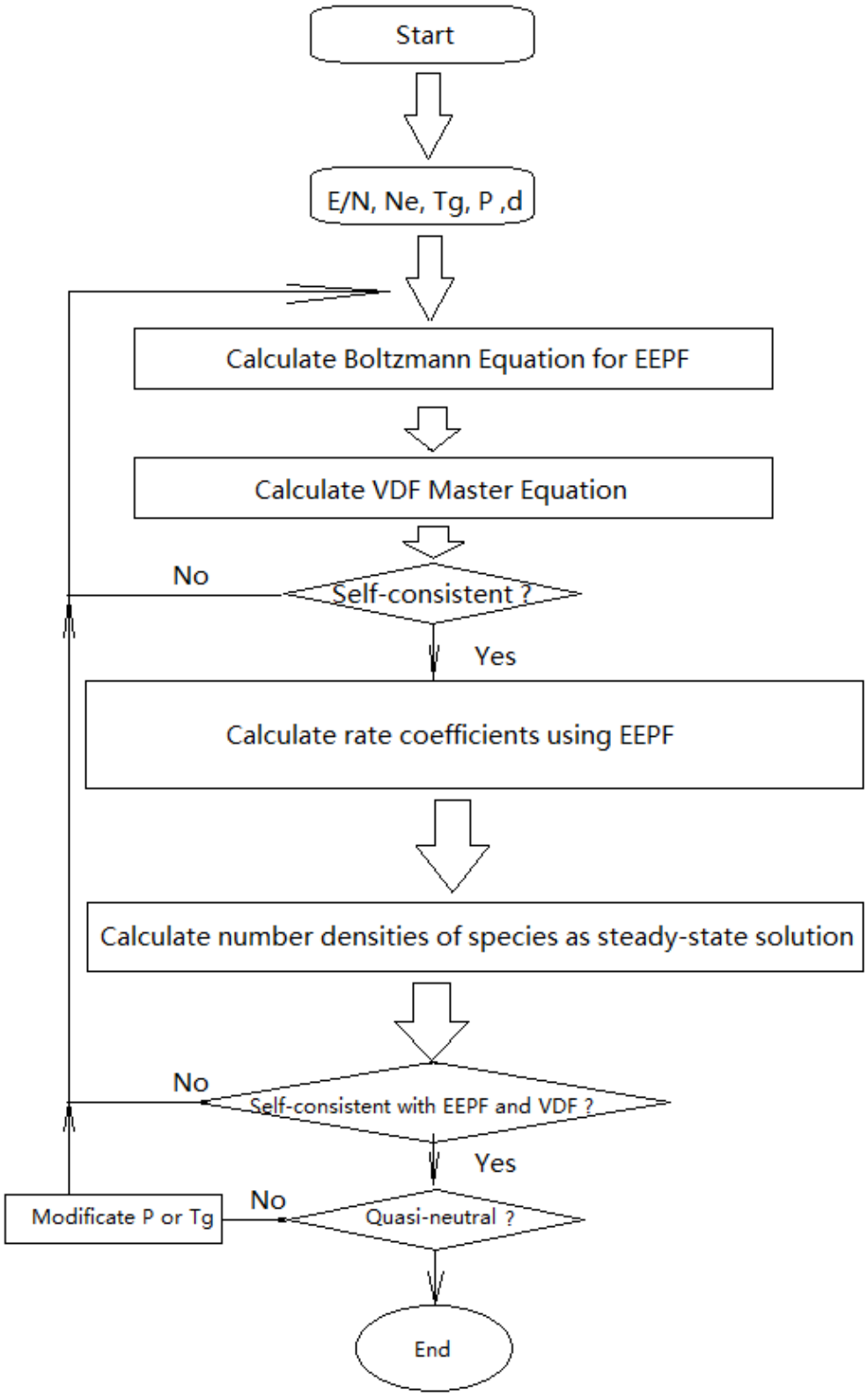

Figure 2.10. Schematic outline of the numerical calculations.

This model solves each species, by self-consistent calculating steps in order to achieve a steady number density for every species when solving the differential equations, beginning with certain initial values corresponding to those for an equilibrium composition. The original model chooses a reduced electric field so that the electron mean energy equals to $(3/2)kT_e$ as 7.5-17 Td, which I modified in my study. This modification will be introduced at Sec. 4.2.

It should be remarked that the electron density is chosen as an input parameter and, consequently, the resultant ion density does not necessarily equal to N_e. In order to maintain quasi-neutrality, the model modify the value of P or T_g and repeat the algorithm in Fig. 2.10 untill the quasi-neutral condition is fulfilled, which results in overall self-consistency. The model repeatedly compare the sum of the number density of negative charges N_- (i.e., electrons and O^-) with that of positive charges involved in the model N+ until the condition $(N_- - N_+)/N_- \leqslant 10^{-4}$ is attained. The model employs the Kaps-Rentrop-Shampine numerical scheme to solve the present simultaneous ordinary differential equations since the equations are extremely stiff.

CHAPTER III: Vibrational and Rotational Temperatures of NO Molecules in N_2-O_2 Discharge using γ-band

Nitrogen oxides (NO_x) have been a hot topic in the last decades from the viewpoint of remediation of atmospheric environment due to their toxicity, while they are also arousing people's interest because of many useful medical applications, such as relaxation of pulmonary hypertension or pulmonary embolism.[51,52] In N_2-O_2 plasmas, as one of main resultants, the NO_x molecular species, nitric monoxide (NO) is clearly highlight in ionosphere to determine physical and chemical processes of the universe investigation. Especially in the extraterrestrial detecting, it is possible to determine the elementary composition of the planets far from the earth by the universal emission lights. Therefore, the observation of NO molecules in N_2-O_2 plasmas, is very necessary for a prediction both on the degree of approximation of the planets with the earth and the temperature or partial ratio of the gaseous environment. Therefore, we focus on the radiation spectrum of NO molecules in this study for an improvement of the understanding for the plasma process.

3.1 NO γ-band Spectrum

The γ-band is radiated at the electronic transition from A $^2\Sigma^+$ excited-state to the X $^2\Pi$ ground-state of NO molecules. It has several band heads with considerable intensity at the ultraviolet region. Even at very lower pressure than N_2, the NO molecules are still able to emit the same magnitude as N_2 2PS. Moreover, the peaks have very good shapes (apparent pinnacle), this makes that the two-photon excitation has already been applied to the γ-band for laser-induced fluorescence spectroscopy (LIFS) measurement of the

number density of the ground state NO X $^2\Pi$ state [53]. As shown in Fig. 3.1, it is easily to recognize the strong NO γ-band emission at about 200 – 290 nm and N_2 2PS at about 290 – 400 nm, the pressure ratio is N_2 : O_2 = 1:1 with a total pressure 1 Torr.

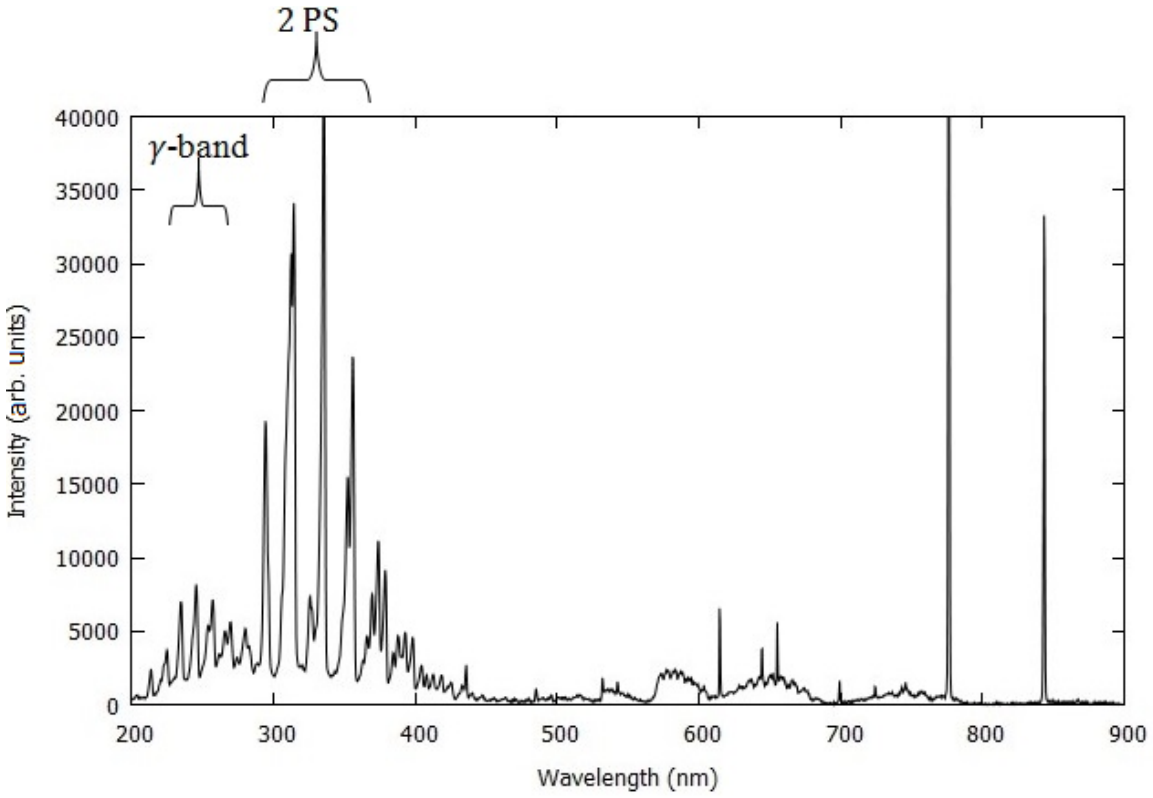

Figure 3.1. Spectrum of N_2-O_2 microwave discharge with total pressure 1 Torr, and N_2:O_2 = 1:1.

In order to study the vibrational and rotational properties of NO, we should carry out some spectroscopic measurements of N_2-O_2 mixture plasma, thus we can examine the dependence of plasma parameters deduced from γ-band spectra, such as vibrational or rotational temperatures, and the discharge conditions, as well as the difference and the dependence between NO and N_2 by comparison of their spectroscopic properties.

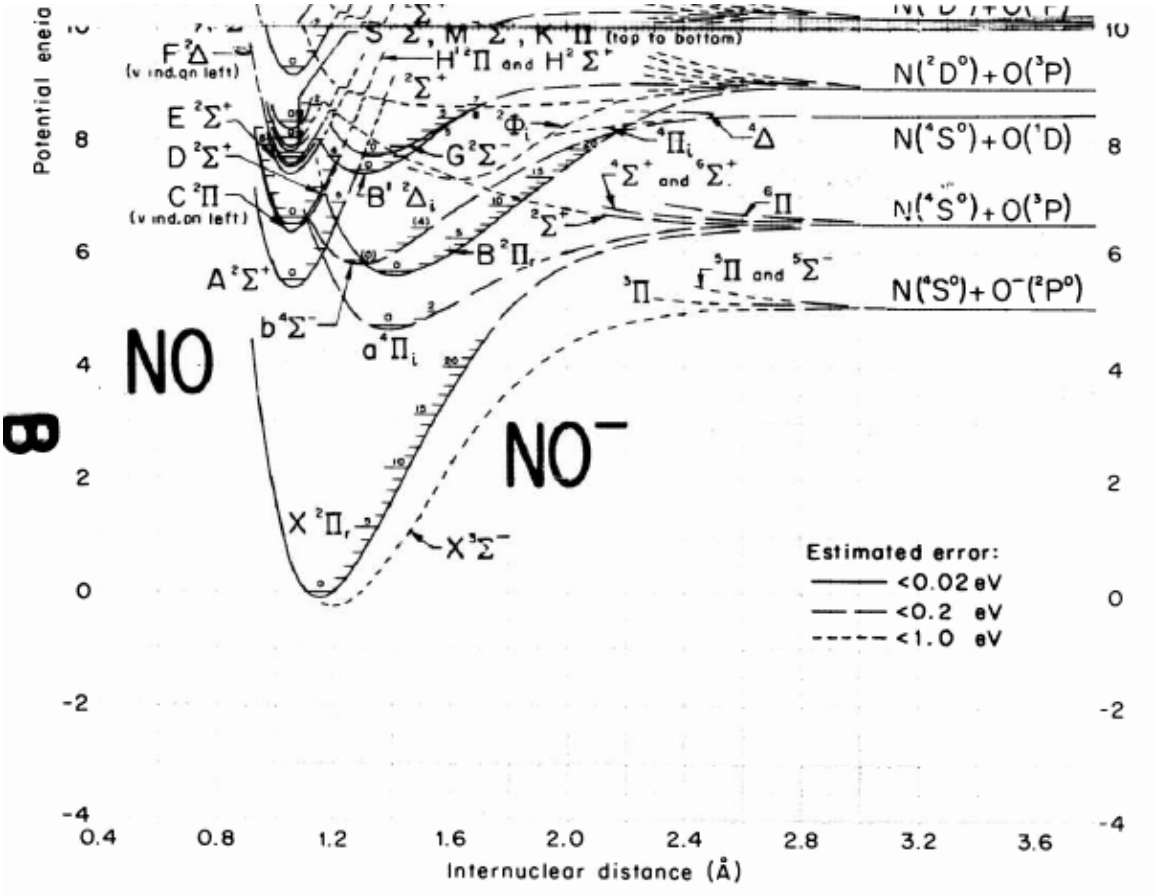

Figure 3.2. Several important potential energy curves of NO molecules. [54]

From the Fig 3.2, we can clearly recognize the molecular constants of some important states of NO molecules, including their vibrational level energies, interatomic distances, and dissociation energies and so forth. But even more important, we can find the NO A $^2\Sigma^+$ state has a more steep potential energy curve than two states (a $^4\Pi_i$ and b $^4\Sigma^-$) which means a longer life time, and a lower excitation energy than the other excited states, these two characteristics makes NO A $^2\Sigma^+$ state the most number density in all the NO excited states. This can explain the strong emission in a way.

3.2 Theory of Spectral Calculation

As we have talked at Chap. 2, if the diatomic molecule is treated as a nonrigid rotor, its vibrational and rotational energy-term formulas can be written as follows:

$$\begin{aligned} G(v) &= \omega_e(v+\frac{1}{2}) - \omega_e x_e(v+\frac{1}{2})^2 \\ F(J) &= B_v J(J+1) - D_v J^2(J+1)^2 \end{aligned}, \tag{3.2.1}$$

The molecular constants are taken from the Herzberg's book [46], electronic excitation energy T_e is taken as 43965.7 for A $^2\Sigma^+$ state, 0 for X $^2\Pi_{1/2}$ and 121.1 for X $^2\Pi_{3/2}$ state all in cm^{-1}. $\omega_e x_e$ is taken as 2371.3 for A $^2\Sigma^+$ and 1904.03 for X $^2\Pi_{1/2}$ and 1903.68 for X $^2\Pi_{3/2}$ state all in cm^{-1}. Here, when we calculate the energy of the rotational levels, we should consider an effect from the centrifugal force. For the X $^2\Pi$ state, normal correction terms are needed both for B_v and D_v as shown below,

$$\begin{aligned} B_v &= B_e - \alpha_e(v+\frac{1}{2}) + \cdots \\ D_v &= D_e + \beta_e(v+\frac{1}{2}) + \cdots \end{aligned}, \tag{3.2.2}$$

where B_v is taken 1.7046 for both X $^2\Pi_{1/2}$ and X $^2\Pi_{3/2}$ state in cm^{-1}. Meanwhile, since the centrifugal force is considered, the rotational terms of the A $^2\Sigma^+$ state are given by [46]:

$$\begin{aligned} F_1(N) &= B_v N(N+1) + \frac{1}{2}\gamma N \\ F_2(N) &= B_v N(N+1) - \frac{1}{2}\gamma(N+1) \end{aligned}, \tag{3.2.3}$$

where the $F_1(N)$ refers to the $J=N+1/2$ and $F_2(N)$ refers to the $J=N-1/2$. However, the γ constant is not available and we still use the classical equations by ignoring the energy

split [55]. It should remark that this ignorance will make the spectra calculated lose some thin peaks when the wavelength resolution is high, but this does not affect the spectral fitting process. Thus, the B_e is taken as 1.9952 for A $^2\Sigma^+$ state and 1.7046 for both X $^2\Pi_{1/2}$ and X $^2\Pi_{3/2}$ state all in cm^{-1}.

Concerning the strength for each vibrational and rotational level, all the line intensities with the Franck-Condon factors [12] and the Hönl-London factors for corresponding transitions [56] should be included. The formula of the Hönl-London factors are taken from the L. T. Earls's work [56], given by:

$$\begin{aligned}
R_2(+), R_{21}(-): &\quad \frac{(2J+1)^2 \pm (2J+1)U(4J^2+4J+1-2\lambda)}{32(J+1)} \\
R_{12}(-), R_1(+): &\quad \frac{(2J+1)^2 \pm (2J+1)U(4J^2+4J-7+2\lambda)}{32(J+1)} \\
Q_2(+), Q_{21}(-): &\quad \frac{(2J+1)[(4J^2+4J-1) \pm U(8J^3+12J^2-2J+1-2\lambda)}{32J(J+1)} \\
Q_{12}(-), Q_1(+): &\quad \frac{(2J+1)[(4J^2+4J-1) \mp U(8J^3+12J^2-2J-7+2\lambda)}{32J(J+1)} \\
P_2(+), P_{21}(-): &\quad \frac{(2J+1)^2 \pm (2J+1)U(4J^2+4J-7+2\lambda)}{32J} \\
P_{12}(-), P_1(+): &\quad \frac{(2J+1)^2 \mp (2J+1)U(4J^2+4J+1-2\lambda)}{32J}
\end{aligned}, \tag{3.2.4}$$

where the + and – are staying the same as the changing part in the formula, and P R and Q branches denote the rotatinoal level differences, which can refer to Fig. 4.3.

$$\begin{aligned}
U &= [\lambda^2 - 4\lambda + (2J+1)^2]^{-1} \\
\lambda &= A_v / B_v
\end{aligned}. \tag{3.2.5}$$

where A_v indicates a coupling constant which determines the multi-split [46]. In Eq. 4.2.5, the λ takes $\pm\infty$ in Hund's case (a) and 0 in case (b). In the NO γ-band case, the upper state A $^2\Sigma^+$ has the constant as 0 and that of the lower state X $^2\Pi$ is given by[57]

$$A_v = 123.26 - 0.1906 \times (v + 0.5) - 0.0108 \times (v + 0.5)^2 . \quad (3.2.6)$$

where v is the vibrational quantum number. The rotational transition structure is shown as following:

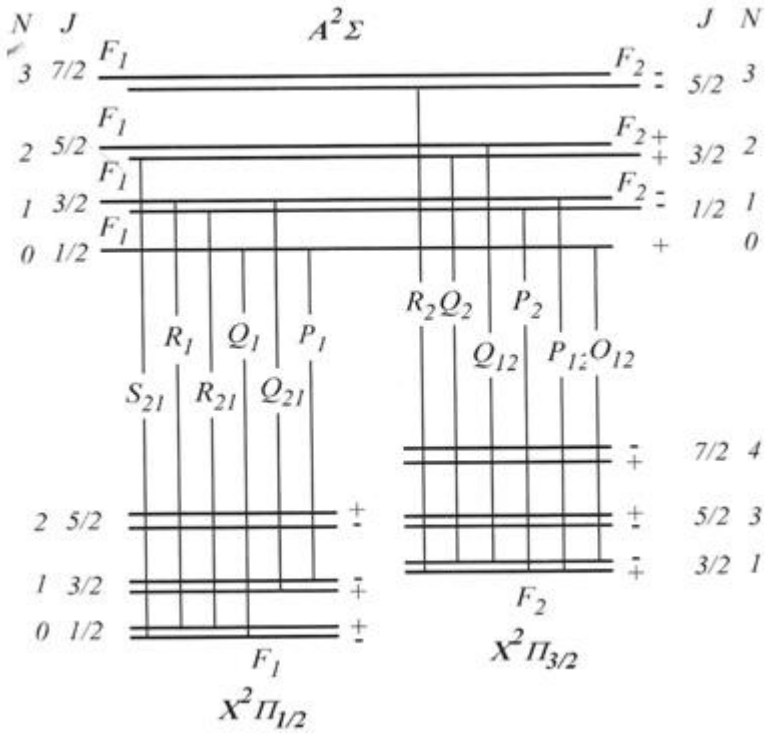

Figure 3.3. Diagram of the rotational structure of NO γ-band. [12]

The wavelength where the line appears is calculated from the energy differences between the initial and final states. Also we consider a Gaussian broadening of each line. Thus, we can finally obtain the calculation result of the γ–band. Fig. 3.4 shows four main peaks of the γ-band calculated, the wavelength position of the peaks match the experiment result

perfectly shown in Fig. 3.1, which means the calculation is sufficient for a vibrational and rotational temperature fitting measurement.

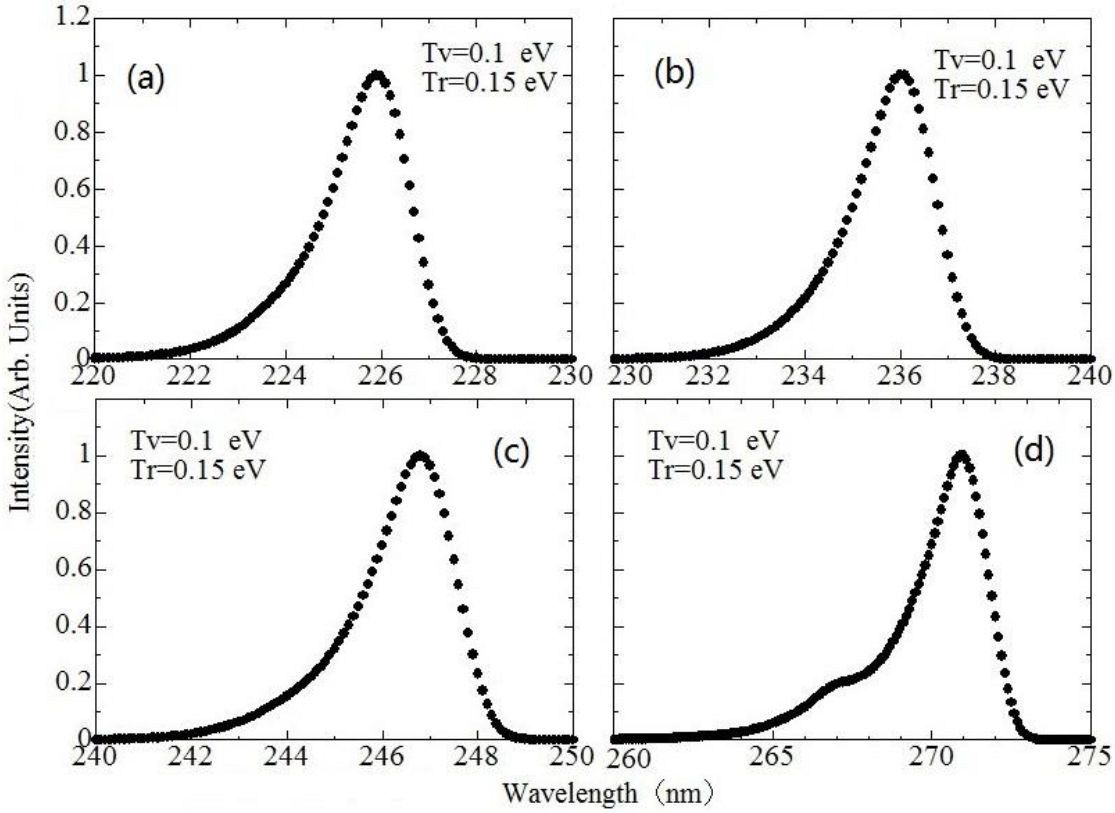

Figure 3.4. Calculation results of γ-band peaks at different transitions between vibrational levels. $\Delta v = v'' - v' = 0$(a),-1(b),-2(c),-3(d) and FWHM = 1 nm.

Using this calculation, we can study the dependence of the γ-band with the plasma conditions which can lead to a variation of the molecular motion. When the vibrational and rotational temperatures change, which means the number densities of different vibrational and rotational levels change, the shape of the spectra calculated change, as shown in Fig 3.5 and Fig. 3.6.

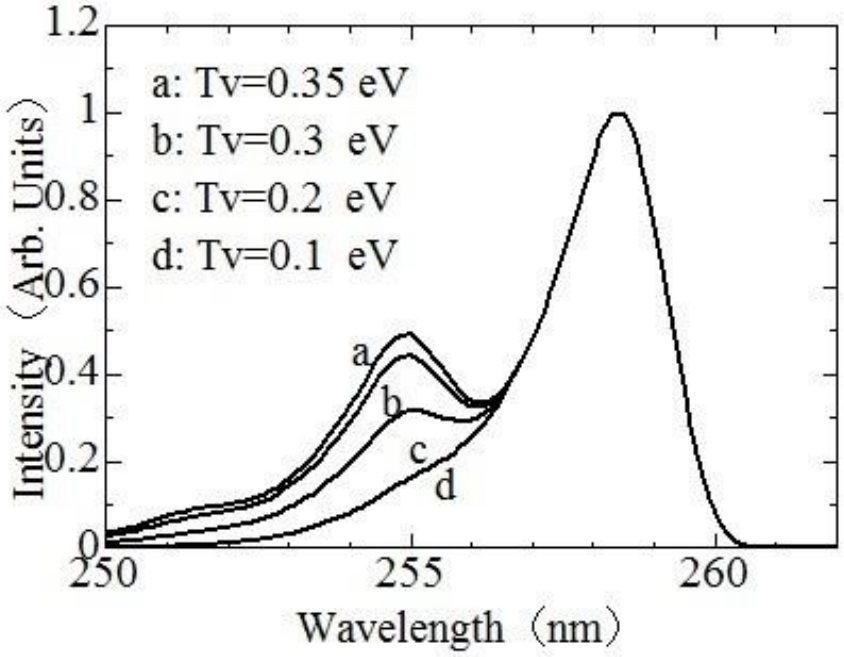

Figure 3.5. Vibrational temperature dependence of γ-band. $\Delta v = v'' - v' = 0$ and FWHM = 1 nm.

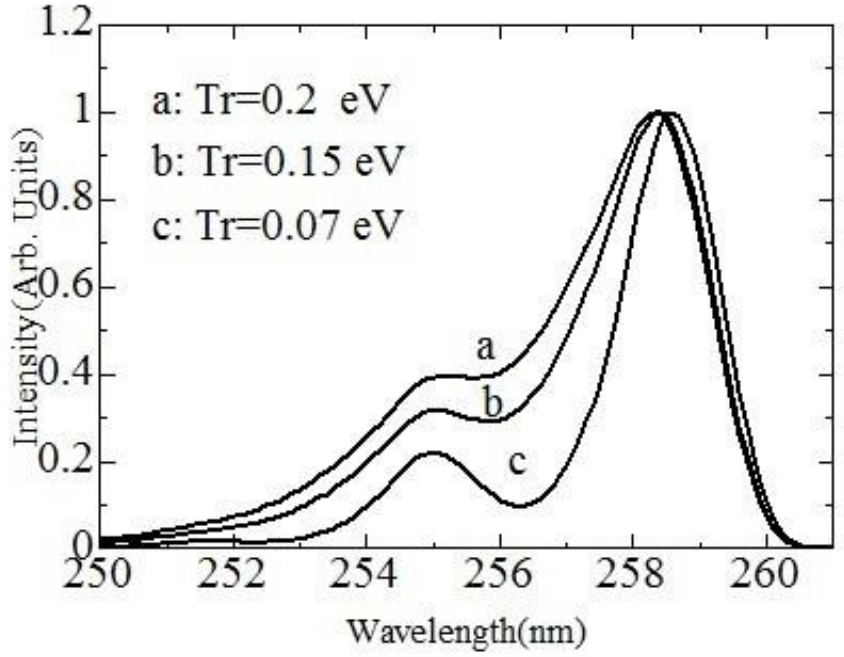

Figure 3.6. Rotational temperature dependence of γ-band. $\Delta v = v'' - v' = 0$ and FWHM = 1 nm.

As described all above, we can compare the experimental spectra with the calculated and assume the best fitting calculation result provides the experimental parameters. Because the fitting results are artificially determined, we found the error range to be about 4% after a large number of repetitions. Meanwhile, to avoid ambiguity due to discharge conditions, we take 30 series of every spectrum in succession and average them as the final fitting data in order to reflect the plasma properties more accurately. There is a fitting example (Fig. 3.7), when the total pressure is 0.5 Torr and the gas mixture is N_2:O_2 = 1:1. From the fitting result, we can see that at the middle area of two neighbouring peaks, the spectra cannot be perfectly fitted because of the overlapping of the peak extension. This will not affect the validity because this peak extension cannot achieve the peak position.

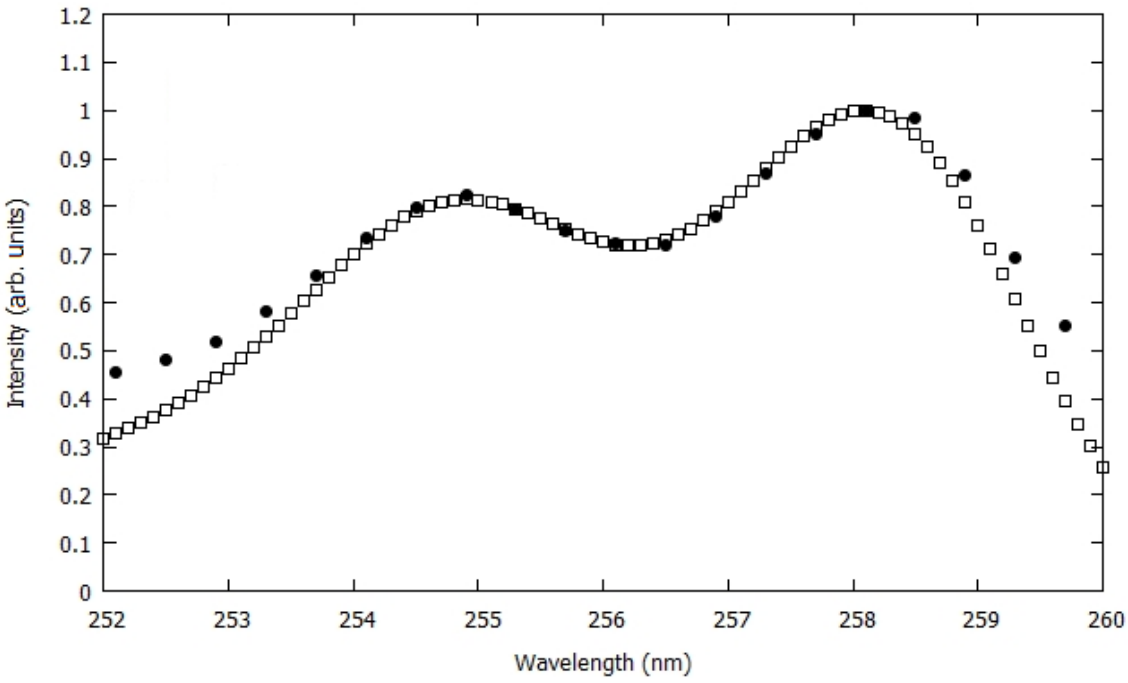

Figure 3.7. An example of the fitting process of γ-band. $\Delta v=v''-v'=0$ and FWHM = 1 nm. Calculation result (hollow rectangles) and experiment result (solid dots).

3.3 Vibrational and Rotational Temperatures of NO in N_2-O_2 Discharge

By using the method introduced above, we set up some experiments to investigate the vibrational and rotational temperatures of NO molecules in N_2-O_2 discharge. We measured the spectra at 0, 60, 100, and 140 mm with the discharge pressure 0.5 to 2 Torr. The output power is set at 600 W, and the gas ratio N_2:O_2 = 1:1. Comparatively, we measured the N_2 spectra and use a similar fitting calculation [58] to obtain its vibrational and rotational temperatures.

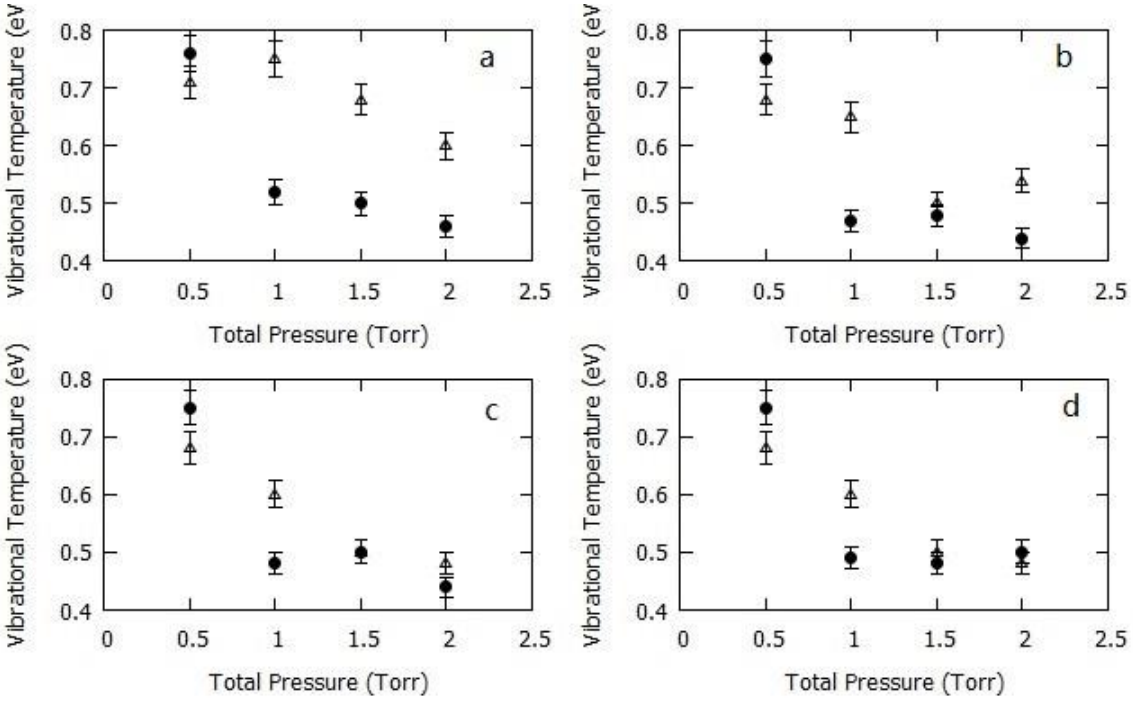

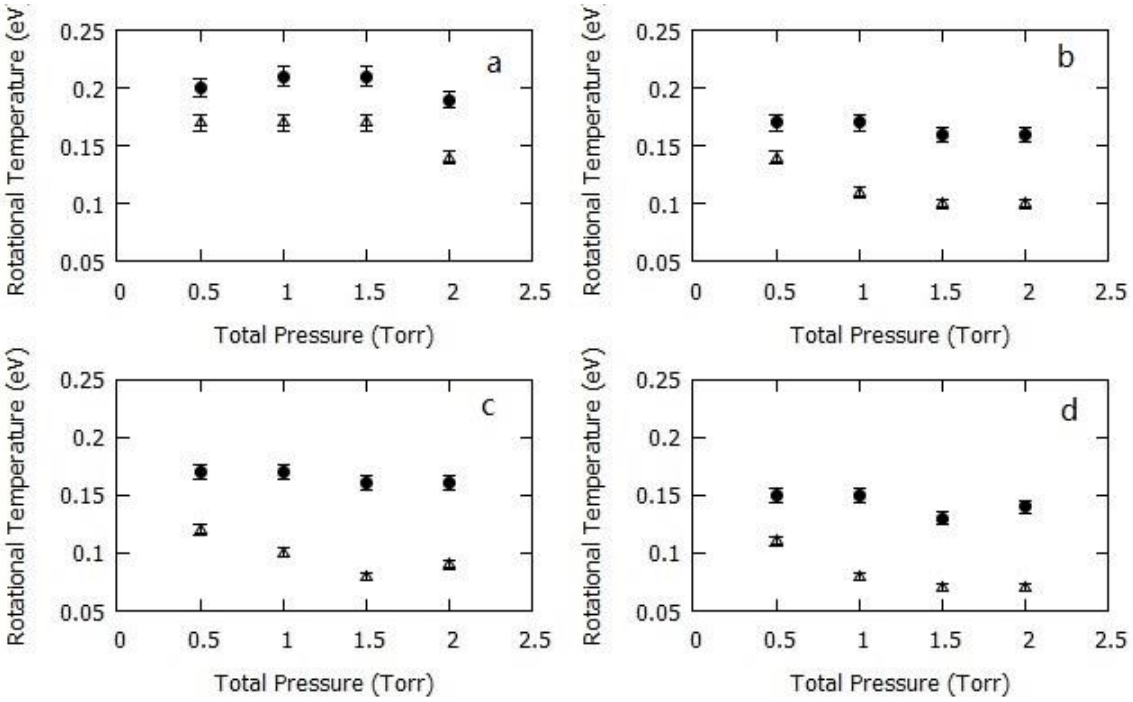

Figure 3.8. Fitting results of vibrational and rotational temperatures of NO (solid dots) and N_2 (hollow triangle) molecules at different position (a: 0 mm, b: 60 mm, c: 100mm, d: 140mm).

From these results, it is easily seen that both NO and N_2 molecules experience a cooling process both on vibrational and rotational temperatures as the plasma flows to the downstream direction along the quartz tube. It is well-known that electronically excited states of atoms and molecules (e.g. N, O, N_2, O_2, NO, and etc.) are generally populated by collisions with electrons in a low-pressure and low-electron density microwave discharge plasmas, and relaxed by collisions with heavy particles as well as with discharge tube wall. As flowing to the downstream direction in the tube, the plasma loses its energy by molecular radiation and recombination. The diffusion loss of charged particles or thermal energy to the plasma tube wall cooling by the atmosphere should be also considered. As a

result, this leads to a decay of the radiation intensity of γ-band, which corresponds to the decrease in the number density of NO A $^2\Sigma^+$ state. We can find that the cooling rates at 100 and 140 mm are obviously smaller than those at 0 and 60 mm. From Fig. 3.8, we can see that in this nonequilibrium plasma, both NO and N_2 molecules tend to get higher energy for vibrational motion than for rotational motion. This is because vibrational energy transformation is more effectively carried out by collisions with energetic electrons in low-pressure plasma. On the other hand, from Fig. 3.8, it is found that the NO molecules always have a higher rotational temperature than N_2, and that rotational relaxation process is slower than that of the vibrational one. This implies that the rotational excitation process of NO molecule is different from that of N_2, which is one of the most important findings in the present study.

In order to widen this research more roundly, we continue to explore the dependence and plasma properties when the N_2 and O_2 pressure partial ratio changes. We focus on the 60 mm position at the tube, where provides a stable plasma relatively and a resolved radiation with less noise. Because of the limitation of the rotary pump and impermeability of the vacuum system, the ratio is limited to 1% ~ 99% for one gas.

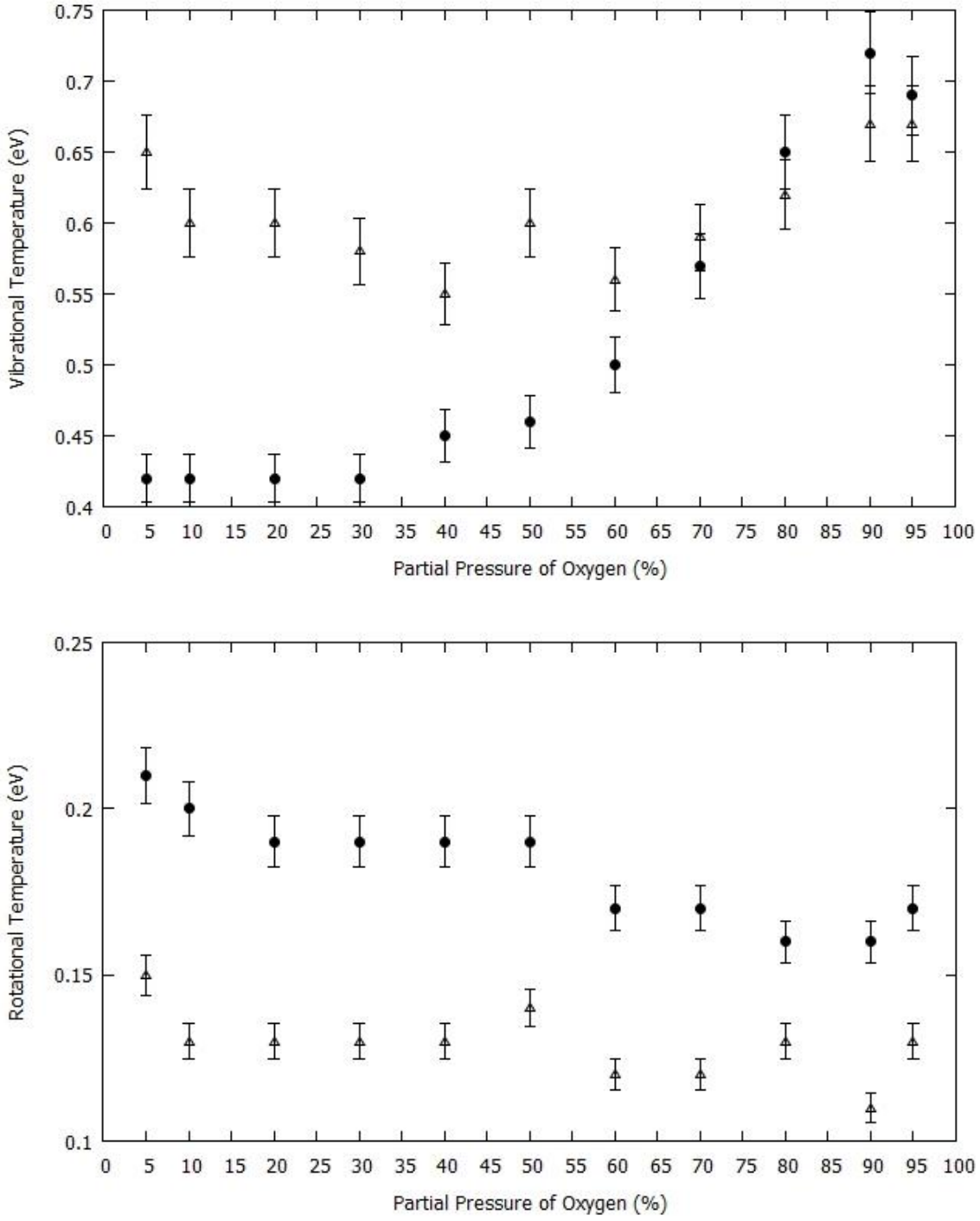

Figure 3.9. Vibrational and rotational temperatures of NO (solid dots) and N_2 (hollow triangle) plotted against partial pressure of oxygen in a plasma feeding gas. (60 mm, 2 Torr).

Figure 3.9 shows vibrational and rotational temperatures of NO A $^2\Sigma^+$ state and of N_2 C $^3\Pi_u$ state plotted against partial pressure of oxygen with the total discharge pressure 2 Torr. We found an irregular vibrational temperature increase as the partial pressure ratio of oxygen increases for the rotational temperature of NO A $^2\Sigma^+$ state, while that of N_2 C $^3\Pi_u$ state has its minimum for O_2 ratio 40 – 60%. The detailed analysis for both Fig. 3.8 and 3.9 is in Chap. 4, because these should be support by some quantitative evidence.

CHAPTER IV: Kinetics Model of NO (A, B, C) in N_2-O_2 Discharge

4.1 Introduction of Kinetics Model

A number of theoretical models have been developed and many experimental examinations on high- and low-pressure N_2-O_2 mixture, as well as other gaseous plasmas have been performed to clarify the physical and chemical kinetics under different plasma conditions.[14,59,60] Nonetheless, in the studies on N_2-O_2 plasma, only the particles with relatively large number densities such as N_2, O_2 molecules, and N and O atoms are fixed people's eyes. Indeed, NO molecules are sometimes mentioned as the nonessential resultant in these models, but typically only the NO ground state is considered. On the one hand, more new findings on the molecular reactions are continually digging out for a possible to improve these models. On the other hand, this basic investigation of NO molecules is still insufficient, especially because their excited states are not considered and there is no accurate experimental examination. On account of the wide applications and complexities for the N_2-O_2 mixture plasma, at atmospheric pressure, some studies proved that, after considering the existence of the NO excited states, the calculated spectra are getting closer agreement with the experimental spectra. [61] This implies that the excited-state of NO molecules are indispensable when studying the chemical kinetics of this kind of plasma. Hence, a precise kinetic model of low-pressure N_2-O_2 mixture discharges is necessary for investigating the reaction kinetics of NO molecules, especially the kinetics of the NO metastable states such as A $^2\Sigma^+$, B $^2\Pi$, and C $^2\Pi$. These three excited states show quite different behaviors in terms of number density as plasma conditions change, which consequently changes the plasma radiation spectra.

In optical emission spectroscopy spectra, the γ–band (from A $^2\Sigma^+$ to X $^2\Pi$) has been frequently observed in N_2-O_2 plasma. The γ–band is even mistakenly called the "third positive system of N_2" [62] long ago because it usually appears along with (and close to) and have a similar intensity with, the N_2 first and second positive systems. Furthermore, the δ–band (from C $^2\Pi$ to X $^2\Pi$) can be observed when the γ–band spectrum broadening is not severe (i.e., with low rotational temperature) and the gas temperature is sufficiently high (at 4000–5000 K to excite the C $^2\Pi$ state).[61] Ultimately, the β–band (from B $^2\Pi$ to X $^2\Pi$) is rarely visible except under harsh conditions (afterglow plasma when N_2% = 96 – 99.5%).[60,63,64]

Consequently, it is necessary to include the excitation kinetics of NO metastable states in N_2-O_2 mixture discharges, since they have different population and depopulation processes theoretically. What is more, as talked in Chap.3, we need a quantitative analysis for the vibrational and rotational temperature dependences of both NO and N_2 to get a convincing conclusion. The molecular properties form through many particle collisional processes, only with rate and number density comparisons, the most important influence can be determined. To this end, the kinetics model is essential.

4.2 Generation and De-excitation of NO (A, B, C) in N_2-O_2 Discharge

This self-consistent kinetic model is based on a previous work by Ichikawa *et al*. [59] It is developed for a microwave discharge in a cylindrical tube under the assumption that the discharge plasma is homogeneous along the tube with a density gradient of the Bessel J_0 distribution along the radial direction. Mr. Ichikawa originally designed the numerical

code to calculate the number densities of important particles in the N_2-O_2 gas mixture microwave discharge plasma as functions of the following parameters: the gas temperature T_g, electron density N_e, total discharge pressure P, reduced electric field E/N, and the N_2 to O_2 partial pressure ratio in the mixture. In his previous study, only the ground state of the NO molecule is considered. I added some reactions involve the excited states of NO and corrected the self-consistency process. In the previous study, the plasma parameters including plasma gas temperature and electron density were modified during the calculation, in order to maintain this quasi-neutrality. In my study, considering that gas temperature is obtained from N_2 2PS experimentally, I decrease the amplitudes of fluctuations in plasma gas temperature and electron density. Also, the reduced electric field E/N is modified on a large scale in order to achieve the quasi-neutrality instead, because E/N cannot be detected precisely and directly in the microwave discharge. Throughout the analysis, gas temperature is approximated by the rotational temperature obtained from the N_2 second positive system (2PS). The electron density obtained from our experiments was also included in the analysis.[59,65-67] In this kind of discharge plasma, all the electrons originate from molecular and atomic ionizations. Moreover, free electrons remain in the quartz tube and can only flow in the downstream direction along the tube. Therefore, we use the quasi-neutral condition as the plasma self-consistent boundary condition.

This model enables the determination of the populations of the vibrational levels of N_2 X $^1\Sigma^+_g(v = 1–8)$ and O_2 X $^3\Sigma^+_g(v = 1–4)$ from the effects of inelastic and superelastic collisions. For other molecules, we consider N_2 A $^3\Sigma^+_u$, B $^3\Pi_g$, C $^3\Pi_u$, a $^1\Pi_g$, a$'$ $^1\Sigma^-_u$, O_2 a$'$ $^1\Delta_g$, b $^1\Sigma^+_g$, and O_3. For ions and atoms, N_2^+, N_4^+, O_2^+, NO^+, and O^- are

included. In this work, three important excited states of NO molecules are calculated including X $^2\Pi$ (ground state), A $^2\Sigma^+$, B $^2\Pi$, and C $^2\Pi$ states. The reactions involving NO molecules are listed in Tables I and II, including those newly added.

Table V. List of reactions where NO X $^2\Pi$ and NO^+ are involved in the kinetic model.

Reactions			Reference of ICS or rate coefficient
$NO(X\ ^2\Pi) + e^-$	→	$NO^+ + 2e^-$	59
$NO^+ + e^-$	→	$N(^4S) + O(^3P)$	59
$N(^4S) + O(^3P) + N_2(X\ ^1\Sigma_g)$	→	$NO(X\ ^2\Pi) + N_2(X\ ^1\Sigma_g)$	59
$N(^4S) + O_2(X\ ^3\Sigma_g)$	→	$O(^3P) + NO(X\ ^2\Pi)$	59
$N_2(B\ ^3\Pi_g) + NO(X\ ^2\Pi, v)$	→	$N_2(X\ ^1\Sigma_u) + NO(X\ ^2\Pi, w)$	59
$N_2(a'\ ^1\Sigma_u) + NO(X\ ^2\Pi, v)$	→	$N_2(X\ ^1\Sigma_u) + NO(X\ ^2\Pi, w)$	59
$N_2^+ + NO(X\ ^2\Pi)$	→	$N_2(X\ ^1\Sigma_u) + NO^+$	59
$N_2^+ + O(^3P)$	→	$N(^4S) + NO^+$	59
$N_4^+ + NO(X\ ^2\Pi)$	→	$N_2(X\ ^1\Sigma_u) + NO^+$	59
$O_2^+ + N(^4S)$	→	$O(^3P) + NO^+$	59
$O_2^+ + NO(X\ ^2\Pi)$	→	$NO^+ + O_2(X\ ^3\Sigma_g)$	59
$O^+ + N_2(X\ ^1\Sigma_u) + O_2(X\ ^3\Sigma_g)$	→	$NO^+ + N(^4S) + O_2(X\ ^3\Sigma_g)$	59
$N_2(a'\ ^1\Sigma_u) + NO(X\ ^2\Pi)$	→	$N_2(X\ ^1\Sigma_u) + O(^3P) + N(^4S)$	59
$N(^4S) + N(^4S) + NO(X\ ^2\Pi)$	→	$N_2(A\ ^3\Sigma_u) + NO(X\ ^2\Pi)$	59
$N(^4S) + N(^4S) + NO(X\ ^2\Pi)$	→	$N_2((B\ ^2\Pi_g) + NO(X\ ^2\Pi)$	59
$O_2(a\ ^1\Delta_g) + NO(X\ ^2\Pi, v)$	→	$O_2(X\ ^3\Sigma_g) + NO(X\ ^2\Pi, w)$	59
$N_2(A\ ^3\Sigma_u) + O(^3P)$	→	$NO(X\ ^2\Pi) + N(^4D)$	86 [a]

[a]This reaction that involving NO is newly added in the present study.

Table VI. List of inelastic collisions in which NO excited states are involved and important reactions are included in the present study.

Reactions			Reference of ICS or rate coefficient
$NO(X\ ^2\Pi) + e^-$	→	$NO(A\ ^2\Sigma^+) + e^-$	68, 69
$NO(X\ ^2\Pi) + e^-$	→	$NO(B\ ^2\Pi) + e^-$	68, 69
$NO(X\ ^2\Pi) + e^-$	→	$NO(C\ ^2\Pi) + e^-$	68, 69
$N_2(A\ ^3\Sigma^+_u) + NO(X\ ^2\Pi)$	→	$N_2(X\ ^1\Sigma^+_g) + NO(A\ ^2\Sigma^+)$	76
$N(^4S) + O(^3P)$	→	$NO(C\ ^2\Pi)$	61

$NO(A\ ^2\Sigma^+)$	→	$NO(X\ ^2\Pi) + h\nu$	80
$NO(B\ ^2\Pi)$	→	$NO(X\ ^2\Pi) + h\nu$	80
$NO(C\ ^2\Pi)$	→	$NO(X\ ^2\Pi) + h\nu$	72
$NO(C\ ^2\Pi)$	→	$NO(A\ ^2\Sigma^+) + h\nu$	72

4.2.1 Cross Sections of Electron Impact Excitation

In this type of low-temperature and low-pressure discharge plasma, electron collision occurs far more frequently than the other types of collision between heavy particles. This implies that the electron impact excitation and ionization processes usually dominate the generation of molecular and atomic excited states. The electronic impact excitation rate coefficient k can be calculated using

$$k = \sqrt{\frac{2}{m_e}} \int_0^\infty \sigma(\varepsilon) f(\varepsilon) \varepsilon d\varepsilon \ , \tag{4.2.1.1}$$

where m_e is the electron mass, $\sigma(\varepsilon)$ is the integral cross section (ICS) of electron impact excitation, $f(\varepsilon)$ is the electron energy probabilistic function (EEPF), which is obtained using the Boltzmann equation [59] and normalized in Eq. (4.2.1.2), and ε is the electron energy, and the dependence schematic diagram of the EEPF is shown in Fig. 4.1,

$$\int_0^\infty f(\varepsilon) \sqrt{\varepsilon} d\varepsilon = 1. \tag{4.2.1.2}$$

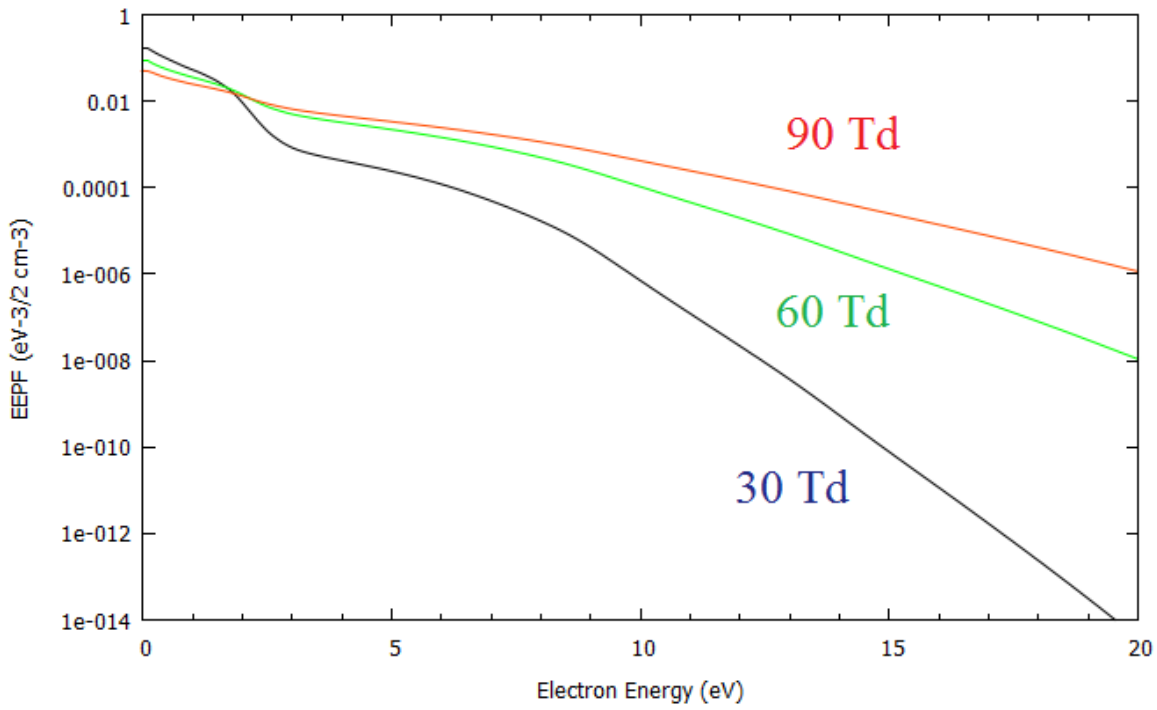

Figure 4.1. Comparision of EEPF calculated for different *E/N* values as functions of electron energy (N_2:O_2 = 1:1, total pressure = 5 Torr).

Fig. 4.1 draws three EEPF curves with different *E/N* at 30, 60 and 90 Td. It is easily seen that as the *E/N* increases, the population at high energy range increases rapidly. That indicates an increase on the rate coefficient with the increasing *E/N* under the same electron temperature. This is the reason that I correct the self-consistency in order to achieve the boundary condition during the calculation. Sometimes, using all the plasma parameters obtained from the experimental detecting, the positive charge sum is always smaller than the negative one. Thus, we can increase the E/N artificially to increase the degree of ionization to increase the positive charge sum, finally the quasi-neutrality can be achieved which means the sum of the N_2^+, N_4^+, and NO^+ number

densities is equal to that of O^- and e^-., and at the same time, all the plasma parameters are not violated.

The second part of the Eq. (4.2.1.1) is the ICS to get the final rate coefficient. Although there have been some studies on the ICS of NO electron impact excitation,[68-70] only the report by Brunger *et al.*[68,69] can provide detailed data both theoretically and experimentally over the low-electron-energy range shown in Fig. 4.2 and 4.3. Therefore, in our calculation, we use the ICS values of Brunger *et al.* for NO A $^2\Sigma^+$, B $^2\Pi$, and C $^2\Pi$. In these ICS curves, we consider that the data from Brunger *et al.* cannot provide a continuous line. Therefore, we make a smooth curve to connect all the data points, and at the same time, the cut-off excitation energy and approximations on both around cut-off point and high energy range are also considered according to the data from Skubenich *et al.* and DW shown in Fig 4.2 and 4.3. Moreover, the reverse processes involved follow the Klein-Rosseland equation [71] are also calculated,

$$\frac{\sigma_{pq}(\varepsilon')}{\sigma_{pq}(\varepsilon'')} = \frac{g_p \cdot (\varepsilon'')}{g_q \cdot (\varepsilon')} \quad , \tag{4.2.1.3}$$

where $\sigma_{pq}(\varepsilon')$ is the ICS for the electron impact excitation from levels p to q under the energy difference $\varepsilon_{pq}>0$ for the electron energy ε', $\sigma_{pq}(\varepsilon'')$ is that for the reversal case for the electron energy $\varepsilon''=\varepsilon'+\varepsilon_{pq}$, and g_p and g_q are the statistical weights of the in states suffix shown.

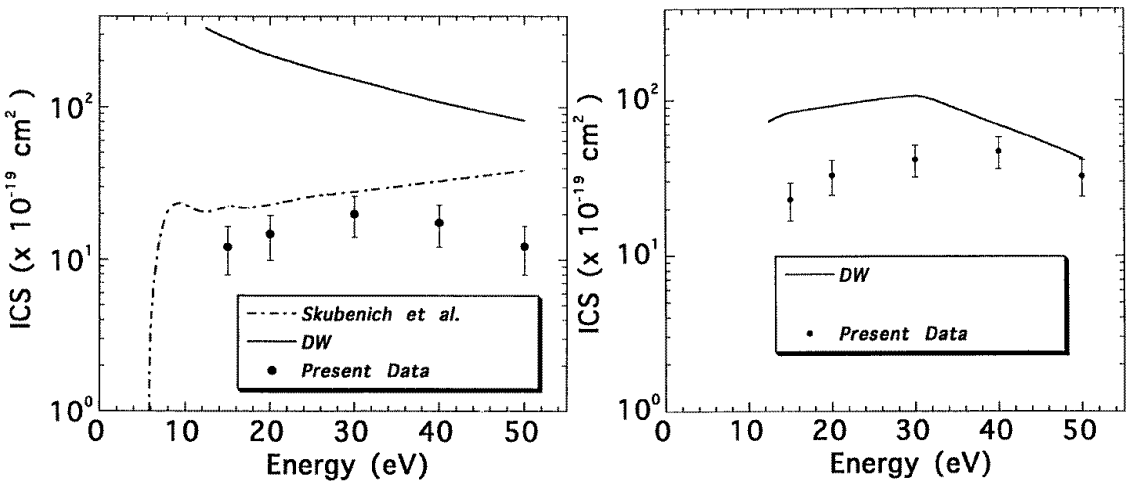

Figure 4.2. Cross sections of NO A $^2\Sigma^+$ (left) and C $^2\Pi$ (right) states quoted from Brunger *et al.*'s study.

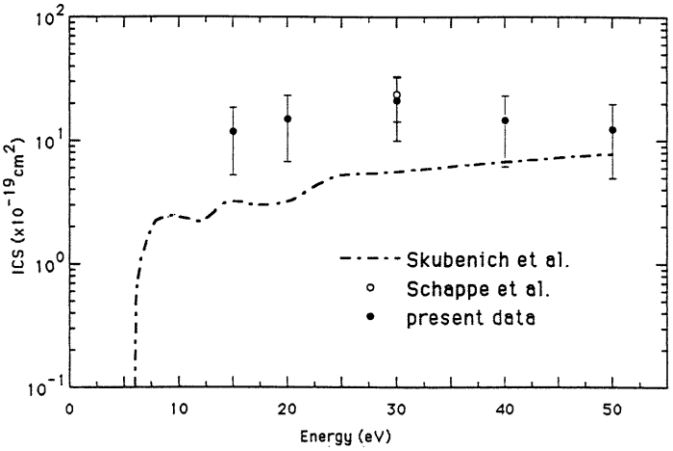

Figure 4.3. Cross sections of NO B $^2\Pi$ (right) state quoted from Brunger *et al.*'s study.

4.2.2 Heavy Particle Collisions

Numerous studies have been performed to understand the population of NO electronic states arising from collisions between molecules and to clarify the recombination reaction

of N and O atoms. [61,72-75] Excitations of the NO A $^2\Sigma^+$ and C $^2\Pi$ states should be considered under our plasma conditions. The elementary excitation processes are summarized in Table II.

All three-body collisions for excitation NO metastable states are ignored because they rarely happen at low temperatures and pressures. The reaction rate 6.9×10^{11} cm^3/s for NO A $^2\Sigma^+$ excited from its ground state by collisions with N_2 A $^3\Sigma^+_u$ is taken from the report of Cao and Setser.[76] Moreover, the NO C $^2\Pi$ state is considered to be populated by inverse predissociation with the ground electronic states of atoms N(^{4}S) and O(^{3}P). Considering our plasma temperature, N and O atoms should be mostly situated in their ground states. If a Boltzmann distribution is assumed for their electronically excited states, the percentages of these two ground states must be more than 90%. Hence, during the calculation, I use the total N and O atom number densities directly for the reactions that involved N and O. For the NO C $^2\Pi$ state, the predissociation rate varies significantly with the vibrational and rotational quantum numbers (v and J).[59] Many studies have been performed experimentally and theroretically to identify the predissociative lifetime of individual rotational levels of the C $^2\Pi$ state. [59,74,77-79] The resulting predissociation rates (inverse of the lifetime) are listed as follows:

$$k^J_{predissociation} = \begin{cases} 3.3\times10^7 \quad s^{-1} \quad for\ v=0, J<4.5, \quad (non-predissociated) \\ 3.3\times10^8 \quad s^{-1} \quad for\ v=0, J>4.5, \\ 3\times10^9 \quad s^{-1} \quad for\ v=1, \\ 2\times10^{10} \quad s^{-1} \quad for\ v=2, \end{cases} , \qquad (4.2.2.1)$$

Under our plasma conditions, the number densities at high vibrational and rotational levels are much lower than those at low levels. Moreover, considering the

predissociation effect, the C $^2\Pi$ state at high vibrational and rotational levels will rapidly return to excited states of N and O atoms. Therefore, we use the non-predissociated rate coefficient to estimate the relative number density of the C $^2\Pi$ state. The kinetics of the NO B $^2\Pi$ state are more complicated than those of the other two states, and the population of NO B $^2\Pi$ state is not related to the inverse predissociation of the C $^2\Pi$ state. There are two possible excitation paths: (1) three-body collision excitation via another NO intermediate state, that is, a $^4\Pi$ state that is also a minority state, as described above, which rarely happens in low-pressure plasma; (2) transferring from the molecular potential energy curve crossing with the NO predissociated state A$'$ $^2\Sigma^+$, which originates from the high-energy collision between N and O with low probability. However, because the rate coefficient is not available, we ignored this process for the generation of the B $^2\Pi$ state in the present calculation.

4.2.3 Radiation

Theoretically, radiative bands should be observable when the number density of the corresponding excited state is sufficiently high. However, interference can make the expected band disappear, caused by the overlap of weak peaks with stronger peaks, the low resolution of spectroscopic equipment, and self-absorption. Nevertheless, I can still calculate the radiative de-excitation even when the bands are not experimentally observed. We take the radiative coefficient for NO A $^2\Sigma^+$ (v = 0) to X $^2\Pi$ as 5.08×10^6 s^{-1} (γ-band), that for B $^2\Pi$(v = 0) to X $^2\Pi$ as 2×10^6 s^{-1} (β-band), [59,80] and that for C $^2\Pi$ to X $^2\Pi$ as 2.1×10^7 s^{-1} (δ-band).[72] Furthermore, we consider another radiative transition from C $^2\Pi$

to A $^2\Sigma^+$, which can produce infrared bands at a rate coefficient of 5.6×10^6 s^{-1} (health band). [72] All these band except the health band can be seen in Fig 4.4.

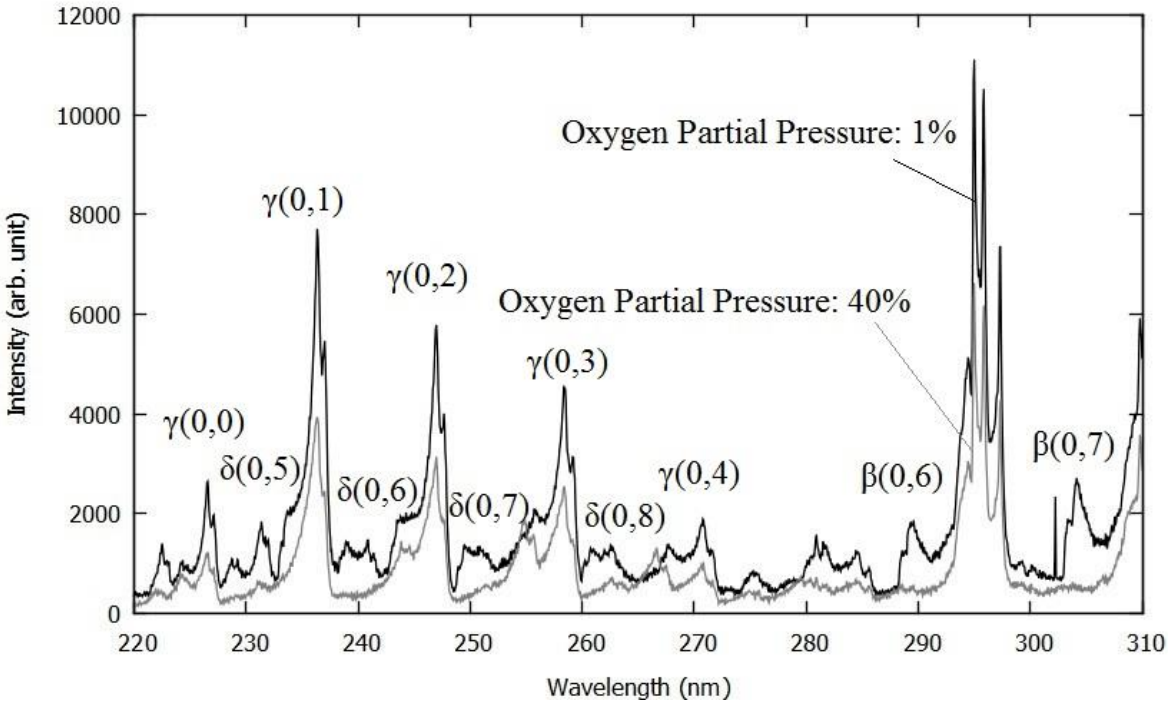

Figure 4.4. Experimentally observed spectra over the 220–310-nm-wavelength range with oxygen partial pressures of 1 (black line) and 40% (grey line). The γ-, β-, and δ-bands are specified. Brackets denote the vibrational quantum numbers (upper, lower) involved.

4.3 Examination Results on Kinetics Model

In order to exam our kinetics model, we set up several experiments and calculations. On one hand, the calculation program can be applied only at less than 5 Torr total pressure, because serial calculation in one core of a normal computer will increase the running time

rapidly when a large total pressure. On the other hand, we need follow the previous experimental conditions in order to a further discussion.

For the numerical simulation, the gas temperature is set at approximately 1500 K and *E/N* is self-consistently determined to be in the range of 75–140 Td (from 5 to 0.5 Torr) as shown in Fig. 4.5.

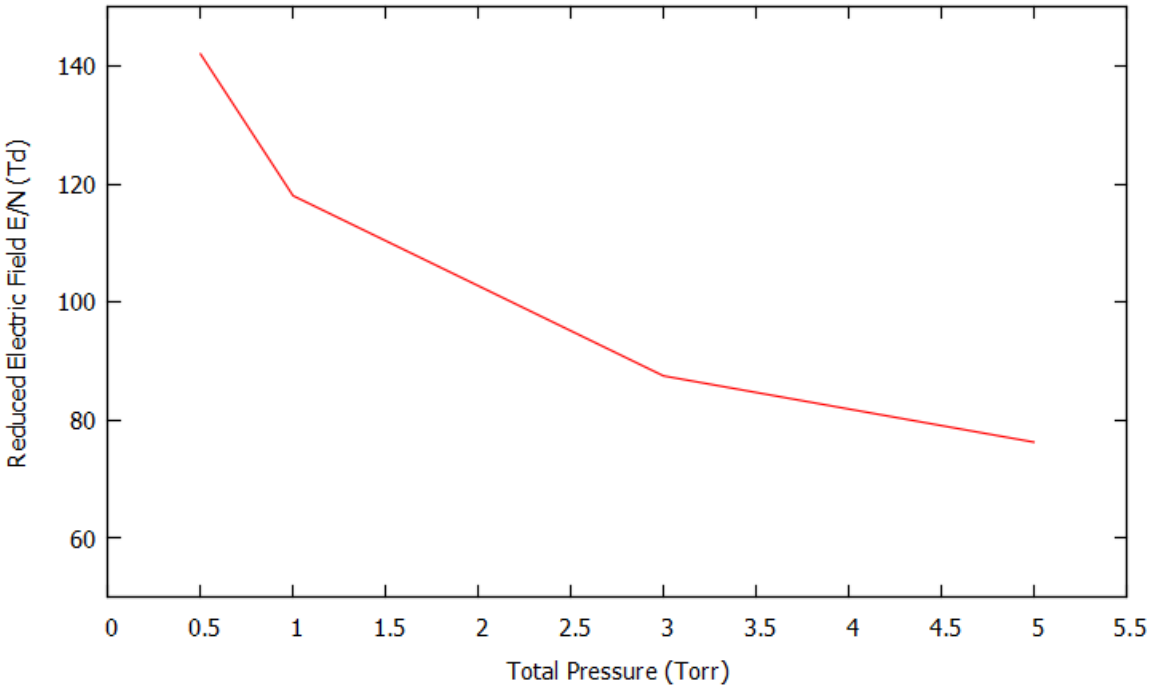

Figure 4.5. Experimental results of γ-band intensities (left vertical axis, closed circles) and numerical results of number density of NO A $^2\Sigma^+$ state (right vertical axis, solid line) plotted against total discharge pressure. $N_2 : O_2 = 1 : 1$.

In this study, we measured the γ-band peak intensity at 230–240 nm (Δv = -1). Fig 4.6 shows the γ-band radiation intensities at different total pressures compared with the calculated results of the NO A $^2\Sigma^+$ number densities.

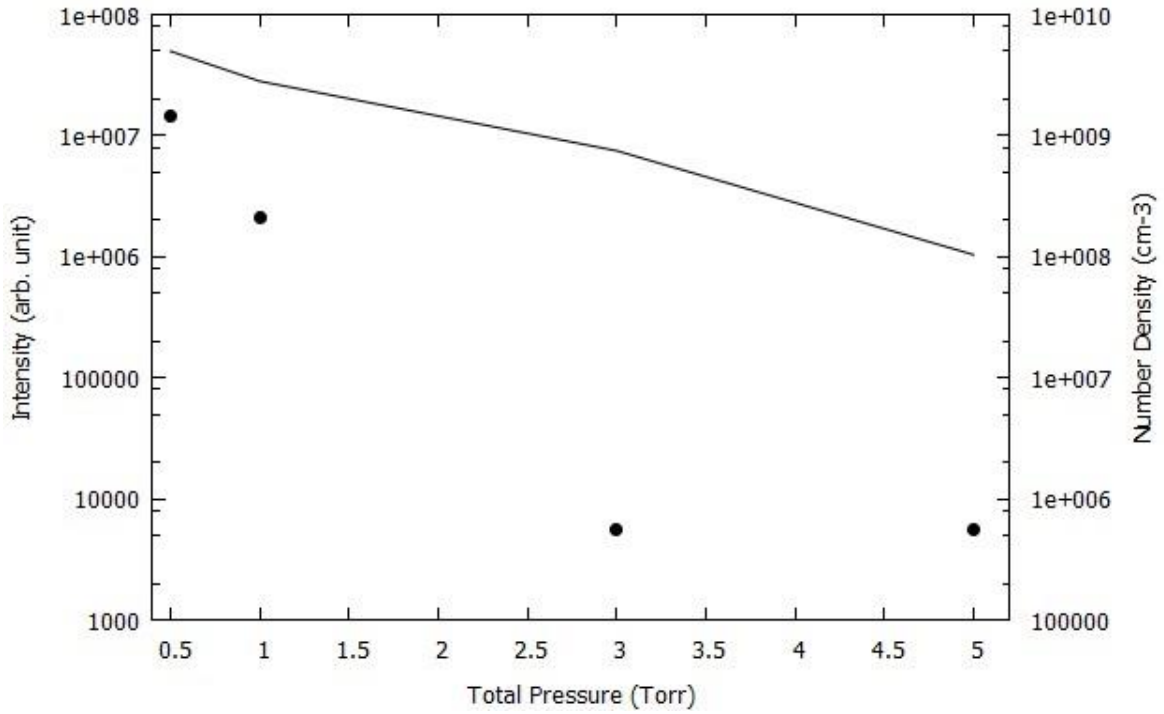

Figure 4.6. Experimental results of γ-band intensities (left vertical axis, closed circles) and numerical results of number density of NO A $^2\Sigma^+$ state (right vertical axis, solid line) plotted against total discharge pressure. $N_2 : O_2 = 1 : 1$.

We see that the observed intensities of the γ-band decrease faster than the numerical results as the total discharge pressure increases. We consider that the reason for this is that the plasma self-absorption becomes stronger as the pressure increases. Indeed, as the total pressure increases (from 0.5 to 5.0 Torr), the electron density decreases slightly (from 5.5×10^{11} cm^{-3} to 2×10^{11} cm^{-3}), which can cause a decrease in both the electron impact excitation rate coefficient and the density of the N_2 A $^3\Sigma^+_u$ state. As we described the heavy-particle collision-induced excitation and electron-impact-induced excitation, two-body collisions dominate the excitation of the NO A $^2\Sigma^+$ state. According

to the numerical results, the rate of the collisional excitation of the N_2 A $^3\Sigma^+_u$ state is nearly always 1000 times higher than that of the electron impact excitation from the NO X $^2\Pi$ state when N_2:O_2=1:1. Hence, in our low-temperature plasmas, γ-band intensity can reflect N_2 (A $^3\Sigma^+_u$) density indirectly.

4.3.1 γ-band

For the numerical procedure of the partial pressure ratio dependence, the gas temperature is set at approximately 2000 K and *E/N* is determined self-consistently at approximately 50 – 75 Td as shown in Fig. 4.7.

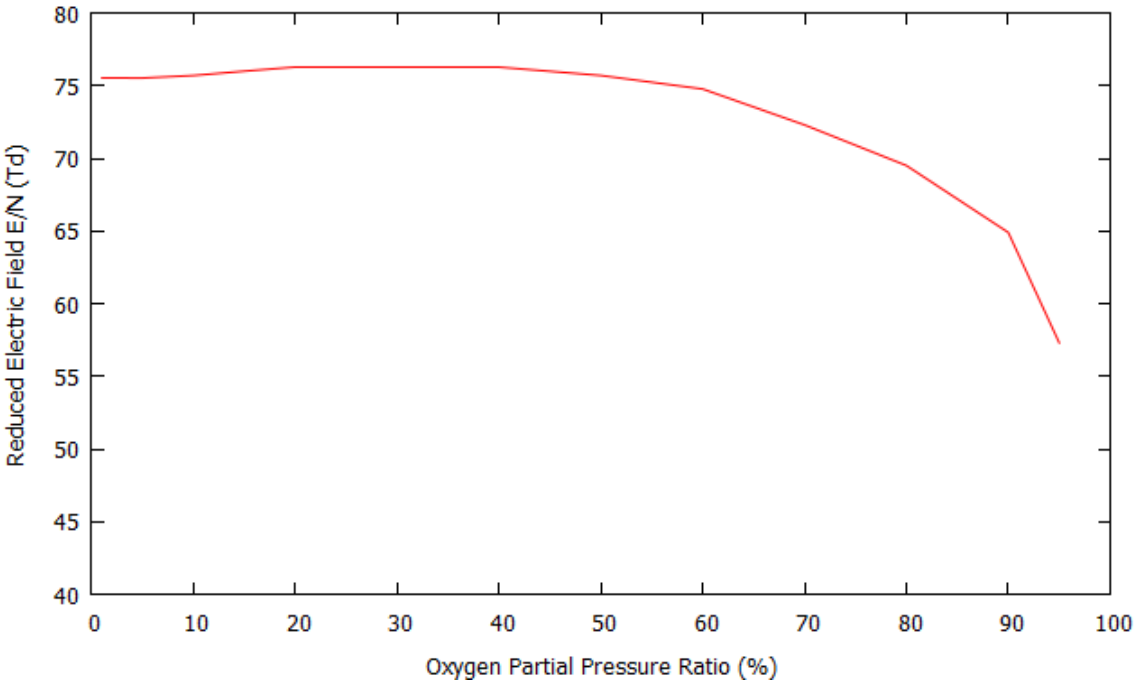

Figure 4.7. Dependence curves of E/N against oxygen partial pressure ratio.

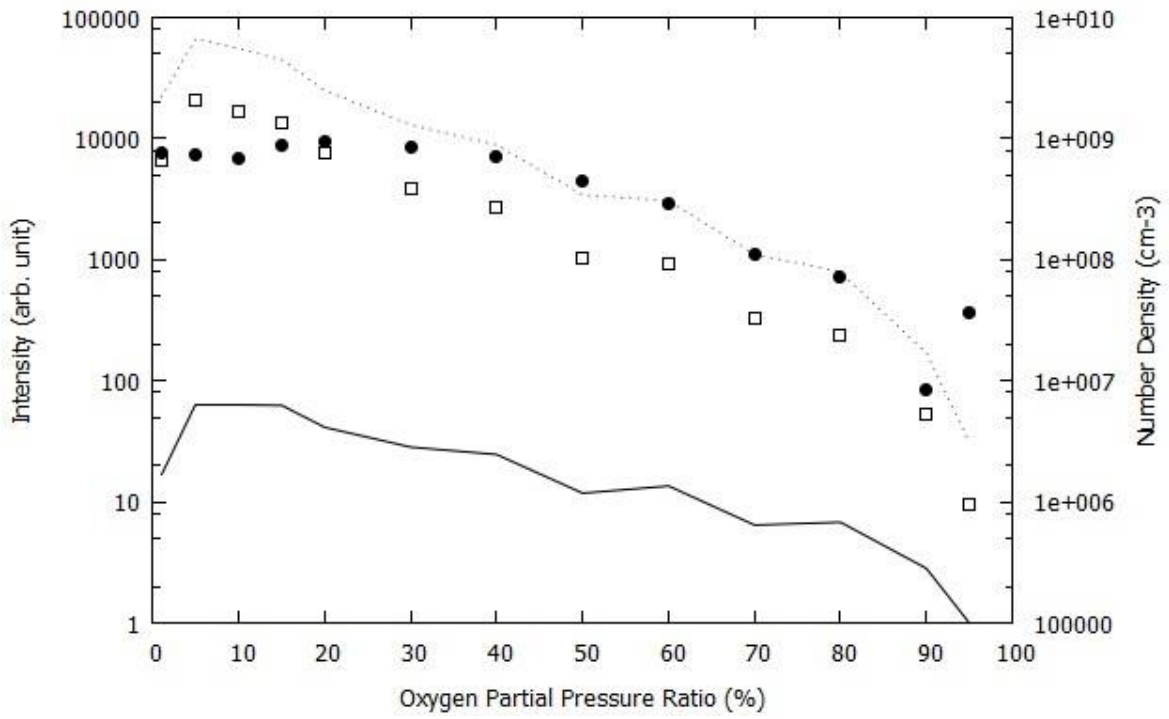

Figure 4.8. Experimental results of the γ-band intensities (left vertical axis, closed circles) and numerical results of number density of NO A $^2\Sigma^+$ state (right vertical axis, open squares), together with generation rate coefficients of NO A $^2\Sigma^+$ state by collisional excitation with N_2 A $^3\Sigma^+_u$ (left vertical axis, dotted line) and electron impacted excitation (left vertical axis, solid line). Generation rates are normalized by the electron impact excitation rate under the oxygen partial pressure of 95%.

Fig. 4.8 shows the numerical and experimental results of the γ-band intensity and the number density of the corresponding upper level, the A $^2\Sigma^+$ state, plotted against oxygen partial pressure. Figure 4.8 shows that the intensity of the experimentally measured γ-band fits the numerically calculated number density of NO A $^2\Sigma^+$ considerably well. They both decrease as the oxygen partial pressure increases, which is

in agreement with the results of Gordiets *et al.* [14] However, according to our calculation, the rates of NO A $^2\Sigma^+$ excitation by collisions with N_2 (A $^3\Sigma^+_u$) are always more than 1000 times higher than the rate of electron impact excitation, which is different from the explanation given by Gordiets *et al.* It is considered that this difference occurs because Gordiets *et al.* independently calculated these two excitation rates and normalized them in the graph by assuming that these two rates are the same at 50% O_2. We discuss the disagreement between the experimental intensity and the simulated number density in the next subsection, particularly for NO C $^2\Pi$.

4.3.2 β and õ-band

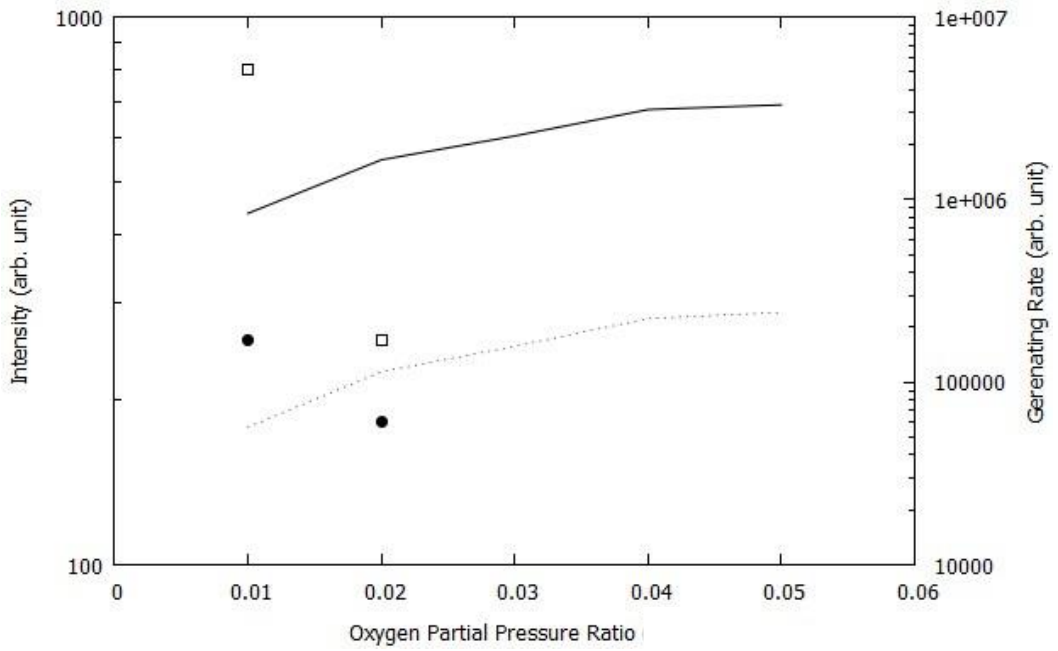

Figure 4.9. Experimental results for the intensities of the β- (open squares) and δ-bands (closed circles) (left vertical axis), and numerical results for population rates of NO B $^2\Pi$ (solid line) and NO C $^2\Pi$ (dotted line) (right vertical axis).

For the β- and δ-bands, we obtained the radiation peaks only when the oxygen partial pressure was suppressed to be very low (< 3%). Therefore, we should discuss the molecular processes involved in this difference. Figure 4.4 shows the experimentally observed spectra over the 220 – 310 nm wavelength range. From the spectra, we can observe the δ-band at 231.3, 240.9, 262.5, and 275.3 nm, and the β-band at 289.4 and 304.1 nm. We added the reference spectra for the oxygen partial pressure ratio of 40% in Fig. 4.4. After the measurement of the wavelength range shown in Fig. 4.4, we subtracted the γ-band and N_2 2PS for the calculation of the intensities of the β- and δ-bands, respectively.

Figure 4.9 shows that the numerical population rates of the NO B $^2\Pi$ and C $^2\Pi$ states increase with increasing oxygen partial pressure ratio, whereas the observed intensities decrease rapidly. This implies that there are essential molecular processes that are not included. Because only the oxygen molecules and atoms change their densities on a large scale under this small variation in plasma conditions, we can limit the discussion to the relevant oxygen molecules for the following reasons:

(i) One of the NO metastable states acts as an intermediate state of transition. This intermediate state is likely the NO a $^4\Pi$ state, which is usually considered to equilibrate with the NO B $^2\Pi$ and C $^2\Pi$ states, because it is quenched by oxygen molecules or atoms. Because the potential curve of B $^2\Pi$ crosses those of C $^2\Pi$ and a $^4\Pi$,[54] this will have a certain probability to transit each other. All of these processes have a common cause, that is, the association between atomic N and O. However, even if this assumption is true, this process cannot make the number densities of NO B $^2\Pi$ and C $^2\Pi$ zero reach a dynamic

equilibrium. Moreover, this process cannot explain the disappearance of the β- and δ-bands at a large partial pressure ratio of O_2, as shown in Fig. 4.4.

(ii) Since Campbell and Mason have reported that the bottom of the NO a $^4\Pi$ potential curve lies almost directly below that of NO B $^2\Pi$,[73] it consequently has a much larger internuclear distance than NO A $^2\Sigma^+$. Moreover, Campbell and Mason proposed an almost exact energy resonance for the process shown in Eq. (4.3.1).

$$O_2(X^3\Sigma_g^-, v''=0) + NO(B^2\Pi, v'=0) \rightarrow O_2(a^1\Delta_g, v'=0) + NO(a^4\Pi, v''=0). \quad (4.3.1)$$

We can also consider a process similar to that in Eq. 4.3.1 for the NO C $^2\Pi$ state, which has even closer energy levels (7918.1 cm^{-1} for NO and 8182.3 cm^{-1} for O_2):[46,81,82]

$$O_2(X^3\Sigma_g^-, v''=0) + NO(C^2\Pi, v'=0) \rightarrow O_2(a^1\Delta_g, v'=0) + NO(A^2\Sigma, v''=0). \quad (4.3.2)$$

The transition for O_2 is optically forbidden in both Eqs. (4.3.1) and (4.3.2). However, if we notice that the reactions occur between molecular collisions, the optically forbidden transitions are often incident. Moreover, Eq. (4.3.2) should be more incident because it includes a spin-allowed transition for the NO molecule (calculated by Laher and Gilmore in 1999 [81]) even though Eq. (4.3.3) has forbidden transitions for both NO and O_2. These two processes are both related to the O_2 ($X\ ^3\Sigma^-_g$) ground state, which generally has a very high number density even when oxygen has a low partial pressure. As we have mentioned, in this low-pressure plasma, molecular collisions only become essential between particles with large number densities. In this case, “high” means particles with considerably higher number densities than others, this is quantitatively shown in Table III.

Table VII. Numerical results of the particle number densities when $N_2 : O_2 = 4 : 1$ at 5 Torr (T_g = 1500 K, T_e = 3 eV, $N_e = 2\times10^{11}$ cm^{-3}, E/N = 76 Td).

Particle type	Number density (cm^{-3})	Particle type	Number density (cm^{-3})
N_2 X $^1\Sigma^+_g$	1.66×10^{16}	O_2 X $^3\Sigma^-_g$	2.86×10^{15}
N_2 A $^3\Sigma^+_u$	1.18×10^{13}	O_2 a $^1\Delta_g$	3.48×10^{14}
N_2 B $^3\Pi_g$	1.00×10^{12}	O_2 b $^1\Sigma^+_g$	7.85×10^{13}
N_2 C $^3\Pi_g$	4.43×10^{9}	O_2^+	1.48×10^{11}
N_2 a $^1\Pi_g$	1.90×10^{12}	O^-	1.50×10^{10}
N_2 a$'$ $^1\Sigma^-_u$	9.02×10^{11}	O_3	3.10×10^{10}
N_2^+	1.12×10^{10}	NO X $^2\Pi$	4.58×10^{12}
N	8.83×10^{10}	NO^+	5.36×10^{10}
N_4^+	1.17×10^{9}	NO A $^2\Sigma^+$	7.04×10^{8}
NO B $^2\Pi$	1.99×10^{6}	NO C $^2\Pi$	1.49×10^{5}

When the lifetime of NO C $^2\Pi$ (v' = 0, 4.982×10^{-8} s) and B $^2\Pi$ (v' = 0, 2.123×10^{-6} s) are considered, we know that the B $^2\Pi$ state has an adequate time to achieve a sufficient number of collisions to transfer to the NO a $^4\Pi$ state instead of radiation. This results in β-band disappearance. On the other hand, the NO C $^2\Pi$ state should simultaneously have δ-band radiation and transformation processes (Eq. 4.3.2) because of its short lifetime. Moreover, in atmospheric plasma, the δ-band often has a stable intensity ratio with respect to the γ-band, while the β-band is still difficult to observe. Concerning the NO C $^2\Pi$ state, Eq. 4.3.2 will decrease the intensity of the δ-band while augmenting the intensity of the γ-band. This is very different from the explanations elsewhere, [83,84] as

$$N_2 + NO(C^2\Pi) \rightarrow N_2 + NO(A^2\Sigma). \quad (4.3.3)$$

Theoretically, most collisions can have a de-excitation effect on these NO excited states including both N_2 and O_2 in N_2-O_2 mixture discharge. We do not deny the validity of Eq. (4.3.3). However, the rate coefficients of molecular collisions are totally different,

and in this case we can see that O_2 dominates the de-excitation of the NO C $^2\Pi$ state instead of N_2.

4.4 More Proof for Our Inference

In order to further prove out inference at last section, we carry out some extra experiments and calculations. According to Eq. (4.3.1) and (4.3.2), we have this proposal: NO C $^2\Pi$ state populates from the combination of N and O atoms, which means the N and O approach towards each other from the infinity (compare to the interatomic distance in the molecular region). As a result, NO C $^2\Pi$ state molecules usually stay at higher vibrational and rotational energy levels shown as Fig. 4.10. While from the potential energy curve (Fig. 4.2), we can imagine that the recombination usually means a high energy level status at the infinity. Thus, if the NO C $^2\Pi$ state is really de-excited to NO A $^2\Sigma^+$ state, the vibrational temperature of NO A $^2\Sigma^+$ state should change as the amount of NO C $^2\Pi$ state number density. Although the number density of NO C $^2\Pi$ state is far less than NO A $^2\Sigma^+$ state, the number density of NO C $^2\Pi$ state is the same level or more than that of high energy levels of NO A $^2\Sigma^+$ state (Fig. 2.5). Therefore, we can expect a positive correlation between the number density of NO C $^2\Pi$ state and the vibrational temperature of NO A $^2\Sigma^+$ state.

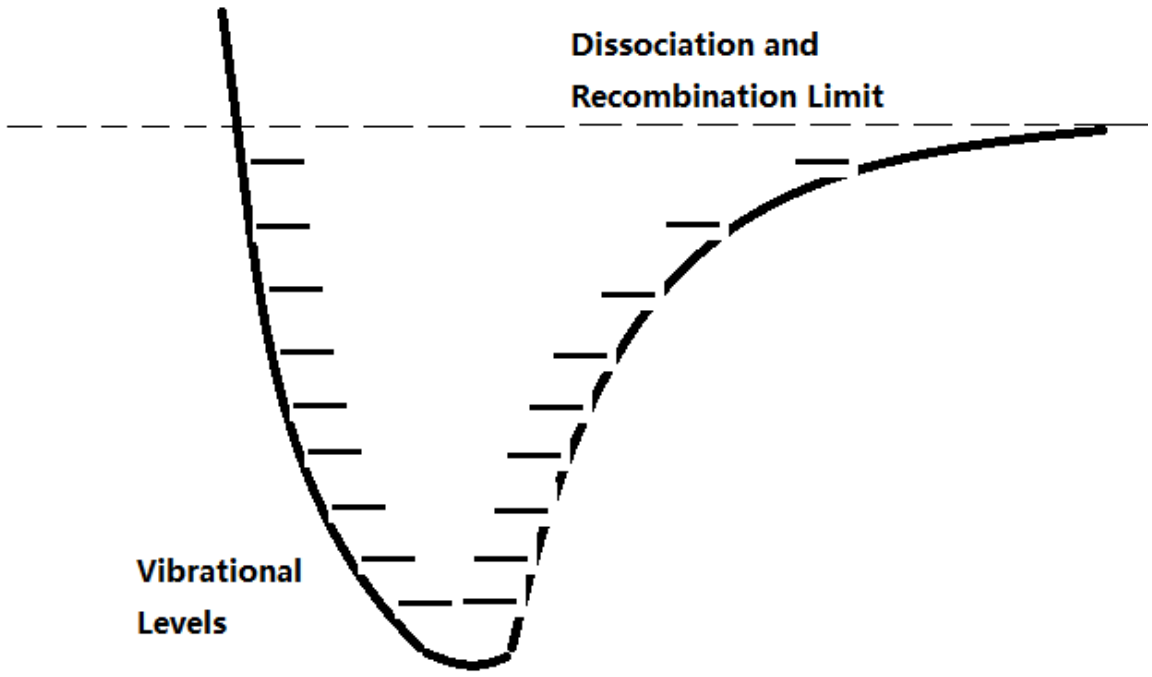

Figure 4.10. Schematic diagram of the high energy level location principle for molecular recombination.

In the numerical procedure, the electron temperature and density adopted were 2 eV and 2×10^{11} cm^{-3}, respectively. These values were obtained by double-probe measurement in the previous study, where we found that as the O_2 partial pressure increases from 0% to 100%, the electron temperature decreases slightly, and the density increases slightly. [59] However, considering that the lens system can collect the emitted light from quite a large area, we only averaged the values of electron temperatures and densities at different distances along the quartz tube and set the values as constant in the calculation. The gas temperature was obtained from the rotational temperature of the N_2 second positive system as 1740 K. We treat these parameters as constant in the calculation because they remain nearly unchanged, even if the O_2 partial pressure changes. It should be noted that,

as mentioned above, the gas temperature will be modified within a small range around the experimental result to achieve quasi-neutrality. The reduced electric field *E/N* is self-consistent during our calculation, and ranges from 47.0 to 77.5 Td.

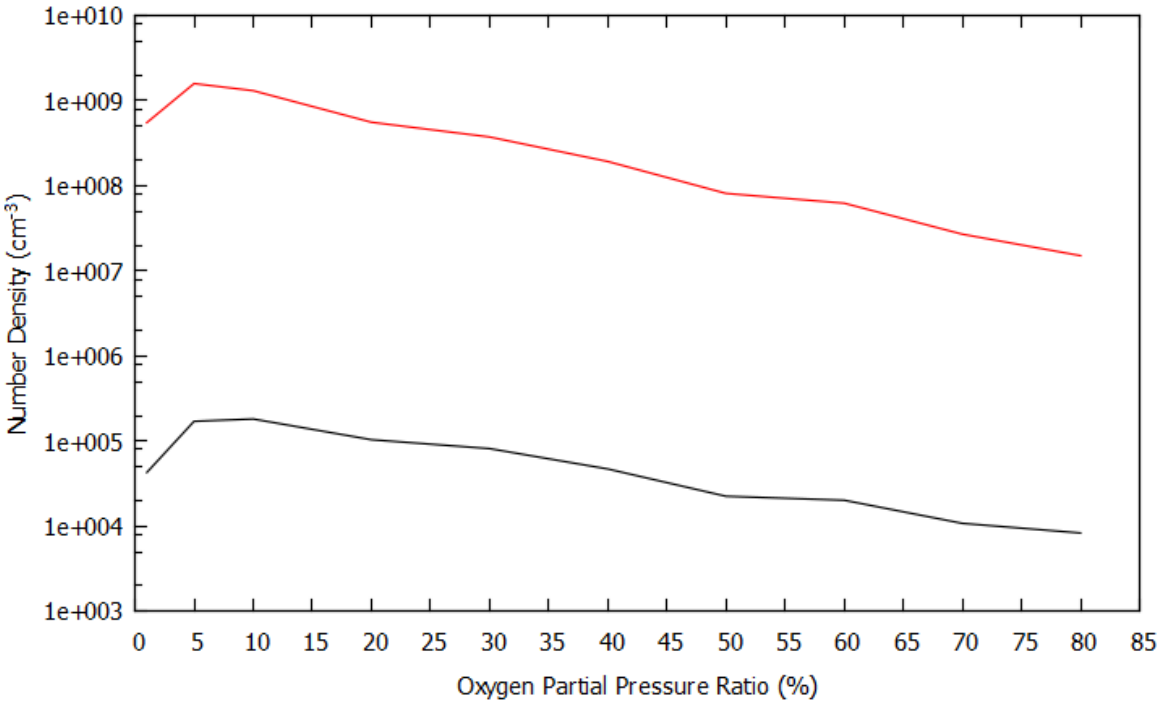

Figure 4.11. Calculation results for the number densities of the NO A $^2\Sigma^+$ state (red line) and the NO C $^2\Pi$ state (black line).

Figure 4.11 shows the calculated number densities of the NO C $^2\Pi$ and A $^2\Sigma^+$ states. From the results, we can easily see that the number densities of both the NO C $^2\Pi$ and A $^2\Sigma^+$ states decrease as the O_2 partial pressure increases. However, it is still not clear whether or not the product of the NO C $^2\Pi$ de-excitation is the A $^2\Sigma^+$ state. Therefore, by using the method of our previous study, we obtained the vibrational and rotational temperatures of the NO A $^2\Sigma^+$ state by fitting the calculated and experimental spectra. In this way, we were able to check whether or not the rovibronic properties of the NO A $^2\Sigma^+$

state change.

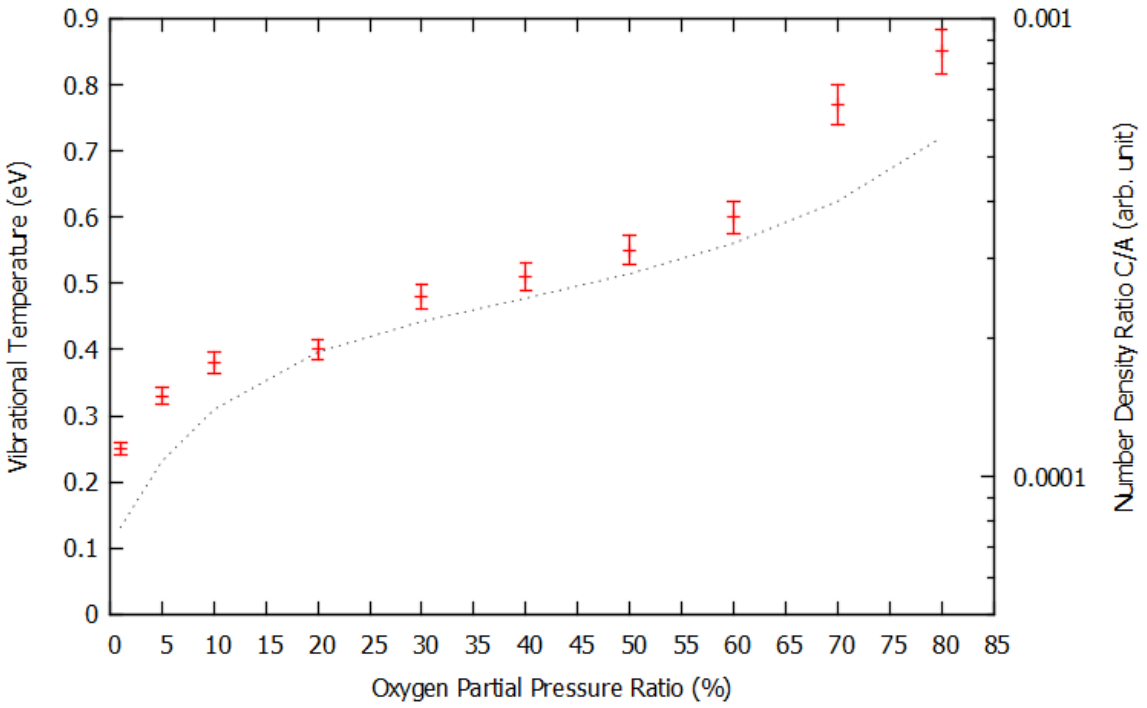

Figure 4.12. Experimental results for the vibrational temperatures of the NO A $^2\Sigma^+$ state (red dots with error bars, left vertical axis), and numerical results for number density ratios of the NO C $^2\Pi$ and NO A $^2\Sigma^+$ states (black dotted line, right vertical axis).

Fig. 4.12 shows the dependence of the vibrational temperature of NO A $^2\Sigma^+$ state with respect to the O_2 partial pressure. From the results, we can observe a good agreement between the O_2 partial pressure dependence of the vibrational temperature for the A $^2\Sigma^+$ state with that of the number density ratio of C $^2\Pi$ and A $^2\Sigma^+$ states. This indicates that, because the NO C $^2\Pi$ state population process involves an atomic collision of N and O, the C $^2\Pi$ state molecules should have higher vibrational populations, because the heavy particle impact association usually generates molecules at higher vibrational

levels.[46,85] After quenching by O_2, the molecules are de-excited to the A $^2\Sigma^+$ states and this leads to an increase in the vibrational temperature of the A $^2\Sigma^+$ state, that is, because the collision occurs too frequently to change its vibrational status. Moreover, we only calculated the non-predissociated processes. If the molecules at higher vibrational levels are included, the number density ratio of the NO C $^2\Pi$ and A $^2\Sigma^+$ states should be larger, which further corroborates to our analysis above. Therefore, as the number density ratio of the NO C $^2\Pi$ and A $^2\Sigma^+$ states increases, the ratio of the A $^2\Sigma^+$ state with high vibrational temperature also increases, which can finally result in the vibrational temperature increase of the NO A $^2\Sigma^+$ state. Thus, we can finally conclude that NO C $^2\Pi$ transfers to NO A $^2\Sigma^+$ and contributes a different vibrational distribution in which O_2 $^3\Sigma^-_g$ can be considered as a catalyst.

CHAPTER V: Conclusions

5.1 Summary

This research has two main parts, spectroscopic measurement of vibrational and rotational temperatures of nitrogen monoxide molecules, and the development of a self-consistent kinetic model for the examination of the number densities of NO A $^2\Sigma^+$, B $^2\Pi$, C $^2\Pi$ states.

The vibrational and rotational temperatures of nitrogen monoxide molecules are obtained for N_2-O_2 mixture microwave discharge plasma through spectroscopic measurement. We experimentally observed the γ-band (195 – 340 nm) spectrum of nitrogen monoxide. We also developed a method of theoretical calculation for its vibrational and rotational spectrum, with which we can fit the experimental results theoretically, so that the vibrational and rotational temperatures can be determined. Some experiments are carried out to examine relaxation process of excited states of the N_2-O_2 mixture gas plasma by changing the N_2 ratio dependence. We find a normal increase on the vibrational temperature of NO molecules when the O_2 ratio approaches to 100%, which is the most important finding in the first part.

At the second part of this research, a self-consistent kinetic model is developed to study the atomic and molecular processes in the microwave discharge plasma of N_2-O_2 mixtures. We focus on the NO A $^2\Sigma^+$, B $^2\Pi$, and C $^2\Pi$ states in the mixture discharge. We find good agreement between the calculated NO A $^2\Sigma^+$ densities and experimental γ-band radiation intensities. On the other hand, the radiation bands from the NO B $^2\Pi$ and C $^2\Pi$ states are observed only when the oxygen partial pressure is less than 3%. We discuss the

de-excitation processes for the NO B $^2\Pi$ and C $^2\Pi$ states in this low-pressure plasma and propose that the de-excitation processes involve collision with O_2 X $^3\Sigma^-_g$ for these levels, which can explain the observed spectral disappearance, which is the most important finding in the second part.

In order to prove our proposal, we carried out some adding experimental and calculation results. This result shows that as the ratio of the number density of NO C $^2\Pi$ and A $^2\Sigma^+$ increases, there is a positive correlation with the vibrational temperature of the NO A $^2\Sigma^+$state. This implies that the NO C $^2\Pi$ state experiences a de-excitation collision and turns into A $^2\Sigma^+$ state, which finally leads to the vibrational temperature increase of NO A $^2\Sigma^+$state.

For the further research of this study, both the spectral calculation and the kinetics model can be improved after more molecular constants are available. Meanwhile, in the kinetics model, if more excited states of NO, as well as N_2 and O_2 are included, the programming procedure should also be improved using the multi-core calculating method, which can decrease the calculating period effectively.

5.2 Concluding Remarks

5.2.1 Future Possibility to Understand Other Diatomic Molecules

For future investigations, it is necessary to develop the calculation of β- and δ-bands. Although they are hard to observe in low-temperature and low-pressure N_2-O_2 plasma, they exist when the pressure is high, for example the atmosphere. If we can combine the

spectral calculation and the number density simulation, the whole unresolved spectra ranged at 200—900 nm, including NO γ-, β- and δ-bands, and other bands of N_2 and O_2, and lines of atoms and ions, can be finally obtained, which would be very helpful for the spectroscopic study of the N_2-O_2 plasma.

For other mixture gases, this method is still available to diagnose a specific molecule, for example, the NH molecule in N_2-H_2 plasma. There is also a strong radiation band of the NH molecule at 336 nm, which origins from the $A^3\Pi$ to $X^3\Sigma^-$ states shown as Fig. 5.1.

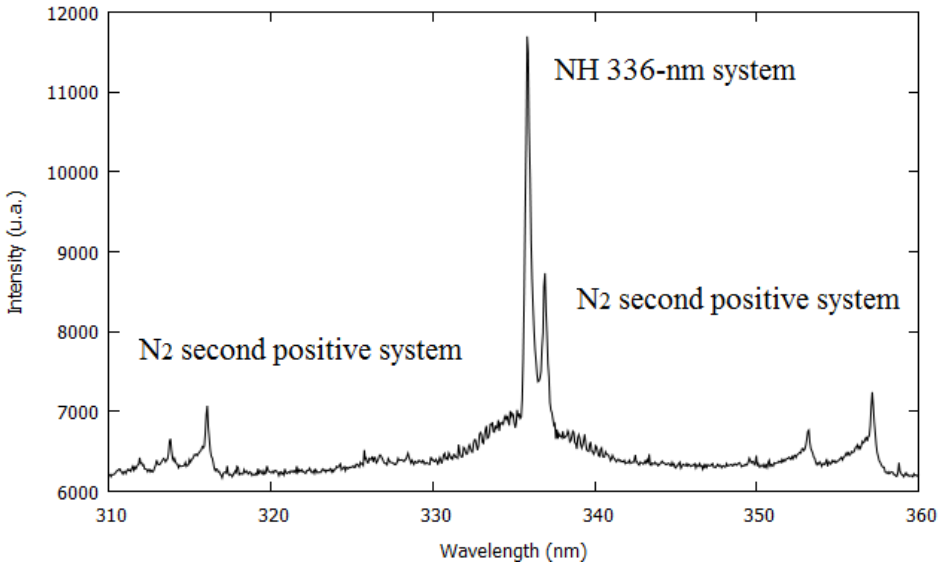

Figure 5.1. Experimentally observed spectra over the 310-360-nm wavelength range with H_2 partial pressure at 90%. The 2nd positive system of N_2 (310~320 nm and 350~360 nm) and 336-nm system (330~340 nm) of NH are specified. The discharge pressure is 1 Torr.

Meanwhile, this spectroscopic method has a basic requirement, that is, two visible vibrational transitions, for example (0,0) and (1,1), should be not too closed to each other.

For the NH case in Fig. 5.1, we can see two strong peaks around 336 nm. However, they are different rotational branches that both belong to the same vibrational transition (0,0). Therefore, it is only possible to obtain the rotational temperature of NH molecules by fitting the calculated and experimental spectra.

5.2.2 Future Research and Development Issues Relevant to NO Molecules

As shown in Table IV, the NO molecule is far less than N_2 and O_2 molecules in the plasma. Meanwhile, we can also find that the NO molecules always exist and the number densities of different states have dependence when O_2 partial pressure changes. From Fig. 4.4, we can find that the intensities of the NO γ-bands when 40% O_2, is smaller than that of 1% O_2. This means in some applications, we can control the NO concentration by changing the O_2 partial pressure. For example as shown in Fig. 1.1, the plasma light source for the therapy requires that, when the plasma is generating, we need the NO concentration to be as much as possible, while when pumping out the exhaust gas, we need the NO concentration to be as little as possible. Therefore, I think according to our research result, an adding gas that only reacts with O_2 can solve this problem perfectly.

ACKNOWLEDGMENTS

Here I would like to say thanks to all the people since I came to Tokyo Tech.

Prof. Akatsuka gave me the opportunity to get my doctoral dream since I was a child. He also gave me fully supports both on my research and my life. I have learned not only the knowledge from him, but also the attitude that a researcher should have. I think the latter is more precious because that will lead me to the rest of my life and career.

To my parents, I never say “thanks” to them, because I feel this word cannot cover all the meaningful feelings that I want to express. No word can. They support me for nearly 30 years which is really a long time. As long as something I missed, someone I lost, they never complain, because they are willing to do so, from heart.

I want to express my grateful appreciation to Mr. Nezu. I didn’t get my master degree in Tokyo Tech., as a result, I need a long time to learn the usage of the experimental apparatus. He did me the favor and spent much time to be with me when I performed an experiment. On the other hand, Mr. Nezu is a very good cooker. He cooed the best Yaki-Soba I ever ate, which I couldn’t achieve even after a long time try. Meanwhile, I feel very happy to be with all the fellows in the laboratory. It is called “Yuan (缘)” in Chinese, which means the gift from the God that you cannot expect. And I will keep this memory in mind though all my life.

I want to thank the financial support from the Saneyoshi founding of Tokyo Tech. for the tuition waiver during my doctor course. And I also thank JASSO (Japan Student Services

Organization) for their scholarship. These two financial support really releases my life at Japan and help me to focus on my research.

REFERENCES

[1] M. Capitelli, C. M. Ferreira, B. F. Gordiets, and A. I. Osipov, *Plasma Kinetics in Atmospheric Gases* (Springer-Verlag Berlin Heidelberg, 2000), Chap. 13.

[2] V. Guerra and J. Loureiro, Plasma Sources Sci. Technol. **8**, 110-124 (1999).

[3] U. von Zahn and E. Murad, Nature **321**, 147 (1986).

[4] J. Winter, M. Dünnbier, A. Schmidt-Bleker, A. Meshchanov, S. Reuter, and K-D.Weltmann, J. Phys. D **45**, 385201 (2012).

[5] K. M. Smith and D. A. Newnham, Chem. Phys. Lett. **308**, 1-6 (1999).

[6] J. Jiang and S. I. Sandler, Langmuir **20**, 25 (2004).

[7] G. M. Sokol, K. P. van Meurs, L. L. Wright, O. Rivera, W. J. Thorn III, P. M. Chu, and R. L. Sams, Clinical Chemistry **45**, 3 (1999).

[8] L. Martinsson, P. E. Bengtsson, and M. Aldén, Appl. Phys. B **62**, 29-37 (1996).

[9] A. Fridman, *Plasma Chemistry* (Cambridge University Press, New York, USA, 2008), Chap. 12.

[10] M. Moisan, K. Boudam, D. Carignan, D. Kéroack, P. Levif, J. Barbeau, J. Séguin, K. Kutasi, B. Elmoualij, O. Thellin, and W. Zorzi, Eur. Phys. J. Appl. Phys. **63**, 10001 (2013).

[11] G. N Rokhlin, *Discharge Light Sources* (Moscow: Energoatomizdat, Russian, 1991).

[12] V. N. Ochkin, *Spectroscopy of Low Temperature Plasma*, (WILEY-VCH Verlag GmbH & Co. KGaA, Russia, 2009).

[13] B. Bordiets and A. Ricard, Plasma Sources Sci. Technol. **2**, 158-163 (1993).

[14] B. F. Gordiets, C. M. Ferreira, V. L. Guerra, J. M. A. H. Loureiro, J. Nahorny, D. Pagnon, M. Touzeau, and M. Vialle, IEEE TRANSACTIONS ON PLASMA SCIENCE **23**, 4 (1995).

[15] J. Nahorny, C. M. Ferreira, B. Gordiets, D. Pagnon, M. Touzeau, and M. Vialle, J. Phys. D **28**, 738-747 (1995).

[16] I. A. Kossyi, A. Y. Kostinsky, A. A. Matveyev, and V. P. Silakov, Plasma Sources Sci. Technol. **1**, 207-220 (1992).

[17] M. Capitelli, R. Celiberto, G. Colonna, G. D'Ammando, O. De Pascale, P. Diomede, F. Esposito, C. Gorse, A. Laricchiuta, S. Longo, L. D. Pietanza, and F. Taccogna, Plasma Phys. Controlled. Fusion. 53, 124007 (2011).

[18] K. Peerenboom, A. Parente, T. Kozák, A. Bogaerts, and G. Degrez, Plasma Sources Sci. Technol. **24**, 025004 (2015).

[19] J. M. Tibbitt, R. Jensen, A. T. Bell, and M. Shen, Macromolecules **10**, 3 (1977).

[20] J. Abdallah Jr, N. Palmer, W. Gekelman, J. Maggs, and R. E. H. Clark, J. Phys. B **32**, 1001-1008 (1999).

[21] A. Garscadden and R. Nagpal, Plasma Sources Sci. Technol. **4**, 268-280 (1995).

[22] B. Gordiets, C. M. Ferreira, M. J. Pinheiro, and A. Ricard, Plasma Sources Sci. Technol. **7**, 363-378 (1998).

[23] B. Gordiets, C. M. Ferreira, M. J. Pinheiro, and A. Ricard, Plasma Sources Sci. Technol. **7**, 379-388 (1998).

[24] C. Park and S. H. Lee, J. Thermophys. Heat Tr. **9**, 9-16 (1995).

[25] D. S. Babikian, N. K. J. L. Gopaul, and C. Park, J. Thermophys. Heat Tr. **8**, 737-743 (1994).

[26] K. Abe, T. Kameyama, H. Kihara, M. Nishida, K. Ito, and H. Tanno, J. Thermophys. Heat Tr. **19**, 428-434 (2005).

[27] S. Hyun, C. Park, and K. Chang, 47th AIAA Aerospace Sciences Meeting Including The New Horizons Forum and Aerospace Exposition, Korea Advanced Institute of Science and Technology, Florida, 2009.

[28] B. F. Gordiets, Yu. N. Kulikov, M. N. Markovand, and M. Ya. Marov, J. Geophys. Res. **87**, 4504-4514 (1982).

[29] I. Langmuir, Proc. Nat. Acad. Sci. **14**, 627 (1926).

[30] N. A. Krall and A. W. Trivelpieece, *Principles of Plasma Physics*, (McGraw-Hill Inc., US, 1973).

[31] 马腾才，胡希伟，陈银华 著, *等离子体物理原理*, (中国科学技术大学出版社, 合肥, 1988).

[32] 徐佳鸾，金尚宪 著, *等离子体物理学*, (原子能出版社, 北京, 1981).

[33] 李定，陈银华，马锦秀，杨维纮 著, *等离子体物理学*, (高等教育出版社, 北京, 2006).

[34] P. Bliokh, V. Sinitsin, and V. Yaroshenko, *Dusty and self-gravitational plasmas in space*, (Kluwer Academic Publishers, US, 1995).

[35] J. Howard, *Introduction to Plasma Physics C17 Lecture Notes*, (Class handout, Australian National University, 2002).

[36] R. O. Dendy, *Plasma Dynamics*, (Clarendon Press, Abingdon, 1990).

[37] J. A. Bittencourt, *Fundamental of Plasma Physics*, (Springer-Verlag, New York, 2004).

[38] S. Koike, T. Sakamoto, H. Kobori, H. Matsuura, and H. Akatsuka, Jpn. J. Appl. Phys. **43**, 5550 (2004).

[39] R. Toyoyoshi, T. Sakamoto, H. Matsuura, and H. Akatsuka, Jpn. J. Appl. Phys. **46**, 3566 (2007).

[40] T. Sakamoto, H. Matsuura, and H. Akatsuka, Jpn. J. Appl. Phys. **45**, 7905 (2006).

[41] T. Sakamoto, H. Matsuura, and H. Akatsuka, J. Appl. Phys. **101**, 023307 (2007).

[42] R. Kashiwazaki and H. Akatsuka, Jpn. J. Appl. Phys. **41**, 5432 (2002).

[43] J. Mizuochi, T. Sakamoto, H. Matsuura, and H. Akatsuka, Jpn. J. Appl. Phys. **49**, 036001 (2010).

[44] K. Kano, M. Suzuki, and H. Akatsuka, Plasma Sources Sci. Technol. **9**, 314 (2000).

[45] K. Kano, T. Sakamoto, and H. Akatsuka, J. Adv. Oxid. Technol. **8**, 25 (2005).

[46] G. Herzberg, *Molecular Spectra and Molecular Structure I. Spectra of Diatomic Molecules* (D. Van Nostrand, Toronto, 1950).

[47] L. Pauling and E. B. Wilson, *Introduction to Quantum Mechanics* (McGraw-Hill, New York, 1937).

[48] M. Born and R. Oppenheimer, Ann. Physik **84**, 457 (1927).

[49] M. Cacciatore, M. Capitelli, and C. Gorse, *Chem. Phys.* **60**, 141 (1982).

[50] G. de Wit, B. R. Heazlewood, M. S. Quinn, A. T. Maccarone, K. Nauta, S. A. Reid, M. J. T. Jordan, and S. H. Kable, Faraday Discuss. **157**. 227-241 (2012).

[51] T. Yumii, T. Yoshida, K. Doi, N. Kimura, and S. Hamaguchi, J. Phys. D **46**, 135202 (2013).

[52] M. Wenig, N. Spichtinger, A. Stohl, G. Held, S. Beirle, T. Wanger, B. Jähne, and U. Platt, Atmos. Chem. Phys. **3**, 387 (2003).

[53] P. Vankan, S. B. S. Heil, S. Mazouffre, R. Engeln, and D. C. Schram, Rev. Sci. Instrum. **75**, 996 (2004).

[54] F. R. Gilmore, J. Quant. Spectrosc. Radiat. Trans. Phys. **5**, 783-808 (1965).

[55] R. S. Mulliken and A. Chirsty, Phy. Rev. **38**, 87 (1931).

[56] L. T. Earls, Phys. Rev. **48**, 423 (1935).

[57] R. Engleman, Jr. , and P. E. Rouse, J. Molecular. Spectroscopy 37, 240-251 (1971)

[58] T. Sakamoto, PhD Thesis, Tokyo Institute of Technology, Tokyo, Japan (2006).

[59] Y. Ichikawa, T. Sakamoto, A. Nezu, H. Matsuura, and H. Akatsuka, Jpn. J. Appl. Phys. **49**, 106101 (2011).

[60] U. H. Kurzweg, A. M. Bass, and H. P. Broida, J. Mol. Spectrosc. **1**, 184 (1957).

[61] C. O. Laux, PhD Thesis, Stanford University, Stanford, CA, USA (1993).

[62] F. A. Jenkins, H. A. Barton, and R. S. Mulliken, Phys. Rev. **30**, 150 (1927).

[63] C. S. Park, M. E. Newfield, D. G. Fletcher, T. Gökçen, and S. P. Sharma, J. Thermophys. Heat Transfer **12**, 190 (1998).

[64] D. S. Babikian, N. K. J. M. Gopaul, and C. Park, J. Thermophys. Heat Transfer **8**, 737 (1994).

[65] T. Sakamoto, K. Naoi, H. Matsuura, and H. Akatsuka, Jpn. J. Appl. Phys. **45**, 243 (2006).

[66] N. Masoud, K. Martus, M. Figus, and K. Becker, Contrib. Plasma Phys. **45**, 32

(2005).
[67]J. Raud, M. Laan, and I. Jõgi, J. Phys. D **44**, 345201 (2011).
[68] M. J. Brunger, L. Campbell, D. C. Cartwright, A. G. Middleton, B. Mojarrabi, and P. J. O. Teubner, J. Phys. B 33, 809 (2000).
[69] M. J. Brunger, L. Campbell, D. C. Cartwright, A. G. Middleton, B. Mojarrabi, and P. J. O. Teubner, J. Phys. B 33, 783 (2000).
[70] L.-F. Zhu, Z.-P. Zhong, Z.-S. Yuan, W.-H. Zhang, X.-J. Liu, X.-M. Jiang, K.-Z. Xu, and J.-M. Li, Chin. Phys. 11, 1149 (2002).
[71] T. Fujimoto, *Plasma Spectroscopy* (Oxford University Press, Oxford, U.K., 2004) p. 69.
[72] W. E. Sharp and D. W. Rusch, J. Quant. Spectrosc. Radiat. Transfer **25**, 413 (1981).
[73] I. M. Campbell and R. S. Mason, J. Photochem. **8**, 321 (1978).
[74] K. Tsukiyama, T. Munakata, M. Tsukakoshi, and T. Kasuya, Chem. Phys. **121**, 55 (1988).
[75] A. A. Matveev, A. M. Pravilov, and A. F. Vilesov, Chem. Phys. Lett. **217**, 582 (1994).
[76] Z. D. Cao and D. W. Setser, J. Phys. Chem. **92**, 1169 (1988).
[77] T. Hikida, T. Suzuki, and Y. Mori, Chem. Phys. **118**, 437 (1987).
[78] W. Groth, D. Kley, and U. Schurath, J. Quant. Spectrosc. Radiat. Transfer **11**, 1475 (1971).
[79] R. de Vivie-Riedle, M. C. van Hemert, and S. D. Peyerimhoff, J. Chem. Phys. **92**, 3613 (1990).
[80] L. G. Piper and L. M. Cowles, J. Chem. Phys. **85**, 2419 (1986).
[81] R. R. Laher and F. R. Gilmore, J. Phys. Chem. Ref. Data **20**, 685 (1991).
[82] F. R. Gilmore, R. R. Laher, and P. J. Espy, J. Phys. Chem. Ref. Data **21**, 1005 (1992).
[83] R. W. Gross and N. Cohen, J. Chem. Phys. **48**, 2582 (1968).
[84] A. B. Callear and I. W. M. Smith, Discuss. Faraday Soc. **37**, 96 (1964).
[85] H. Tan, A. Nezu, H. Matsuura, and H. Akatsuka, Jpn. J. Appl. Phys. **54**, 01AB06 (2015).
[86] B. F. Gordiets, C. M. Ferreira, V. L. Guerra, J. M. A. H. Nahomy, D. Pagnorn, M. Touzeau, and M. Vialle Rowe, IEEE Trans. Plasma Sci. **23**, 750 (1995).

Overview

Doctor Oral Defense

Time:

Place:

Supervisor: Prof. Hiroshi Akatsuka

Presenter

Name: Hao Tan

Birthday: 1987.2.11

Nationality: China

Study Experience

2006.9 ~ 2010.7: Zhejiang University (China) / Information and Communication Technology / Bachelor of Engineering

2011.4 ~ 2013.3: Utsunomiya University (Japan) / Electrical, Electronic and System Engineering / Master of Science

2013.4 ~ 2016.3: Tokyo Institute of Technology (Japan) / Energy Science / Ph. D

Achievement

Published Paper

Spectroscopic determination of vibrational and rotational temperature of NO molecules in N_2-O_2 mixture microwave discharge.

H. Tan, A. Nezu, H. Matsuura, and H. Akatsuka.

Japanese Journal of Applied Physics, **54**, 01AB06, 6 (2015).

Kinetic model and spectroscopic measurement of NO (A, B, C) states in low-pressure N_2-O_2 mixture microwave discharge.

H. Tan, A. Nezu, and H. Akatsuka.

Japanese Journal of Applied Physics, **54**, 096103, 6 (2015).

Spectroscopic investigation of the NO C $^2\Pi$ de-excitation process by collision with O_2 X $^3\Sigma_g^-$ in a low-pressure N_2-O_2 mixture microwave discharge.

H. Tan, A. Nezu, and H. Akatsuka.

Japanese Journal of Applied Physics, **55**, 01AH04, 4 (2016).

International Conference

- Hao Tan, Atsushi Nezu, Hiroshi Akatsuka.

Spectroscopic Examination of Molecular Spectra in Mixture Gaseous Microwave Discharge (N_2-O_2 and N_2-H_2), 68th Annual Gaseous Electronics Conference/9th International Conference on Reactive Plasmas/33rd Symposium on Plasma Processing, Bulletin of the American Physical Society, The American Physical Society, Vol. 60, No. 9, p. 41, Oct. 2015.

- Hao Tan, Atsushi Nezu, Haruaki Matsuura, Hiroshi Akatsuka.

Spectroscopic Examination Of Vibrational and Rotational Properties of NO(A $^2\Sigma^+$) Metastable State From NO gamma–Band Spectra By Using Microwave Discharge N_2-O_2 Mixture Plasma, 17th International Congress on Plasma Physics (ICPP2014), ICPP2014_Book_of_Abstracts, Instituto Superior Técnico (IST), Sep. 2014.

- Hao Tan, Atsushi Nezu, Haruaki Matsuura, Hiroshi Akatsuka.

Calculation and Spectroscopic Examination of γ–band Spectra of NO Molecule by Using Microwave Discharge N_2-O_2 Mixture Plasma, 8th International Conference on Reactive Plasmas/31st Symposium on Plasma Processing, The Conf. Proc. 8th International Conference on Reactive Plasmas/31st Symposium on Plasma Processing, Japan Society of Applied Physics, Feb. 2014.

- Hao Tan, Atsushi Nezu, Hiroshi Akatsuka.

Vibrational and rotational temperatures of NO A $^2\Sigma^+$ metastable state in N2-O2 mixture microwave discharge, The 42nd IEEE International Conference on Plasma Science (ICOPS2015), ICOPS 2015 Abstract Book, IEEE, NPSS, p. 45, May. 2015.

- Hao Tan, Atsushi Nezu, Haruaki Matsuura, Hiroshi Akatsuka. Kinetic model of NO molecular states (X $^2\Pi_r$, A $^2\Sigma^+$, B $^2\Pi_r$ and C $^2\Pi_r$) in a low- pressure N_2-O_2 discharge, 7th International Symposium on Advanced Plasma Science and its Applications for Nitrides and Nanomaterials/ 8th International Conference on Plasma-Nano Technology & Science (ISPlasma2015/IC-PLANTS2015), Proc. ISPlasma2015/IC-PLANTS2015, Organizing Commmittee of ISPlasma2015/IC-PLANTS2015, Mar. 2015.

- Hao Tan, Atsushi Nezu, Haruaki Matsuura, Hiroshi Akatsuka. Spectroscopic Examination of Vibrational and Rotational Properties of NO A $^2\Sigma^+$ Metastable State from NO γ-Band Spectra in N^2-O^2 Mixture Microwave Discharge, 67th Annual Gaseous Electronics Conference, Bull. Am. Phys. Soc., APS, Vol. 59, No. 16, p. 19, Nov. 2014.
- Hiroshi Akatsuka, Hirokazu Kawano, Koichi Naoi, Hao Tan, Atsushi Nezu, Haruaki Matsuura.

Difference in Rotational Temperatures between Neutral Molecules and Molecular Ions of Low-Pressure Discharge N_2-O_2 Plasmas, 67th Annual Gaseous Electronics Conference, Bull. Am. Phys. Soc., APS, Vol. 59, No. 16, p. 33, Nov. 2014.

- Hao Tan, Atsushi Nezu, Haruaki Matsuura, Hiroshi Akatsuka. Vibrational and Rotational Temperature Spectroscopic Determination of NO Molecule in N_2-O_2 Microwave Discharge, Plasma Conference 2014, Plasma 2014 Online Procedings, The Japan Society of Plasma Science and Nuclear Fusion Research, Nov. 2014.

Domestic Conference

- Hao Tan, Atsushi Nezu, Hiroshi Akatsuka.

Vibrati onal and Rotational Te mperature Dependence of NH in Microwave N2 - H2 Mixture Gas Discharge, The 76th JSAP Autumn Meeting, 2015, Extended Abstracts of The 76th JSAP Autumn Meeting, 2015, The Japan Society of Applied Physics, p. 07-038, Aug. 2015.

- Hiroshi Akatsuka, Hao Tan, Atsushi Nezu, Haruaki Matsuura.

Optical Emission Spectroscopic Observation of Low-pressure N2-O2 Mixture Plasma and its Excitation Kinetics in a Lab-scale Discharge Experiment, The Annual Meeting of the Spectroscopical Society of Japan, Proc. the Annual Meeting of the Spectroscopical Society of Japan, The Spectroscopical Society of Japan, p. 2, Jun. 2015.

- 譚 浩, 根津 篤, 松浦 治明, 赤塚 洋. マイクロ波放電 N_2-O_2 混合気体プラズマ中の NO 分子 B, C 励起状態の分光測定と粒子数の計算, 第 62 回応用物理学会春季学術講演会, 第 62 回応用物理学会春季学術講演会 講演予稿集, 07-004, Feb. 2015.
- 赤塚 洋, 川野 泰和, 直井 浩一, 清水 良浩, 譚 浩, 根津 篤, 松浦 治明. 分子気体放電プラズマ中の各励起種の回転温度差に関する考察, 電気学会プラズマ研究会, 電気学会プラズマ研究会資料, 一般社団法人電気学会, Sep. 2014.
- Tan Hao, Nezu Atsushi, Matsuura Haruaki, Akatsuka Hiroshi.

Calculation of γ-band Spectra of NO Molecule in Microwave Discharge N_2-O_2 Mixture Plasma and Determination of Vibrational and Rotational Temperature, Technical Meeting on "Plasma Science and Technology", IEE Japan, The Papers of Technical Meeting on "Plasma Science and Technology", IEE Japan, The Institute of Electrical Engineers of Japan, Vol. PST-13-104-113, pp. 29-32, Sep. 2013.